APPLICATION OF SUPERCRITICAL CARBON DIOXIDE IN LIPID VESICLE DESIGN AND EXTRACTION OF OIL FROM POTATO CHIPS

A Dissertation

Presented to the Faculty of the Graduate School

of Cornell University

In Partial Fulfillment of the Requirements for the Degree of

Doctor of Philosophy

by

Michael Emil Wagner

January 2015

APPLICATION OF SUPERCRITICAL CARBON DIOXIDE IN LIPID VESICLE DESIGN AND EXTRACTION OF OIL FROM POTATO CHIPS

Michael Emil Wagner, Ph.D.

Cornell University 2015

Supercritical carbon dioxide (SC-CO_2) has emerged as a non-toxic and environmentally friendly alternative to conventional organic solvents with many applications. A novel method of non-ionic surfactant based lipid vesicle (niosome) production coupling a gas ejector with the rapid expansion of a supercritical solution was studied. Niosomes were prepared using Tween61, which was shown to be 4-6% soluble (wt. basis) in SC-CO_2 ranging from 40 to 60°C and 10 to 20 MPa, and cholesterol at a 1:1 molar ratio. Niosome lamellarity was shown to depend on the degree of precipitation of the lipid formulation at the point of aqueous cargo introduction. Niosome particle size distributions were bimodal, with the 80-99% of the liposomal volume contributed niosomes ranging in size from 3-7 μm and the remaining niosomes ranging from 239-969 nm, depending on the system configuration. Using the gas ejector for cargo introduction, the maximum encapsulation efficiency of a 0.2 M sucrose solution was 28%. Niosome size and encapsulation efficiency were shown to be influenced by aqueous cargo droplet formation and the aerodynamic forces of the expanding gaseous stream. Simultaneous encapsulation of ferrous sulphate and cholecalciferol achieved encapsulation efficiencies of 25.1 ± 0.2% and 95.9 ± 1.5%, respectively. Niosomes showed good physical stability at 20°C, but storage at 4°C showed an initial burst release of ferrous iron, indicating possible rupture of the niosomal membrane.

Extraction of oil from potato chips was investigated as a means for the simultaneous production of low fat potato chips and flavor extract. Extraction conditions range 27.6-41.4MPa, 35-80°C and solvent flow rate of 0.5-5.0g CO_2/min. Up to 100% of the oil was recovered from the potato chips at the highest pressure and temperature conditions. Two process conditions were chosen for comparison of performance with a larger scale (1:5) system, maintaining the same CO_2 flow rate to feed mass ratio with Good agreement between scales observed at the higher pressure and temperature settings. Kinetic parameters, calculated using a literature model, indicated that the extraction was limited by internal diffusion. Costs associated with the process were assessed using a method described in the literature.

BIOGRAPHICAL SKETCH

Michael Emil Wagner was born in Wayne, New Jersey. His early education was in the Wayne public school system's accelerated learning programs. In 2006, Michael entered Cornell University as an undergraduate. He pursued a majored in Food Science and supplemented this curriculum by minoring in Nurtritional Science. He held a product development internship with French's Foods during the summer of 2009 and did undergraduate research in the lab of Professor Syed S.H. Rizvi on the production of yeast free bread using Supercritical Fluid Extrusion. Michael graduated early in January 2010, but stayed on as a technician in the Rizvi lab working on Supercritical Fluid Extrusion and other projects. He was accepted into the Master's Degree program at Cornell under Professor Rizvi in 2010 and transferred to the PhD program in 2011. He minored in Applied Economics and Management and Biological and Environmental Engineering during the course of his graduate study. Michael also held five separate Teaching Assistantships and won the Outstanding Teaching Assistant Award for the department of Food Science in 2013. His research has focused on the application of Supercritical CO_2 in food processing through extraction, extrusion, and novel particle design.

This dissertation is dedicated to my family and friends, who have stood by me throughout my journey

ACKNOWLEDGEMENTS

I would like to thank Professor Syed. S.H. Rizvi, my advisor, for giving me this opportunity and providing guidance throughout my research. I have learned more than I ever intended and am forever grateful. I would also like to thank my minor advisors, Professor Todd Schmit and Professor Kifle Gebremedhin, for their guidance and assistance.

I would like to thank Pepsico for their generosity in partially funding my graduate education and the scientists that I worked with for their good advice.

I would like to thank Sean Schell and Tom Burke, for the practical education that they gave me. I certainly would not have been able to do as much without their teaching and support.

I would like to thank my labmates and friends in the Department of Food Science, for many enlightening discussions and enjoyable moments throughout our common struggle.

Lastly, I would like to thank my family, whose unconditional love and support carried me this far.

TABLE OF CONTENTS

Section I

LIST OF FIGURES

LIST OF TABLES

Section I

Chapter 1: Literature review

1.1. Introduction

Supercritical fluids (SCFs) have emerged as a potential alternative to organic solvents. A fluid becomes supercritical when it is pushed beyond its critical temperature and pressure and under these conditions, it has properties intermediary between a gas and a liquid. With gas like diffusivity and almost no surface tension, SCFs will readily penetrate solid and liquid matrices. With liquid like density, SCFs can readily dissolve polar or non-polar compounds, depending on the properties of the fluid being used. Additionally, the density, and therefore the solvating power of a SCF is tunable according to the system temperature and pressure. In the region of the critical point, the properties of a SCF can change drastically, which can allow for the selective solvation of certain compounds. Supercritical carbon dioxide (SC-CO_2) has gained considerable attention as a non-toxic alternative to conventional organic solvents for the solvation of non-polar compounds. With a relatively low critical temperature and pressure (31.1°C, 7.38 MPa), it is suitable for use with thermolabile compounds and leaves no solvent residue. As a linear molecule with no dipole moment, CO_2 is generally considered a poor solvent for polar and ionic species but can be modified with the addition of co-solvents, such as ethanol, for the solvation of poorly soluble compounds. SC-CO_2 is typically used in separation processes for non-polar compounds, but has also been used for enzyme and bacterial inactivation (Balaban and Ferrentino, 2012), polymer foaming (Sauceau et al. 2011), synthetic chemistry (Han and Poliakoff, 2012), and even as an alternative working fluid in power cycles (Dostal et al., 2006) The benefits and applications of SCFs have been extensively reviewed (Hauthal, 2001; McHugh and Krukonis, 1994; Rizvi et al., 1986a; Rizvi et al., 1986b).

1.2 Liposomes

Liposomes are colloidal particulates composed of spherical bimolecular phospholipid bilayers, which enclose part of the surrounding aqueous media into their interior. Because of the presence of both lipid and aqueous phases in the structure, liposomes are ideally suited for the entrapment, delivery, and release of water-soluble, lipid-soluble, and amphiphilic bioactive materials. Delivery of bioactive materials to various locations in the body is directly related to particle size, therefore nanoencapsulation has greater potential to enhance bioavailability, improve controlled release, and enable precision targeting of the bioactive material than microencapsulation does (Mozafari et al., 2006). Their controllable and narrow size distribution also increase therapeutic benefits, leading to small dosages required and avoiding undesirable side effects (Banerjee, 2001). They are particularly ideal for site specific delivery of actives to the body due to their similarity to natural cells. Used as a biocompatible carrier system, liposomes can also promote the physiological activity and safety of the entrapped components. In addition, liposomes passively target organs and tissues with discontinuous endothelium such as liver, kidney, spleen, lung liver, etc. (Chang and Yeh, 2012). For these reasons, liposomes have been the subject of extensive research, and several related technologies have been developed for specialized applications in the pharmaceutical (Banerjee, 2001) and cosmetic industries (Hougeir and Kircik, 2012). Liposomes have many potential applications including targeted anti-cancer drug delivery (Li et al., 2009), gene therapy (Suzuki et al., 2008), and immunization(van den Berg et al., 2010). Their non-toxic and biodegradable nature makes them suitable for delivery of many active compounds in biological systems (Lesoin et al., 2011). Some efforts have been made to use liposomes in food systems for the delivery of proteins, enzymes, antioxidants, flavors, and antibacterial peptides (Mozafari et al., 2006; Mozafari et al., 2008; Taylor et al., 2005a; Taylor et al., 2005b; da Silva Malheiros et al., 2010)). Such physically inspired approach

to designing novel structures to accomplish a specific function such as stabilization and controlled release of bioactive ingredients and flavors in foods while preserving good taste and perception properties is rapidly increasing in demand. Creating novel systems to accomplish it based on the fundamental knowledge at the nanoscale of structural and physical properties of materials provides a new platform for stimulating and challenging research.

1.2.1. Liposome forms and formulation

Liposomes can be made with a single bilayer of phospholipids, called unilamellar vesicles (UV), or multiple bilayers, called multilamellar vesicles (MLV) when the vesicles are concentric and multivesicular vesicles (MVV) when they are not concentric. Liposomes can also be classified by size, as single bilayer liposomes with a diameter less the 100 nanometers are called small unilamellar vesicles (SUV) and liposomes larger than 100 nanometers are called large unilamellar vesicles (LUV). The bilayer structure of liposomes allows for the simultaneous encapsulation of hydrophobic and hydrophilic compounds (Lesoin et al., 2011), as shown in Figure 1.1. Liposomes also offer enhanced physical and chemical stability in environments with high water activity when compared to conventional microencapsulation techniques, such as spray drying or extrusion which are stable in dry environments, but release their cargo readily in systems with high water activity (Gouin, 2004).

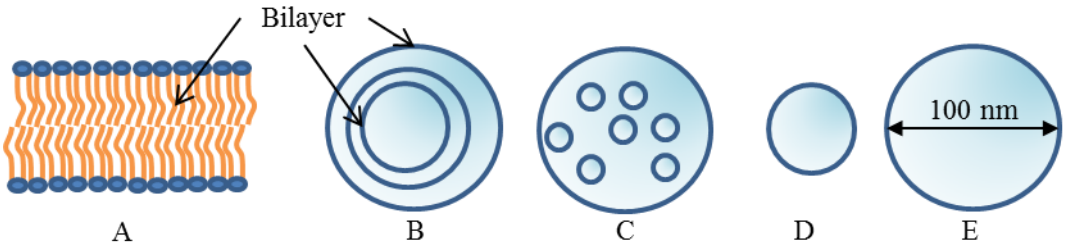

Figure 1.1. Liposome structural varieties. (A) Phospholipid bilayer, (B) MLV, (C) MVV, (D) SUV, (E) LUV.

Liposomes typically consist of amphipathic lipids combined in some proportion with cholesterol. Lipid selection can greatly influence the properties of the liposome including: surface charge, bilayer fluidity, permeability and cargo retention (Gregoriadis and Perrie, 2001). Some of the commonly used lipids and their relevant properties are listed in Table 1.1**.**

Table 1.1. Lipids commonly used in liposomes

Category	Name	Abbreviation/Trade name	T_c(°C)[a,b]	Head group type[ac]
Phospholipid based	Egg phosphatidylcholine	EPC	-10	I
	Hydrogenated soy phosphatidylcholine	HSPC	50-60	I
	Dioleoylphosphatidylcholine	DOPC	-20	I
Synthetic surfactant based	Sorbitan monostearate	Span 60	45	NI
	Polyoxyethylene sorbitan monostearate	Tween 61	40.6	NI
	Polyoxyethylene lauryl ether	Brij 30	<10	NI

[a] phospholipid based lipids at pH 7.4,(Avanti Polar Lipids); [b]Synthetic surfactants,(Manosroi et al., 2003); [c] I = ionic, NI = non-ionic

Blok *et al.* (1975) investigated the effect of chain length and phase transition temperature of different prepared lecithins on the permeability of liposomes. The transition temperature (T_c) is defined as the temperature at which the lipid changes from an ordered gel, where the hydrocarbons are extended and packed, to a liquid crystalline phase, where the hydrocarbon chains are randomly oriented. They showed that greater release of the entrapped substance occurred in the vicinity of the transition temperature of the phospholipid. The transition temperature is critical in the application of the liposome. For example, liposomes designed for drug delivery in the human body will leak their cargo rapidly if the T_c is well below

physiological temperatures. Cholesterol is also commonly used in liposomes to increase the rigidity of the bilayer. The ratio of cholesterol to phospholipid depends on the application, but at high concentrations (~30% molar), cholesterol can totally eliminate phase transition and make the liposome more stable even after delivery to the body (Sharma and Sharma, 1997).

The pH of the hydrating solution may also play a role in membrane characteristics. Sulkowski *et al.* (2005) prepared liposomes using TRIS buffer with pH ranging from 1.9-8.4. Liposomes prepared with TRIS buffer at lower pH (1.9 and 5) tended to have greater membrane rigidity (physical stability) below their T_c than liposomes produced under identical conditions using a buffer with alkaline pH (8 and 8.4). The authors hypothesized that this enhanced rigidity may be due to the formation of hydrogen bonds between the protonated head groups on adjacent phospholipids at lower pH. They showed that the effect of pH was less pronounced when cholesterol was also included in the liposome.

Liposomes can be anionic, cationic, or neutral depending on the polarity of the head group of the phospholipid. The surface charge of the liposome appears to greatly effect interactions between the liposome and the cell (Sharma and Sharma, 1997). Negative surface charge may increase intracellular uptake, accelerate plasma clearance after uptake, and result in the release of their cargo in the blood (Gabizon et al., 1990; Sharma and Sharma, 1997). Cationic liposomes may differ from anionic in their uptake by the cell.

Due to chemical instability, cost of materials, phospholipid degradation during storage, liposomes formed using synthetic non-ionic surfactants, called niosomes, offer advantages over phospholipid based liposomes (Uchegbu and Vyas, 1998). Non-ionic surfactants are structurally more consistent when compared with lecithin, which contains a mixture of phospholipids with varying chain length. They can also be designed with saturated alkyl chains, reducing oxidative

instability. In a direct comparison of liposomes and niosomes, Nasr *et al.* (2008) showed that niosomes offered greater physical stability over time than liposomes. Over a ninety day storage period, the most effective niosome formulation retained 72% of the entrapped hydrophilic drug, whereas the most effective liposome formulation only retained 63%. These researchers also found a minor difference in size distribution of stored niosomes compared to that of liposomes, which tended to show increased average diameter with storage. Overall, niosomes offer greater stability, lower cost, and easier production than phospholipid based liposomes (Desai and Finlay, 2002).

1.2.2. Liposome preparation

There are a variety of methods that can be used to prepare liposomes. Lesoin *et al.* (2011) outlined some of the most commonly used methods, including the Bangham method, detergent depletion method, ether/ethanol injection method, reverse phase evaporation method, and the double emulsion method. The Bangham method (Bangham et al., 1965) involves dissolving the phospholipids in organic solvent, typically chloroform, and subsequently evaporating the solvent to form a thin film. The film is then hydrated and with the solution to be encapsulated and agitated. This typically results in MLV ranging from 0.05-10 μm. The detergent depletion method involves forming micelles composed of phospholipid and detergents, such as bile salts or sodium dodecyl sulfate, followed by removal of the detergent through a variety of methods including dilution, dialysis, filtration, or adsorption (Schubert, 2003). The detergent depletion method typically yields UVs in ranging from 0.1-1μm in diameter (Lesoin et al., 2011). The injection methods involve dissolving the phospholipids in solvent, such as methanol or ethanol, and subsequent injection into an aqueous system, resulting in ULV ranging from 0.03-0.11μm in diameter (Lesoin et al., 2011). The reverse phase evaporation method involves the formation of

reverse micelles (single layer of phospholipids with the hydrophilic heads directed inward to the core of the vesicle) in solvent, such as isopropyl or diethyl ether, and subsequent evaporation of the solvent resulting in UV and MLV. Similarly the double emulsion method involves forming a water-in-oil emulsion in organic solvent and subsequent solvent evaporation (Shum et al., 2008). The reverse phase evaporation method and the double emulsion method result in liposomes with diameters of 0.18-0.45μm and 0.05μm, respectively.

1.2.3. Limitations to current methods of liposome assembly

There are several limitations to the preparation and use of liposomes and niosomes. During storage, liposomes undergo chemical and physical degradation, leading to loss of stability and leakage of the cargo material. Chemical instability may be due to hydrolysis of the lipids or oxidation of unsaturated bonds in the hydrocarbon chains (Sharma and Sharma, 1997). Physical defects in the lattice structure of the membrane can lead to leakage and fusion of individual liposomes. Liposomes less the 40 nm in diameter tend to fuse due to physical stresses as a result of the high curvature of the membrane (Risch and Reineccius, 1995). Aggregation will naturally occur due to Van der Waals forces between neutrally charged vesicles, but this can be minimized by using a small amount of charged phospholipid such as phosphatidic acid or phosphatidyl glycerol (Risch and Reineccius, 1995). Lyophilization may enhance the physical stability during storage (Sharma and Sharma, 1997). Liposomes are also limited by relatively low encapsulation efficiencies, ranging from 5-50% (Zuidam and Nedović, 2009). Sterilization is also critical for liposomes that are destined for biological systems. Microfiltration is the current preferred method, but γ-irradiation and heat treatments have been used. However, microfiltration is not suitable for larger liposomes or to remove viruses and irradiation and heat both can damage the vesicle and the cargo it is intended to deliver (Sharma and Sharma, 1997). Another major

drawback to conventional liposome preparation is that it requires a post processing step, such as sonication or the removal of organic solvents (Lesoin et al., 2011). The use of organic solvents is particularly limiting, as any residual solvent could render the liposomal preparations cytotoxic, thereby making them unsuitable in most biological applications. An ideal process would bypass the use of organic solvents entirely and eliminate the need for post processing.

1.4. Lipid vesicles formed using SCFs

1.4.1. Supercritical fluids in encapsulation

For at least two decades, SCFs, SC-CO_2 in particular, have been applied in alternative processing techniques for encapsulation (Cocero et al., 2009). These techniques can be divided according to the role of the SCF in the process: solvent, anti-solvent, co-solvent, or propellant. Reviews of these processes have been published (Cocero et al., 2009; Jung and Perrut, 2001). Additionally, SC-CO_2 provides a sterile production environment (Meure et al., 2008), which eliminates the need for the post-production sterilization step that is required for micro and nanocapsules designed for use in humans and animals.

1.4.2. Liposomes using SC-CO_2

Several studies have used SC-CO_2 as an alternative solvent in liposome formation, using a variety of methods. These methods can be divided into two classes: those based on the rapid expansion of supercritical solutions (RESS) and those based on reverse phase evaporation. RESS is a process where a supercritical solution is depressurized through a nozzle, causing the rapid nucleation of solute particles. As the supercritical fluid drops from high pressure to low pressure, it transitions into the gas phase where its solvating power is considerably lower, thus the dissolved solute nucleates. Originally noted in 1879 by Hannay and Hogarth, the RESS process has gained attention recently due to its use of clean solvents, like SC-CO_2, in particle design (Jung and Perrut, 2001). Much of the early work with the RESS process was focused on

production of pure, crystalline particles for pharmaceutical and other purposes (Coffey and Krukonis, 1988; Matson et al., 1987; Mohamed et al., 1989).

Castor and Chu (1994) described the injection and decompression methods, which are based on RESS. The injection method involves dissolving the lipid in SC-CO_2 with a cosolvent and subsequently injecting the supercritical solution through a nozzle into an aqueous solution to be encapsulated. The decompression method is similar except that is the aqueous solution to be encapsulated is mixed with the supercritical solution before depressurization through the nozzle. Using the injection method they found that increasing pressure of the supercritical solution from 13.4 to 33.5 MPa increased the average liposome diameter 339.5nm to 1.5μm. However, this is complicated by the varying density of SC-CO_2 and the solubility of lecithin. They achieved the most uniform particle size distribution at their optimum conditions for lecithin solubility, indicating that the solubility of the lipid at the process conditions can affect liposome formation. They also found that a smaller nozzle diameter produced smaller diameter liposomes, with 0.5mm and 0.06mm nozzle diameters resulting in particle sizes of 478nm and 326nm respectively. A similar injection method was described by Frederiksen *et al.,* (1997) who expanded a supercritical solution through a capillary and used 5-7% ethanol as a cosolvent to produce SUVs ranging from 20-50nm. The encapsulation efficiency achieved by this method was around 20%, which was 50% lower than the conventional ethanol injection method, though much less ethanol was required.

Another method for liposome preparation using SC-CO_2 is the reverse phase evaporation method. Developed by Otake *et al.* (2001), this method involves the combination of lipid, ethanol as a cosolvent, and supercritical fluid in a variable volume view cell and the gradual injection of an aqueous phase. As more aqueous solution is added, the original water/CO_2

emulsion transitions into a CO_2/water emulsion and upon depressurization, liposomes are formed. Otake et al. (2001) reported LUVs with a particle size range of 100nm to 1.2μm and comparable encapsulation efficiency to conventional LUV preparation. The same group observed that different levels of ethanol additions resulted in different types of emulsions (water-in-CO_2 or CO_2-in-water) prior to decompression, which influenced the lamellarity of the liposomes generated (Imura et al., 2003). Otake *et al.* (2006) presented an improved method that did not use ethanol, which increased encapsulation efficiency. They also noted that a slower rate of phase inversion produced larger liposomes with greater encapsulation efficiency. They reported very high physical stability, as much as 30 days, compared to liposomes produced using the Bangham method (~6 hrs).

Limited research is available for the formation of niosomes using SC-CO_2. Kinka *et al.* (2005) used reverse phase evaporation to form niosomes using polyoxyethylene sorbitan monostearate (TWEEN 61) as the primary bilayer constituent. They claim to have produced LUV, but their encapsulation efficiency was relatively low, around 9%. Manosroi *et al.* (2008) used the reverse phase evaporation method described previously (Otake et al., 2001) to produce niosomes using a Tween 61 /cholesterol formulation to encapsulate glucose. They also reported the formation of LUVs with relatively low encapsulation efficiency (12%). However, a later study published by that group reported comparable size distribution of niosomes prepared using the reverse phase evaporation method and the conventional sonication method for the encapsulation of rice bran extract (Manosroi et al., 2010a). Additionally, this group reported on the formation of niosomes for the encapsulation of semi-purified rice bran bioactives (Manosroi et al., 2010b). This study reported higher encapsulation efficiencies of two hydrophilic compounds produced by the SC-CO_2 method (55% and 83%) compared to the conventional

sonication method (50% and 72%, respectively). They reported an encapsulation efficiency of 47% for the hydrophobic compound they encapsulated using the SC-CO_2 method, which was slightly lower than the conventional sonication method at 51%.

1.4.3. Limitations of current SC-CO_2-based systems

There are however, limitations to the current application of SC-CO_2 in liposome production. Though these methods technically bypass the need for organic solvents by using SC-CO_2, they generally still require ethanol as a co-solvent for optimized performance. Some degree of size control is achievable, particularly through supercritical reverse phase evaporation, but this method is still largely limited to unilamellar vesicle preparation. The RESS-based injection and decompression methods require the aqueous cargo solution to be held under pressure and to be forced through the nozzle, which could limit the use of cargo that might be affected by SC-CO_2, like proteins. Additionally, little attention has been given to the dynamics of particle growth in these RESS based methods. Furthermore, none of the methods described are continuous processes and suffer from lack of economies of scale. This ultimately limits their use in many industries, which typically have high volume requirements.

1.4.4. Designing unilamellar or multilamellar liposomal assembly

Though unique, all of these processes using SC-CO_2 can be broken down into three segments: dissolution of the carrier in SC-CO_2 (or solvent mixture), precipitation of the carrier from the solvent, and hydration of the carrier solution with the aqueous cargo solution. These methods can be divided based on whether the carrier solution is hydrated before nucleation of the carrier from the solvent or after. Particular attention is drawn to the injection and decompression methods (Castor and Chu, 1994) described previously. These processes are very similar to each

other, except that in the injection method, the carrier/SC-CO_2 solution is decompressed through a nozzle into the aqueous cargo solution, whereas in the decompression method, the carrier/SC-CO_2 solution is mixed with the aqueous cargo under pressure and then decompressed through a nozzle. Among these and other methods of liposome formation using SC-CO_2, it appears as though if the carrier/SC-CO_2 solution is hydrated with the cargo solution before nucleation (decompression of the solution) unilamellar vesicles are formed. If the carrier/SC-CO_2 solution is hydrated with the cargo after nucleation is initiated, MLVs or MVVs tend to form.

This is also somewhat consistent with conventional methods. In the Bangham method (Bangham et al., 1965), carrier is dissolved in organic solvent and then a thin film is formed by evaporating the solvent. The solvent-free thin film is then hydrated and MLVs are formed. Conventional methods that form UVs, such as the injection method or reverse phase evaporation method, involve hydration of the carrier/solvent solution, followed by removal of the solvent through evaporation or other means (Jesorka and Orwar, 2008). Lasic (1988) proposed that vesicle formation is reliant on the formation of precursor bilayer flakes in phospholipid based liposomes. Bilayer flakes can either be formed by the removal of solvent and subsequent disruption of the packed bilayer network in the presence of an aqueous phase, as in the Bangham method, or they can be grown at the aqueous/organic interface of reverse micelles by precipitation from the organic phase, as in the injection or reverse phase evaporation methods. The former tends to result in the formation of MLVs, that latter tends to result in the formation of UVs.

Though the mechanism for liposome formation in SC-CO_2 is not fully understood, it should follow a similar pattern. In organic solutions, surfactants typically exist as reverse micelles. Upon addition of water the micelles will swell and the amount of water added

influences micelle shape, size, and polar headgroup packing according to the ratio of water concentration to surfactant concentration in the organic solution (Willard et al., 1998). When the aqueous cargo droplets are introduced into the carrier/SC-CO_2 solution, a similar reverse micelle is formed and formation of these precursor emulsion structures was shown to be critical to the resultant vesicle morphology (Imura et al., 2003). As pressure drops the monolayer of carrier at the aqueous droplet surface could provide a favorable site for heterogeneous nucleation, so liposome formation occurs more uniformly around single droplets. In RESS methods, such as the injection method of Castor and Chu (1994), the carrier is precipitated from SC-CO_2 before it comes in contact with the aqueous cargo. This may allow for the formation and aggregation of bilayer flakes before hydration. The rate of nucleation of carrier from the expanding CO_2 stream would allow for growth and differentiation in bilayer flake size and could explain the observed formation of MLVs in accordance with the vesicle formation theory proposed by Lasic (1988). Thus controlling the precipitation of the carrier and point of hydration with the cargo solution could be critical to the resultant vesicle morphology.

References

Avanti Polar Lipids. Lipids for liposome formation.<www.avantipolarlipids.com> , 2012(Accessed November 2012).

Balaban, M. O, & Ferrentino, G. (2012). Dense phase carbon dioxide: food and pharmaceutical applications. Hoboken: John Wiley & Sons.

Banerjee R. (2001). Liposomes: Applications in Medicine. *Journal of Biomaterials Applications*, 16(1), 3-21.

Bangham A.D., Standish M.M., & Watkins J.C. (1965). Diffusion of univalent ions across the lamellae of swollen phospholipids. *Journal of Molecular Biology*, 13(1), 238-IN27.

Blok M.C., Van Der Neut-Kok E.C.M., Van Deenen L.L.M., & De Gier J. (1975). The effect of chain length and lipid phase transitions on the selective permeability properties of liposomes. *Biochimica et Biophysica Acta (BBA) - Biomembranes*, 406(2), 187-196.

Castor T.P., Chu L. (1994). Methods for making liposomes containing hydrophobic drugs. (WO9615774).

Chang H.I., Yeh M.K. (2012). Clinical development of liposome-based drugs: formulation, characterization, and therapeutic efficacy. *International journal of nanomedicine*, 7, 49.

Cocero M.J., Martín Á., Mattea F., & Varona S. (2009). Encapsulation and co-precipitation processes with supercritical fluids: Fundamentals and applications. *The Journal of Supercritical Fluids*, 47(3), 546-555.

Coffey M.P., Krukonis V.J. (1988). Supercritical Fluid Nucleation. An Improved Ultrafine Particle Formation Process. *Phasex Corp final report to NSF*, ISI 8660823.

da Silva Malheiros P., Daroit D.J., & Brandelli A. (2010). Food applications of liposome-encapsulated antimicrobial peptides. *Trends in Food Science & Technology*, 21(6), 284-292.

Desai T.R., Finlay W.H. (2002). Nebulization of niosomal all-trans-retinoic acid: an inexpensive alternative to conventional liposomes. *International journal of pharmaceutics*, 241(2), 311-317.

Dostal, V., Hejzlar, P., & Driscoll, M. J. (2006). The supercritical carbon dioxide power cycle: comparison to other advanced power cycles. Nuclear technology, 154(3), 283-301.

Frederiksen L., Anton K., Hoogevest P.v., Keller H.R., & Leuenberger H. (1997). Preparation of liposomes encapsulating water-soluble compounds using supercritical carbon dioxide. *Journal of pharmaceutical sciences*, 86(8), 921-928.

Gabizon A., Price D.C., Huberty J., Bresalier R.S., & Papahadjopoulos D. (1990). *Cancer Research*, 50, 6371-6378.

Gouin S. (2004). Microencapsulation: industrial appraisal of existing technologies and trends. *Trends in Food Science & Technology*, 15(7–8), 330-347.

Gregoriadis G., Perrie Y. (2001). Liposomes. In Anonymous *eLS*. (). John Wiley & Sons, Ltd.

Han, X., & Poliakoff, M. (2012). Continuous reactions in supercritical carbon dioxide: problems, solutions and possible ways forward. Chemical Society Reviews, 41(4), 1428-1436.

Hauthal W.H. (2001). Advances with supercritical fluids [review]. *Chemosphere*, 43(1), 123-135.

Hougeir F.G., Kircik L. (2012). A review of delivery systems in cosmetics. *Dermatologic Therapy*, 25(3), 234-237.

Imura T., Gotoh T., Otake K., Yoda S., Takebayashi Y., Yokoyama S., Takebayashi H., Sakai H., Yuasa M., & Abe M. (2003). Control of physicochemical properties of liposomes using a supercritical reverse phase evaporation method. *Langmuir*, 19(6), 2021-2025.

Jesorka A., Orwar O. (2008). Liposomes: technologies and analytical applications. *Annu.Rev.Anal.Chem.*, 1, 801-832.

Jung J., Perrut M. (2001). Particle design using supercritical fluids: Literature and patent survey. *The Journal of Supercritical Fluids*, 20(3), 179-219.

Kinka, R., Gotoh, T., Wongtrakul, P., Hashimoto, S.,Abe, M.,. (2005). Preparation of niosomes by a supercritical reverse phase evaporation method without using co-solvents-Effects of the pressure on the trapping efficiency-. *MATERIAL TECHNOLOGY*, 23(4), 241-246.

Lasic D.D. (1988). The mechanism of vesicle formation. *The Biochemical journal*, 256(1), 1-11.

Lesoin L., Boutin O., Crampon C., & Badens E. (2011). CO2/water/surfactant ternary systems and liposome formation using supercritical CO2: A review. *Colloids and Surfaces A: Physicochemical and Engineering Aspects*, 377(1–3), 1-14.

Li X., Ding L., Xu Y., Wang Y., & Ping Q. (2009). Targeted delivery of doxorubicin using stealth liposomes modified with transferrin. *International journal of pharmaceutics*, 373(1–2), 116-123.

Manosroi A., Chutoprapat R., Abe M., & Manosroi J. (2008). Characteristics of niosomes prepared by supercritical carbon dioxide (scCO< sub> 2</sub>) fluid. *International journal of pharmaceutics*, 352(1), 248-255.

Manosroi A., Chutoprapat R., Abe M., & Manosroi J. (2010a). Characteristics of niosomes entrapped with rice bran bioactive compounds prepared by supercritical carbon dioxide. In *Nanoscience and Nanotechnology (ICONN), 2010 International Conference on*, .

Manosroi A., Ruksiriwanich W., Abe M., Sakai H., Manosroi W., & Manosroi J. (2010b). Biological activities of the rice bran extract and physical characteristics of its entrapment in niosomes by supercritical carbon dioxide fluid. *The Journal of Supercritical Fluids*, 54(2), 137-144.

Manosroi A., Wongtrakul P., Manosroi J., Sakai H., Sugawara F., Yuasa M., & Abe M. (2003). Characterization of vesicles prepared with various non-ionic surfactants mixed with cholesterol. *Colloids and Surfaces B: Biointerfaces*, 30(1–2), 129-138.

Matson D.W., Fulton J.L., Petersen R.C., & Smith R.D. (1987). Rapid expansion of supercritical fluid solutions: solute formation of powders, thin films, and fibers. *Industrial & Engineering Chemistry Research*, 26(11), 2298-2306.

McHugh M.A., Krukonis V.J. (1994). *Supercritical Fluid Extraction Principles and Practice.* (2nd edn.). Butterworth-Heinemann, Boston.

Meure L.A., Foster N.R., & Dehghani F. (2008). Conventional and dense gas techniques for the production of liposomes: a review. *Aaps Pharmscitech*, 9(3), 798-809.

Mohamed R.S., Debenedetti P.G., & Prud'homme R.K. (1989). Effects of process conditions on crystals obtained from supercritical mixtures. *AIChE Journal*, 35(2), 325-328.

Mozafari M.R., Flanagan J., Matia-Merino L., Awati A., Omri A., Suntres Z.E., & Singh H. (2006). Recent trends in the lipid-based nanoencapsulation of antioxidants and their role in foods. *Journal of the science of food and agriculture*, 86(13), 2038-2045.

Mozafari M.R., Khosravi-Darani K., Borazan G.G., Cui J., Pardakhty A., & Yurdugul S. (2008). Encapsulation of Food Ingredients Using Nanoliposome Technology. *International Journal of Food Properties*, 11(4), 833-844.

Nasr M., Mansour S., Mortada N.D., & Elshamy A.A. (2008). Vesicular aceclofenac systems: A comparative study between liposomes and niosomes. *Journal of microencapsulation*, 25(7), 499-512.

Otake K., Imura T., Sakai H., & Abe M. (2001). Development of a new preparation method of liposomes using supercritical carbon dioxide. *Langmuir*, 17(13), 3898-3901.

Otake K., Shimomura T., Goto T., Imura T., Furuya T., Yoda S., Takebayashi Y., Sakai H., & Abe M. (2006). Preparation of liposomes using an improved supercritical reverse phase evaporation method. *Langmuir*, 22(6), 2543-2550.

Risch S.J., Reineccius G. (1995). *Encapsulation and controlled release of food ingredients.* (). ACS Publications.

Rizvi S.S.H., Benado A.L., Zollweg J.A., & and Daniels J.A. (1986a). Supercritical fluid extraction: Fundamental principles and modeling methods. *Food Technology*, 40(6), 55-65.

Rizvi S.S.H., Benado A.L., Zollweg J.A., & and Daniels J.A. (1986b). Supercritical fluid extraction: Operating principles and food applications. *Food Technology*, 40(7), 57-64.

Sauceau, M., Fages, J., Common, A., Nikitine, C., & Rodier, E. (2011). New challenges in polymer foaming: a review of extrusion processes assisted by supercritical carbon dioxide. Progress in Polymer Science, 36(6), 749-766.

Schubert R. Liposome Preparation by Detergent Removal. (2003) *Methods in Enzymology.* (pp. 46-70). Academic Press.

Sharma A., Sharma U.S. (1997). Liposomes in drug delivery: Progress and limitations. *International journal of pharmaceutics*, 154(2), 123-140.

Shum H.C., Lee D., Yoon I., Kodger T., & Weitz D.A. (2008). Double emulsion templated monodisperse phospholipid vesicles. *Langmuir*, 24(15), 7651-7653.

Sułkowski W.W., Pentak D., Nowak K., & Sułkowska A. (2005). The influence of temperature, cholesterol content and pH on liposome stability. *Journal of Molecular Structure*, 744–747(0), 737-747.

Suzuki R., Takizawa T., Negishi Y., Utoguchi N., & Maruyama K. (2008). Effective gene delivery with novel liposomal bubbles and ultrasonic destruction technology. *International journal of pharmaceutics*, 354(1–2), 49-55.

Taylor T.M., Davidson P.M., Bruce B.D., & Weiss J. (2005a). Ultrasonic Spectroscopy and Differential Scanning Calorimetry of Liposomal-Encapsulated Nisin. *Journal of Agricultural and Food Chemistry*, 53(22), 8722-8728.

Taylor T.M., Weiss J., Davidson P.M., & Bruce B.D. (2005b). Liposomal Nanocapsules in Food Science and Agriculture. *Critical reviews in food science and nutrition*, 45(7-8), 587-605.

Uchegbu I.F., Vyas S.P. (1998). Non-ionic surfactant based vesicles (niosomes) in drug delivery. *International journal of pharmaceutics*, 172(1–2), 33-70.

van den Berg J.H., Oosterhuis K., Hennink W.E., Storm G., van der Aa L.J., Engbersen J.F.J., Haanen J.B.A.G., Beijnen J.H., Schumacher T.N., & Nuijen B. (2010). Shielding the cationic charge of nanoparticle-formulated dermal DNA vaccines is essential for antigen expression and immunogenicity. *Journal of Controlled Release*, 141(2), 234-240.

Willard D.M., Riter R.E., & Levinger N.E. (1998). Dynamics of polar solvation in lecithin/water/cyclohexane reverse micelles. *Journal of the American Chemical Society*, 120(17), 4151-4160.

Zuidam N.J., Nedović V. (2009). Encapsulation technologies for active food ingredients and food processing. .

Chapter 2: Solubility of polyoxyethylene (4) sorbitan monostearate in supercritical carbon dioxide

2.1. Abstract

The solubility of polyoxytheylene (4) sorbitan monostearate (Tween61) in supercritical carbon dioxide was determined using a static recirculation method. Three pressures (10, 15, and 20 MPa) and three temperatures (40, 50, and 60°C) were investigated. Mole fraction of Tween61 in the vapor phase increased with pressure at 40°C, but did not change with pressure at 50 or 60°C. Two phases, liquid and vapor, were observed at all conditions tested. Solubility data was correlated using the Peng Robinson equation of state with the Panagiotopoulos and Reid mixing rule along with Chrastil's empirical equation. Better fit to experimental data was obtained with the Peng Robinson equation of state.

2.2. Introduction

Supercritical carbon dioxide (SC-CO_2) has emerged as a promising alternative to organic chemicals in separation processes with strict processing requirements. It is non-toxic, inexpensive, easily recycled, and with its relatively low critical temperature and pressure (31.1°C and 7.38 MPa), can be applied to heat sensitive materials. One major drawback of processing with SC-CO_2 is the limited solubility of many compounds, particularly large polar molecules. Co-solvents, such as methanol or ethanol, are often added to the enhance solubility of these poorly soluble compounds, but there is a great deal of interest in the applications of surfactants that could be used to emulsify polar compounds in a continuous CO_2 phase (Woods et al., 2004) and for the formation of lipid vesicles (Lesoin et al., 2011).

Many synthetic surfactants have been designed expressly for use in SC-CO_2. Fluorinated

acrylates (Desimone et al., 1992), fluorinated ethers (Hoefling et al., 1991), and fluorocarbon-hydrocarbon hybrids (Harrison et al., 1994) have been developed and applied with success in the formation of water-in-CO_2 emulsions. However, there are concerns over the safety and cost of these fluorinated compounds (Woods et al., 2004). Poly-dimethylsiloxanes have also been studied for potential applications in SC-CO_2 emulsions (da Rocha et al., 2001), however solubilization pressures for these compounds are often higher than those required for fluorinated surfactants (Liu et al., 2002). Non-ionic surfactants have also been used for the formation of emulsions (da Rocha et al., 2001; Liu et al., 2002) and lipid vesicles in SC-CO_2 (Manosroi et al., 2008; Manosroi et al., 2010) Liu *et al.* (2002) investigated the phase behavior of Ls-36 and Ls-45 non-ionic surfactants (CAS 68439-51-0) and suggested that the relatively high water loading capacity of the micelles formed by these surfactants in SC-CO_2 was directly related to their solubility.

Polyoxyethylene (4) sorbitan monostearate (Tween61) is a non-ionic surfactant that has been used for the production of lipid vesicles in SC-CO_2 (Manosroi et al., 2008; Manosroi et al., 2010; Ri et al., 2005). The chemical stability and relative purity of non-ionic surfactants provide an advantage in the generation of lipid vesicles over more traditional phospholipids (Desai and Finlay, 2002; Nasr et al., 2008). However, no data is available in the literature regarding the solubility of Tween61 in SC-CO_2. Greater understanding of the solubility of this compound could offer insight into its behavior in SC-CO_2 solutions and is essential to its application in novel SC-CO_2 based processes.

The objectives of this study are:

1) Investigate the equilibrium solubility of Tween 61 in SC-CO_2
2) Assess the fit of literature models in describing experimental data

2.3. Materials and methods

2.3.1. Materials and reagents

Polyoxyethylene (4) sorbitan monostearate (CAS 9005-67-8; purity >99.8%, moisture content 0.2% w/w) was supplied by Croda, Inc. (Edison, NJ, USA) and stored at room temperature. Carbon dioxide (purity > 99.5%, moisture content <0.001% w/w) was supplied by Airgas (Elmira, NY, USA). All assay reagents were purchased from Sigma Aldrich (St. Louis, MO, USA) unless otherwise specified.

2.3.2. Static solubility method

The static solubility method and apparatus (Figure 2.1.) described by Yu and Rizvi (1992) was used in this study. The system consists of an insulated enclosure containing a high pressure view cell (50 cm^3) with vapor and liquid phase recirculation loops, driven by a magnetic pump, and vapor and liquid expansion vessels. The temperature of the enclosure was maintained by proportional heat controllers and circulation fans to ± 0.3°C. Tween 61 was melted at 45°C in a water bath and 15 ml was loaded into the view cell. Liquid CO_2 was pumped into the view cell Model 396 Minipump (Milton Roy (Ivyland, PA, USA) and the pressure was regulated within $\pm$0.05 MPa of target pressure using a high pressure generator (Model 87-6-5, High Pressure Equipment, Erie, PA, USA). The vapor and liquid phases were recirculated using a specially designed magnetic pump for 1 hour to ensure equilibrium solubility of Tween 61 was achieved. After the equilibration period, sections VSL1 and LSL in the recirculation loops (Figure 2.1.) were sealed, trapping the vapor and liquid samples, respectively and the trapped samples were expanded into separate high pressure vessels. The pressure was then slowly reduced to atmospheric pressure by releasing the CO_2 through the solvent reservoir. The vapor and liquid phase samples were recovered by flushing the respective expansion loops with 125 mL of 100%

ethanol. The ethanol was circulated through each loop using FMI Model RP-D centrifugal pumps (Oyster Bay, NY, USA) for 5 minutes and then drained into a collection flask. The flushing for each loop was repeated three times and compressed air was forced through the tubing after the third flushing to ensure recovery of the sample. The ethanol was removed from the sample at 60°C under vacuum (13.3kPa) and the solvent free samples were stored at 4°C until analysis. Solubility determinations were performed in duplicate.

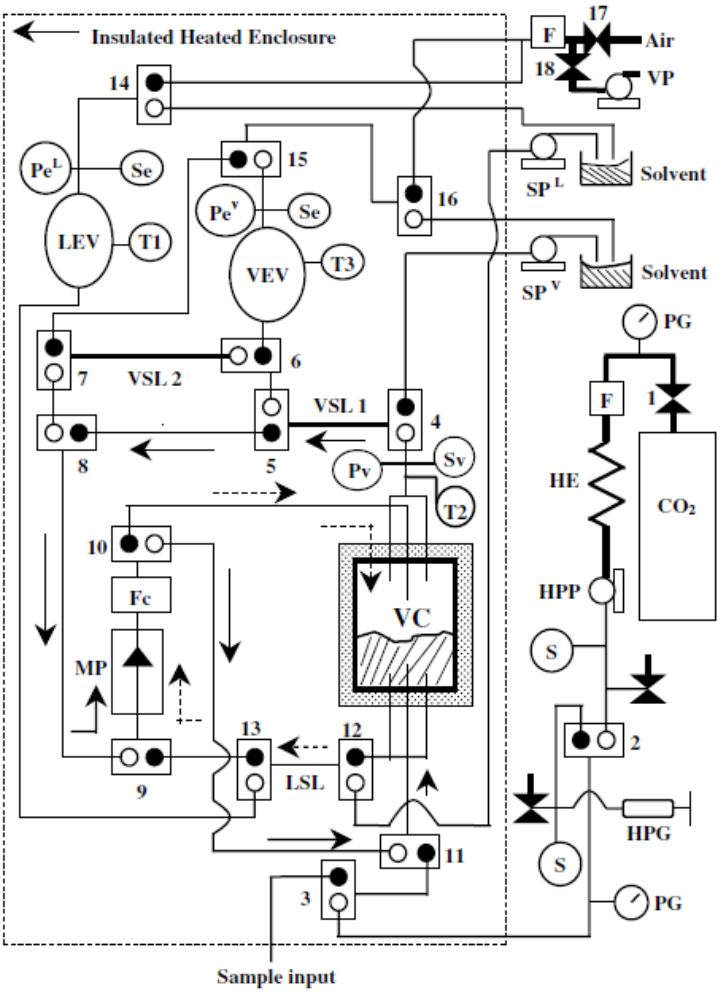

Figure 2.1. Schematic diagram of the static fluid–liquid equilibrium apparatus. , three-way/two-stem combination valve (○, front side; ●, back side); HPP, high-pressure pump; MP, magnetic pump; VP, vacuum pump; SPV and SPL, solvent pumps for fluid and liquid, respectively; HPG,high-pressure generator; HE, heat exchanger; T, thermocouple; Pv, pressure transducer of view cell; PG, pressure gauge; PeV and PeL, pressures transducer for expansion

vessels of fluid and liquid phases, respectively; S, Se and Sv, safety valves; F and Fc, filters; VEV and LEV, expansion vessels of fluid and liquid phases, respectively; VC, view cell; VSL1 and VSL2, fluid sample loops; LSL, liquid sample loop.

2.3.3. Spectrophotometric analysis

In order to determine the amount of Tween61 in the vapor and liquid phases, the spectrophotometric method of Brown and Jaffe (2001) was used. Briefly, 10 mL of deionized water was added to each sample, which was then warmed in a water bath at 45°C for 10 minutes to ensure melting of the Tween 61. The tubes were then vortexed for ten seconds and 500 μL were transferred to a new tube and diluted to 10mL with deionized water. Then 250 μL of an iodine-iodide (I-I) solution (1% iodine and 2% potassium iodide, w/v) was added to each tube and then the tube was vortexed for 5 seconds. The tubes were allowed to equilibrate at room temperature for 30 minutes and the absorbance at 500nm was measured using a Spectronic 20D spectrophotometer (Milton Roy, Ivyland, PA, USA) against a blank containing the same concentration of iodine-iodide solution in deionized water. Tween 61 concentration in the SC-CO_2 equilibrium samples was determined using a standard curve. Analyses were performed in duplicate.

2.3.4. Mathematical modeling

In order to extend the applicability of the equilibrium solubility data gathered in this study, two methods were used to correlate and predict Tween 61 solubility in SC-CO_2.

2.3.4.1. Chrastil Equation

The widely used equation developed by Chrastil (1982) is a semi-empirical correlation of solubility of a given compound to the density of CO_2 according to the equation:

$$\ln C = k \ln \rho + a/T + b \qquad (2.1)$$

Where C is solute solubility (g/L), ρ is the solvent density (g/L), T is the operating temperature (K), and k is a constant dependent on the number of molecules in the solvato-complex, a is constant dependent on molecular weights of the compounds, and b is a constant dependent on the heat of reaction. The model assumes a log-linear relationship between solvent density and solute concentration. Through originally applied to the solubility of fatty acids, the Chrastil equation has been used to model many other solutes in SC-CO_2 (Ding et al., 2011; Tomita et al., 2014; Tsai et al., 2006) .

2.3.4.2 Peng Robinson equation of state

Due to its simplicity and comparative accuracy, the Peng Robinson equation of state (Peng and Robinson, 1976) has been employed to model the equilibrium solubility of many solutes in SC-CO_2. In order to apply the Peng Robinson equation of state (PREOS) to mixtures, the P-V-T relationship is modified to make the equation parameters composition dependent, according to the following equations:

$$P = RT/ (v-b_m) – a_m/(v^2 + 2vb_m –b_m^2) \quad (2.2)$$

$$a_m = \Sigma\Sigma x_i x_j a_{ij} \quad (2.3)$$

$$b_m = \Sigma x_i b_i \quad (2.4)$$

$$a = (0.45724R^2T_c^2/P_c)\{1 + m[(1-(T_r)^{0.5})]\}^2 \quad (2.5)$$

$$b = 0.07780RT_c/P_c \quad (2.6)$$

$$m = 0.37464 + 1.54226\omega – 0.26992\omega^2 \quad (2.7)$$

Where P is pressure, R is the universal gas constant, T is the temperature, v is the molar volume, x is the mole fraction in the fluid or liquid phases, subscripts i and j are mixture component designations, T_c and P_c are the critical temperature and pressure of a component, T_r is the reduced temperature, ω is the acentric factor, and a_m, b_m, a, b, a_{ij}, and m are equation parameters.

The cross parameter a_{ij} was related to the pure component properties using the Panagiotopoulos and Reid (1986) mixing rule:

$$a_{ij} = (a_i a_j)^{0.5} [1-k_{ij}+(k_{ij}-k_{ji})x_i] \quad (2.8)$$

where k_{ij} and k_{ji} are the binary adjustable interaction parameters. The binary interaction parameters were optimized using PE 2000 (Ver. 2.085) phase equilibria software (Pfohl et al., 2000).

Critical properties and acentric factor of CO_2 were obtained from the NIST chemistry webbook (Lemmon et al.). Due to lack of experimental data, the critical properties of Tween 61, T_c and P_c, were determined using the PE 2000 (Ver. 2.085) phase equilibria software (Pfohl et al., 2000) applying the group contribution method of Joback:

$$T_b = 198 + \Sigma\Delta T_b \quad (2.9)$$

$$T_c = T_b / [0.584 + 0.965\Sigma\Delta T_c - (\Delta T_c)^2] \quad (2.10)$$

$$P_c = 1 / (0.113 + 0.0032n_A - \Sigma\Delta P_c)^2 \quad (2.11)$$

Where T_b is the boiling point, ΔTc and ΔPc are the contributions to the critical temperature and critical pressure, respectively, from each molecular group as defined by Joback and Reid(1987), and n_A is the total number of atoms in the molecule. The boiling point estimate was adjusted using the correction of Stein and Brown (1994) prior to calculation of the critical temperature and pressure. The acentric factor of Tween 61 was also estimated using the PE phase equilibria software applying the Lee and Kesler (1975) equation:

$$\omega = (\ln Pc - 5.92714 + 6.09648\theta^{-1} + 1.28862 \ln \theta - 0.169347\theta^6) / (15.2518 - 15.6875\theta^{-1} - 13.4721 \ln \theta + 0.43577\theta^6) \quad (2.12)$$

Where $\theta = T_b/T_c$.

2.3.5. Statistical analysis

Solubility data was analyzed using one way ANOVA and means were compared using Tukey's Honestly Significant Difference test with $\alpha = 0.05$. All statistical analyses were performed using JMP Pro 11 (SAS, Cary, NC, USA). The goodness of fit of each model was assessed using the absolute average deviation (AAD):

$$AAD = \frac{1}{N}\sum_{i=1}^{N}|d_i| \quad (2.13)$$

Where N is the number of data points, and d_i is the difference between the predicted value and the experimental value.

2.4. Results and Discussion

2.4.1. Equilibrium solubility

Equilibrium solubility of Tween 61 in SC-CO_2 was determined at three different pressures (10, 15, and 20 MPa) and three different temperatures (40, 50, and 60°C). Under all conditions examined, two distinct phases were observed in the high pressure view cell, subsequently referred to as the vapor (upper) and liquid (lower) phases. The vapor and liquid mole fraction of Tween 61 are presented in Table 2.1.

Under all conditions, the concentration of Tween 61 was greater in the liquid phase than in the vapor phase. The liquid phase mole fraction of Tween 61 was observed to decrease with increasing pressure. This is likely due to increased solubility of CO_2 in the liquid phase with increased pressure, according to Henry's law. Conversely, increased temperature at a fixed pressure tended to result in an increase concentration of Tween 61 in the liquid phase due to the reduced solubility of CO_2 in the liquid phase. Overall change in the vapor phase mole fraction of Tween 61 was minor, in part due to the large discrepancy in molecular weight of Tween 61 and CO_2 and the limited solvating power of SC-CO_2 for high molecular weight compounds. At 40°C, the mole fraction of Tween 61 in the vapor phase increased with increasing pressure. This is typical of SC-CO_2, as its solvating power increased with increasing pressure (McHugh and

Krukonis, 1994). However at 50°C and 60°C, increasing pressure resulted in no statistically significant difference in Tween61 mole fraction. This behavior has been observed in other systems consisting of solids or liquids of low volatility and high molecular weight (Bartle et al., 1991).

Table 2.1. Equilibrium vapor and liquid mole fractions of Tween 61 in SC-CO_2

Temperature (°C)	Pressure (MPa)	Tween 61 mole fraction*† x 10^3 Vapor	Tween 61 mole fraction*† x 10^3 Liquid
40	10	$2.01 \pm 0.45^{A,a}$	$45.6 \pm 7.7^{A,a}$
	15	$3.87 \pm 0.44^{B,a}$	$35.4 \pm 5.9^{A,a}$
	20	$4.33 \pm 0.37^{B,a}$	$28.4 \pm 3.8^{A,a}$
50	10	$3.11 \pm 0.69^{A,a}$	$95.0 \pm 11^{A,b}$
	15	$2.68 \pm 0.89^{A,a}$	$47.6 \pm 1.8^{B,b}$
	20	$3.19 \pm 0.36^{A,ab}$	$31.3 \pm 6.2^{B,a}$
60	10	$3.39 \pm 0.31^{A,a}$	$107.1 \pm 2.0^{A,b}$
	15	$2.34 \pm 0.34^{A,a}$	$57.4 \pm 2.4^{AB,b}$
	20	$2.84 \pm 0.28^{A,b}$	$28.3 \pm 3.8^{B,a}$

*Data reported as mean ± standard deviation. N=2

†In each column, values at the same temperature with different uppercase superscripts are significantly different and values at the same pressure with different lowercase superscripts are significantly different and values using Tukey's HSD test at $\alpha = 0.05$

At 4-6% (wt. basis), the solubility of Tween61 in SC-CO_2 vapor phase was comparable to, if not slightly higher than that of LS-36 and LS-45 non-ionic surfactants as determined by Liu *et al.* (Liu et al., 2002) at similar conditions (1-4% wt. basis). While fairly similar in molecular weight to Tween61, LS-36 and LS-45 have linear structures of repeating ethylene oxide and propylene oxide units attached to an alkyl chain. This linear arrangement of the "head group" of LS-36 and LS-45 surfactants most likely facilitates greater hydrogen bonding, in comparison to the ethoxylated sorbitan head group of Tween61, which is known to reduce solubility of

compounds in CO_2 (Dandge et al., 1985).

The standard curve for the I-I assay used to determine Tween 61 concentration showed a good linear fit with an $R^2 = 0.9986$. However, it was determined that keeping the Tween 61 initially in a liquid state was critical to properly dispersing it in the deionized water during vortexing prior to introduction of the I-I reagent.

2.4.2. Mathematical Modeling

2.4.2.1. Chrastil Equation

Semi-empirical correlations provide a relatively simple and rapid means of modeling experimental solubility data in supercritical fluids. Chrastil (1982) related the solubility of a compound in supercritical fluids directly to the fluid density under the assumption that the solute associates with the fluid molecules in a solvato-complex, which is in equilibrium with the gas. The equation derived by Chrastil gives a linear relationship between the logarithm of solubility of a solute and logarithm of supercritical fluid density. This relationship between Tween61 solubility and SC-CO_2 density is shown in Figure 2.2. According to the constraints of the model, only the solubility of Tween61 in the vapor phase of the equilibrium mixture was considered.

The equation parameters were determined to be k = 0.695, a = 4501.689, and b = -15.138. At 40°C and 50°C, the Chrastil equation reasonably modeled the experimental data, with AAD of 0.079 and 0.111 respectively. However, at 60°C the model under-predicted solubility in comparison to the experimental values considerably, resulting in an AAD of 0.272. Further, the data does not appear to obey the log-linear relationship between density and solute concentration assumed by the model. The Chrastil model, though relatively simple to implement, does have certain limitations in terms of the temperature and pressure range it is applicable to and the solute-solvent system being studied (Kraska et al., 2002; Sparks et al., 2008). The tendency of

surfactant molecules form pre-micellar aggregates in SC-CO_2 may complicate the phase behavior of surfactant/ CO_2 mixtures (Yee et al., 1992), thus requiring a more sophisticated approach for accurate modeling.

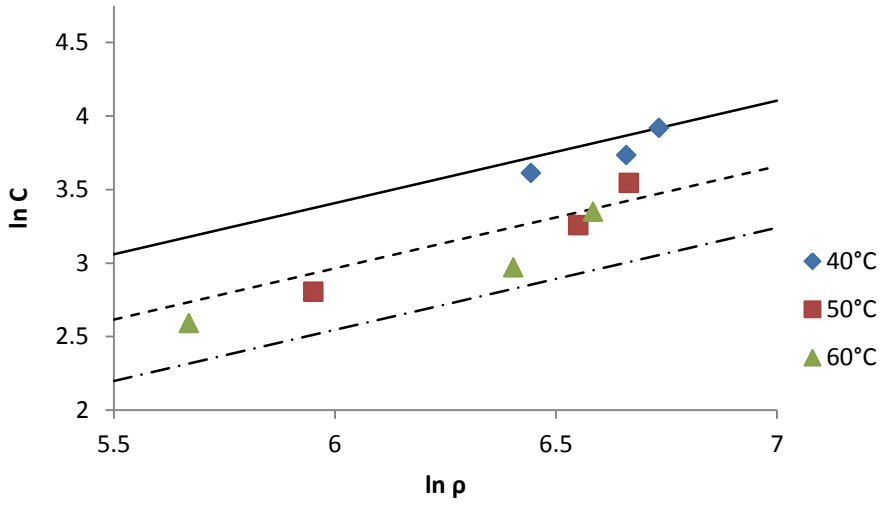

Figure 2.2. Experimental vapor phase solubility C (g/L) of Tween61 in carbon dioxide with density ρ(g/L) in comparison with correlation using Chrastil model. Model prediction indicated by solid line(-) at 40°C, dashed line (--) at 50°C, and dot-dash line (-·-) at 60°C, respectively.

2.4.2.2. PR EOS

The physical properties of Tween 61 and CO_2 are listed in Table 2.2. Binary interaction parameters for the Tween61/CO_2 mixture were determined to be dependent on temperature (Table 2.3.). The temperature dependence of the binary interaction parameters has been discussed by several authors (Jaubert and Mutelet, 2004; Privat et al., 2008), and the absolute value of the interaction parameters determined in the current study followed a similar quadratic pattern with respect to temperature as described by (Coutinho et al., 1994).

Table 2.2. Physical properties of Tween61 and Carbon dioxide

	Boiling point, T_b (°C)	Critical Temperature, T_c (°C)	Critical pressure, P_c (MPa)	Accentric factor, ω
Tween61	965.25*	1134.86*	1.151*	1.727**
Carbon dioxide†	-78.40	30.98	7.38	0.224

*Estimated by the group contribution method of Joback and Reid (1987) using PE 2000 software
**Estimated using the method of Lee and Kessler (1975)
†Data taken from NIST Webbook (Lemmon *et al.*, 2014)

Table 2.3. Binary interaction coefficients for PREOS with Panagiotopoulos and Reid mixing rule and the deviation of the model from the experimental values in the liquid and vapor phases

	Binary interaction coefficients		AAD	
Temperature (°C)	K_{ij}	K_{ji}	Liquid	Vapor
40	-0.1831	-0.1529	0.0252	0.0025
50	-0.1245	-0.0599	0.0151	0.0012
60	-0.4520	-0.1067	0.0084	0.0037

The deviations of the PREOS prediction from the experimentally determined mole fractions of CO_2 in the vapor and liquid phases are listed in Table 2.3. The PREOS more accurately predicted the vapor phase mole fraction of CO_2 than the liquid mole fraction in all cases, though the change in CO2 mole fraction with pressure was very small, as described previously. The greatest deviation was observed for the liquid phase mole fraction at 40°C. The proximity of these conditions to the critical point of CO_2 may have contributed to this error, as two parameter cubic EOS can be fairly inaccurate for the prediction of liquid densities, which increases as the critical point is approached (Orbey et al., 1998). The PREOS with the Panagiotopoulos and Reid mixing rule modeled the experimental vapor phase mole fraction data more accurately than the Chrastil equation. The comparison of the experimental values and the PREOS prediction of the liquid and vapor phase mole fractions of CO_2 in the Tween 61/CO_2 mixture at 40°C, 50°C, and 60°C

are shown in figures 2.3., 2.4., and 2.5., respectively. The open liquid-vapor envelope observed in each of these figures indicates fluid and vapor phases coexistence at all conditions examined. However, flash calculations showed closure of the vapor-liquid envelope near 23 MPa at all temperatures studied, indicating that a single fluid phase may exist beyond this pressure. This is below the value observed by (Consan and Smith, 1990) for the cloud point of non-ethoxylated sorbitan esters and polyethoxylated alcohols of comparable molecular weight in SC-CO_2.

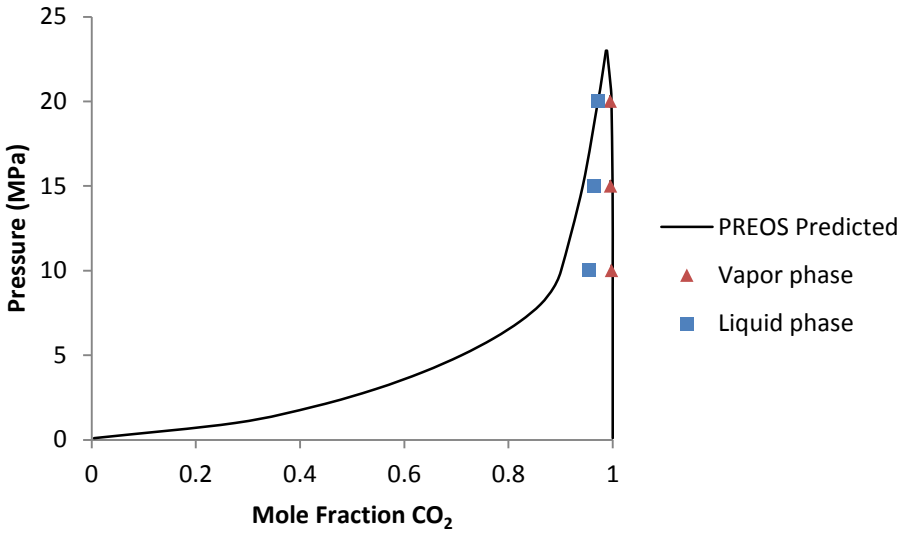

Figure 2.3. Comparison of experimental vapor and liquid phase mole fractions of CO_2 in Tween61/CO_2 mixture at 40°C with values predicted using the Peng-Robinson equation of state

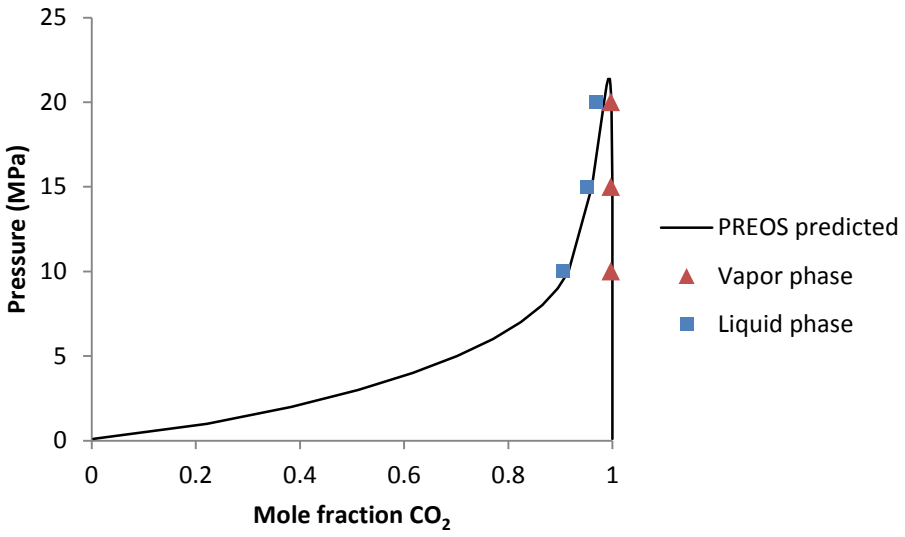

Figure 2.4. Comparison of experimental vapor and liquid phase mole fractions of CO_2 in Tween61/CO_2 mixture at 50°C with values predicted using the Peng-Robinson equation of state

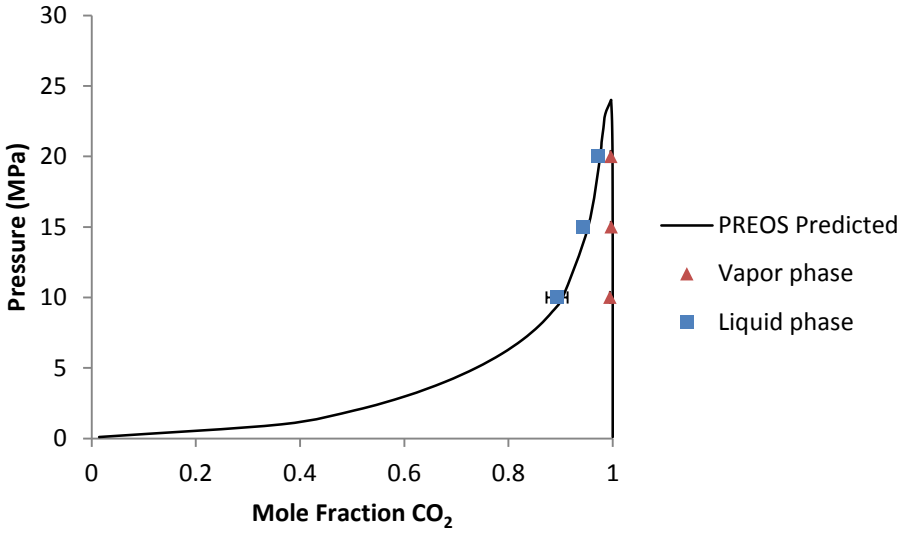

Figure 2.5. Comparison of experimental vapor and liquid phase mole fractions of CO_2 in Tween61/CO_2 mixture at 60°C with values predicted using the Peng-Robinson equation of state

2.5. Conclusion

Understanding the solubility of surfactant compounds is critical to their application in

SC-CO_2, particularly for novel processes such emulsion and vesicle formation. The following conclusions can be drawn from based on the current study:

1) A liquid-vapor miscibility gap was observed for the mixture of Tween61 and SC-CO_2 at all conditions tested. CO_2 showed fairly high solubility in the liquid phase, which decreased with pressure at each temperature.
2) Tween61 solubility in the vapor phase was limited to 4-6% (w/w) due to its relatively high molecular weight, which was similar the solubility of other non-ionic surfactants in SC-CO_2.
3) The PREOS with the Panagiotopoulos and Reid mixing rule showed good agreement with experimental solubility values of Tween61 in SC-CO_2.
4) Though relatively easier to implement, the Chrastil equation was slightly less accurate in predicting Tween61 solubility, especially at 60°C.

References

Bartle K.D., Clifford A., Jafar S., & Shilstone G. (1991). Solubilities of solids and liquids of low volatility in supercritical carbon dioxide. *Journal of Physical and Chemical Reference Data*, 20(4), 713-756.

Brown D.G., Jaffé P.R. (2001). Spectrophotometric assay of POE nonionic surfactants and its application to surfactant sorption isotherms. *Environmental science & technology*, 35(10), 2022-2025.

Chrastil J. (1982). Solubility of solids and liquids in supercritical gases. *The Journal of physical chemistry*, 86(15), 3016-3021.

Consan K.A., Smith R.D. (1990). Observations on the solubility of surfactants and related molecules in carbon dioxide at 50 C. *The journal of supercritical fluids*, 3(2), 51-65.

Coutinho J.A.P., Kontogeorgis G.M., & Stenby E.H. (1994). Binary interaction parameters for nonpolar systems with cubic equations of state: a theoretical approach 1. CO2/hydrocarbons using SRK equation of state. *Fluid Phase Equilibria*, 102(1), 31-60.

da Rocha S.R.P., Psathas P.A., Klein E., & Johnston K.P. (2001). Concentrated CO2-in-Water Emulsions with Nonionic Polymeric Surfactants. *Journal of colloid and interface science*, 239(1), 241-253.

Dandge D.K., Heller J.P., & Wilson K.V. (1985). Structure solubility correlations: organic compounds and dense carbon dioxide binary systems. *Industrial & engineering chemistry product research and development*, 24(1), 162-166.

Desai T.R., Finlay W.H. (2002). Nebulization of niosomal all-trans-retinoic acid: an inexpensive alternative to conventional liposomes. *International journal of pharmaceutics*, 241(2), 311-317.

Desimone J.M., Guan Z., & Elsbernd C.S. (1992). Synthesis of fluoropolymers in supercritical carbon dioxide. *Science (New York, N.Y.)*, 257(5072), 945-947.

Ding Y.G., Huang H.T., Ding Y., Yang C.Y., Ji J., & Wu Y.X. (2011). Study of Metal Complexes' Solubility in Supercritical Carbon Dioxide. *Advanced Materials Research*, 236, 411-416.

Harrison K., Goveas J., Johnston K.P., & O'Rear III E.A. (1994). Water-in-carbon dioxide microemulsions with a fluorocarbon-hydrocarbon hybrid surfactant. *Langmuir*, 10(10), 3536-3541.

Hoefling T., Enick R., & Beckman E. (1991). Microemulsions in near-critical and supercritical carbon dioxide. *The Journal of physical chemistry*, 95(19), 7127-7129.

Jaubert J., Mutelet F. (2004). VLE predictions with the Peng–Robinson equation of state and temperature dependent< i> kij</i> calculated through a group contribution method. *Fluid Phase Equilibria*, 224(2), 285-304.

Joback K.G., Reid R.C. (1987). Estimation of pure-component properties from group-contributions. *Chemical Engineering Communications*, 57(1-6), 233-243.

Kraska T., Leonhard K.O., Tuma D., & Schneider G.M. (2002). Correlation of the solubility of low-volatile organic compounds in near and supercritical fluids: Part II. Applications to Disperse Red 60 and two disubstituted anthraquinones. *Fluid Phase Equilibria*, 194–197(0), 469-482.

Lee B.I., Kesler M.G. (1975). A generalized thermodynamic correlation based on three-parameter corresponding states. *AIChE Journal*, 21(3), 510-527.

Lemmon E.W., McLinden M.O., & Friend D.G. Thermophysical Properties of Fluid Systems. In P. J. Linstrom, W. G. Mallard (Eds.), *NIST Chemistry WebBook, NIST Standard Reference Database Number 69.* National Institute of Standards and Technology, Gaithersburg, MD, 20899.

Lesoin L., Boutin O., Crampon C., & Badens E. (2011). CO2/water/surfactant ternary systems and liposome formation using supercritical CO2: A review. *Colloids and Surfaces A: Physicochemical and Engineering Aspects*, 377(1–3), 1-14.

Liu J., Han B., Wang Z., Zhang J., Li G., & Yang G. (2002). Solubility of Ls-36 and Ls-45 surfactants in supercritical CO2 and loading water in the CO2/water/surfactant systems. *Langmuir*, 18(8), 3086-3089.

Manosroi A., Chutoprapat R., Abe M., & Manosroi J. (2008). Characteristics of niosomes prepared by supercritical carbon dioxide (scCO< sub> 2</sub>) fluid. *International journal of pharmaceutics*, 352(1), 248-255.

Manosroi A., Chutoprapat R., Abe M., & Manosroi J. (2010). Characteristics of niosomes entrapped with rice bran bioactive compounds prepared by supercritical carbon dioxide. In *Nanoscience and Nanotechnology (ICONN), 2010 International Conference on,* .

McHugh M.A., Krukonis V.J. (1994). *Supercritical Fluid Extraction Principles and Practice.* (2nd edn.). Butterworth-Heinemann, Boston.

Nasr M., Mansour S., Mortada N.D., & Elshamy A.A. (2008). Vesicular aceclofenac systems: A comparative study between liposomes and niosomes. *Journal of microencapsulation*, 25(7), 499-512.

Orbey, Hasan., Sandler,Stanley I.,,. (1998). *Modeling vapor-liquid equilibria : cubic equations of state and their mixing rules.* Cambridge University Press, New York.

Panagiotopoulos A., Reid R. (1986). New mixing rule for cubic equations of state for highly polar, asymmetric systems. In ACS Symposium series. 300. 571-582.

Peng D., Robinson D.B. (1976). A new two-constant equation of state. *Industrial & Engineering Chemistry Fundamentals*, 15(1), 59-64.

Pfohl O., Petkov S., & Brunner G. (2000). *PE 2000: a powerful tool to correlate phase equilibria.*. Herbert Utz Verlag.

Privat R., Jaubert J., & Mutelet F. (2008). Addition of the sulfhydryl group (–SH) to the PPR78 model (predictive 1978, Peng–Robinson EOS with temperature dependent kij calculated through a group contribution method). *The Journal of Chemical Thermodynamics*, 40(9), 1331-1341.

Ri K., Yamaguchi S., Wongtrakul P., Hashimoto S., Otake K., Ohkubo T., Sakai H., & Abe M. (2005). Preparation and characterization of nonionic surfactant vesicles using supercritical carbon dioxide. *Material Technology*, 23(5), 340.

Sparks D.L., Hernandez R., & Estévez L.A. (2008). Evaluation of density-based models for the solubility of solids in supercritical carbon dioxide and formulation of a new model. *Chemical Engineering Science*, 63(17), 4292-4301.

Stein, S. E., & Brown, R. L. (1994). Estimation of normal boiling points from group contributions. Journal of Chemical Information and Computer Sciences, 34(3), 581-587.

Tomita K., Machmudah S., Fukuzato R., Kanda H., Quitain A.T., Sasaki M., & Goto M. (2014). Extraction of rice bran oil by supercritical carbon dioxide and solubility consideration. *Separation and Purification Technology*, 125, 319-325.

Tsai W., Ruan Y., & Rizvi S.S. (2006). Solubility measurement of methyl anthranilate in supercritical carbon dioxide using dynamic and static equilibrium systems. *Journal of the science of food and agriculture*, 86(13), 2083-2091.

Woods H.M., Silva M.M., Nouvel C., Shakesheff K.M., & Howdle S.M. (2004). Materials processing in supercritical carbon dioxide: surfactants, polymers and biomaterials. *Journal of Materials Chemistry*, 14(11), 1663-1678.

Yee G.G., Fulton J.L., & Smith R.D. (1992). Aggregation of polyethylene glycol dodecyl ethers in supercritical carbon dioxide and ethane. *Langmuir*, 8(2), 377-384.

Yu Z., Rizvi S.S.H., & Zollweg J.A. (1992). Phase equilibria of oleic acid, methyl oleate, and anhydrous milk fat in supercritical carbon dioxide. *The Journal of Supercritical Fluids*, 5(2), 114-122.

Chapter 3. Mechanics of a continuous liposomal self-assembly process using supercritical carbon dioxide

3.1. Abstract

A novel method for the production of non-ionic surfactant vesicles (niosomes) using an RESS based process coupled with a gas ejector is presented along with an investigation of parameters affecting niosome morphology, size, and encapsulation efficiency of a 0.2 M D-glucose solution in Tris buffer at physiological pH. Vesicles were either multilamellar or unilamellar, depending on the degree of precipitation of the lipid formulation at the point of aqueous cargo introduction. Vesicle particle size distributions were shown to be bimodal, with the 80-99% of the liposomal volume contributed niosomes ranging in size from 3-7 μm and the remaining niosomes ranging from 239-969 nm, depending on the system configuration. Encapsulation efficiency as high as 28% using the gas ejector to introduce the glucose cargo solution was achieved. Vesicle particle size and encapsulation efficiency were shown to be dependent on cargo droplet formation. Physical stability of the produced niosomes was assessed using Vitamin D_3 and iron (II) sulphate as lipophilic and hydrophilic cargo, respectively. Initial encapsulation efficiency was 25.1 ± 0.2% for ferrous sulphate and 95.9 ±1.5% for Vitamin D_3. Niosomes showed good physical stability at 20°C, but storage at 4°C showed an initial burst release, indicating possible rupture of the niosomal membrane.

3.2. Introduction

Lipid vesicles, such as liposomes and niosomes, have been investigated extensively for use in the pharmaceutical (Chang and Yeh, 2012), cosmetic (Hougeir and Kircik, 2012) and food industries (Taylor et al., 2005). Their non-toxic and biodegradable nature along with their ability to simultaneously encapsulate hydrophilic and lipophilic cargo makes them suitable for delivery of many active compounds in biological systems (Jesorka and Orwar, 2008). Non-ionic

surfactant based vesicles, niosomes, are less susceptible to oxidative damage than phospholipid based liposomes (Uchegbu and Vyas, 1998) and have been shown to have greater physical stability (Nasr et al., 2008). However, conventional preparation techniques for lipid vesicles are reliant on the use of toxic organic solvents, like chloroform, making them unsuitable for many applications. In addition, removal and disposal of the organic solvent residues can be time consuming and expensive. These methods are also difficult to scale-up and typically require a post processing step, such as sonication or filtration (Lesoin et al., 2011).

Supercritical fluids, such as supercritical carbon dioxide (SC-CO_2) have emerged as a potential alternative to organic solvents. Liquid like density and gas like diffusivity give SC-CO_2 suitable solvating potential and the non-toxic, non-flammable, inexpensive nature of CO_2 provide distinct advantages over conventional solvents. In recent years, SC-CO_2 has been applied in novel processing techniques for encapsulation (Cocero et al., 2009; Jung and Perrut, 2001) and specifically for the production of lipid vesicles (Lesoin et al., 2011; Meure et al., 2008). Much of the research on lipid vesicle formation using SC-CO_2 has been focused around methods based on the rapid expansion of supercritical solutions (RESS) (Castor and Chu, 1994; Frederiksen et al., 1997) and supercritical reverse phase evaporation (SCRPE)(Otake et al., 2001; Otake et al., 2006) for the production of phospholipid liposomes. However, several non-ionic surfactants have be shown to have reasonably high solubility in SC-CO_2 (Liu et al., 2002), and a few studies have used non-ionic surfactants for the production of niosomes in SC-CO_2 using the SCRPE method (Kinka et al., 2005; Manosroi et al., 2008; Manosroi et al., 2010).

Desirable processes must allow for control of vesicle properties, such as size and lamellarity, while efficiently encapsulating the cargo compounds. Without post processing, vesicle size can be influenced by a variety of factors including nozzle dimensions for RESS and

other spray based production methods (Beh et al., 2012) and depressurization rate for SCRPE-based methods (Otake et al., 2006) . Some evidence suggests that lamellarity is determined by the point of hydration of the lipid with the aqueous cargo (Lesoin et al., 2011), though many SC-CO_2 methods lack the flexibility to vary the point of cargo introduction. Control of encapsulation efficiency, the ratio of encapsulated cargo to cargo introduced in the system, is often more complicated and has been shown to depend on a variety of factors including lipid formulation (Imura et al., 2003; Manosroi et al., 2008), compound to be encapsulated (Manosroi et al., 2010), pH of the aqueous cargo (Kunastitchai et al., 2006), and the presence of modifiers such as ethanol (Wen et al., 2010).

In order to be effectively utilized, lipid vesicles must also remain stable throughout storage and the release of the cargo must be thoroughly understood. Many equations describing the release of drugs from encapsulation matrices are useful for the modeling of bioactive compound release from lipid vesicles (Bayindir and Yuksel, 2010; Fathi et al., 2012). Higuchi (1963) described the release rate of solid drugs dispersed in solid matrices based purely on Fickian diffusion. Korsmeyer et al. (1983) proposed a generalized power law that could describe release ranging from Fickian diffusion to zero-order release kinetics. Hixon-Crowell (1931) described the release from a degrading particle, developing a model where bioactive release is dependent on the change in in surface area and diameter of the particle. Several other strictly empirical models have been applied to cargo release from niosomes (Bayindir and Yuksel, 2010), but those offering insight into the mechanism of release are often more valuable.

A novel system has been developed for lipid vesicle generation that uses the venturi effect to introduce cargo into an expanding supercritical solution, bypassing the need for separate pump and utilizing the inherent energy associated with the high pressure stream. The objectives

of the current study are to:

1) Investigate the factors affecting particle size, lamellarity, and encapsulation efficiency of niosomes produced using a novel method coupling a gas ejector with the RESS particle formation process, the present study has.
2) Demonstrate the viability of this process through simultaneous encapsulation of bioactive hydrophilic and lipophilic cargo
3) Assess the physical stability of niosomes containing bioactive cargo throughout a storage period.

3.3. Materials and Methods

3.3.1. Materials

Polyoxyethylene (4) sorbitan monostearate (Tween61) was supplied by Croda, Inc. (Edison, NJ, USA) and stored at room temperature. Carbon dioxide (purity > 99.5%) was supplied by Airgas (Elmira, NY, USA). Cholesterol (94%), Dimyristoyl-phosphoethanolamine (DMPE), Trinitrobenzensulfonic acid (TNBS; 5% w/v in H_2O),Triton X-100, Nile red, and fluorescein isothiocyanate (FITC) were purchased from Sigma-Aldrich (St. Louis, MO, USA). All other reagents were purchased from Fisher Scientific (Pittsburgh, PA, USA).

3.3.2. Experimental SC-CO_2 system

A schematic diagram of the system used for the generation of niosomes is shown in Figure 3.1. The system consisted of three basic regions: SC-CO_2 generation, pre-expansion, and expansion. In the SC-CO_2 generation section, liquid CO_2 was drawn from a cylinder (1) through ethylene glycol bath (3) maintained at -5°C and then pumped to pressure using a high pressure pneumatic pump (4) (DHF-60, Haskel, Burbank, CA, USA). Pressure was maintained at 10 MPa using a back pressure regulator (5) (Tescom, Elk River, MN, USA). The high pressure CO_2 was brought up to temperature in a water bath (6) maintained at 60°C before entering a high pressure

vessel (9) , which was also maintained at 60°C using heating tape and a CN9000 temperature controller (Omega, Stamford, CT, USA). The lipid formulation was dissolved in SC-CO_2 in a high pressure vessel (10) maintained at 60°C. This solution then passed through a pre-expansion tube, (ID: 0.35cm, L: 30 cm) which was heated to 60°, 70°, or 80°C. A high pressure solenoid valve (Clark Cooper, Roebling, NJ,USA) equipped with an on/off timer was used to meter the SC-CO_2 solution into the expansion zone. The expansion zone consisted of high pressure venturi-based ejector device (11) (PA SpA, Rubiera, Italy) modified with a threaded fitting in the suction port to accommodate the insertion of metal tubing into the path of the high pressure jet. The SC-CO_2 solution was depressurized through a nozzle in the body of the ejector, into which the cargo solution (12) was introduced via a stainless steel tube (Figure 3.1A).

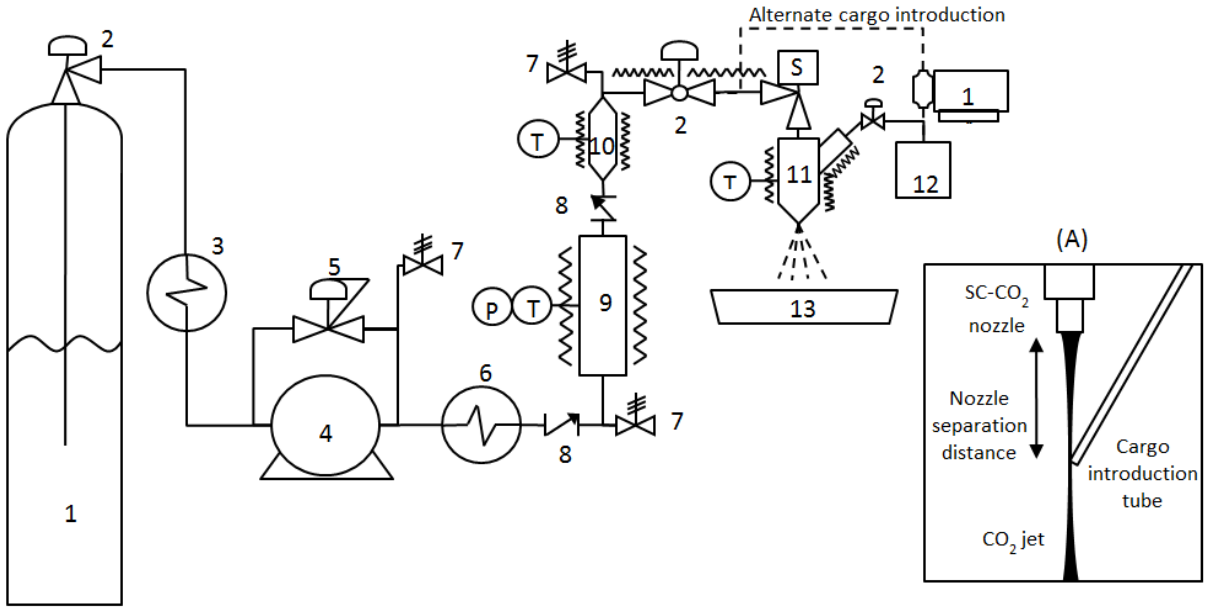

Figure 3.1. SC-CO2 niosome generation system diagram. 1) CO_2 reservoir 2) Valve 3) Cooler 4) High pressure pump 5) Back pressure regulator 6) Preheater 7) Pressure relief valve 8) Check valve 9) SC-CO2 reservoir 10) Solubilization vessel 11) Ejector venturi 12) Cargo reservoir 13) Niosome collection. Inset (A) shows alignment of SC-CO_2 nozzle and cargo introduction tube inside the ejector venturi. P = pressure gauge, T= Thermocouple, S = solenoid valve, zig-zag line represent thermally controlled zone. Dashed line represents alternative pathway.

Three nozzles were used in this study with diameters of 0.762mm (L/D = 6) and 1.003 mm (L/D = 4), and 1.270 (L/D =2.5), respectively, to assess the influence of CO_2 jet on vesicle formation. Three stainless steel tubes were used for cargo introduction with internal diameters of 0.508 mm, 0.838 mm, and 1.372 mm to assess the influence of cargo droplet formation on final vesicle properties. The high velocity of the SC-CO_2 exiting the nozzle creates a vacuum inside the body of the ejector according to Bernoulli's principle, thus the cargo solution is drawn into the lipid-containing CO_2 jet without any additional energy input. Adjustment of the depth of the nozzle within the venturi body via the built-in threaded connection allowed for adjustment of the vacuum created within the venturi body. The greatest vacuum inside the venturi body (absolute pressure of 80 kPa) was generated when the distance between the SC-CO_2 nozzle tip and the end of the cargo introduction tube (nozzle separation distance, Figure 3.1A) was adjusted to 2.5 cm, indicating alignment with the vena contracta of the CO_2 jet. Nozzle separation distance was also varied to 3.75 cm and 0.60 cm from the cargo introduction tube to produce absolute pressures of 85 kPa and 83 kPa respectively. As an alternative pathway (shown in Figure 3.1 as dashed lines), the cargo solution was pumped directly into the pre-expansion tube through a 15μm sintered disk using a Model 396 Minipump (14) (Milton Roy, Ivyland, PA, USA), then expanded with the SC-CO_2 solution through the expansion device with no additional cargo being drawn into the expansion device. Due to the large temperature drop upon CO_2 expansion, the venturi device was heated to the same temperature as the pre-expansion tube (60°, 70°, or 80°C) using heating cord (Brisk Heat, Columbus, OH, USA) and a CN2110 temperature controller (Omega, Stamford, CT, USA). The niosome suspension was collected below the device which was housed inside a ventilated box.

3.3.3. Niosome formulation

Tween61 and cholesterol were mixed at a 1:1 molar ratio, as this ratio has been shown to give high physical stability using an SC-CO_2 based process for niosome formation (Manosroi et al., 2008). DMPE was also included as a marker lipid for lamellarity determination at 1:1000 molar ratio with Tween61. The mixture was heated in a water bath at 45°C and stirred vigorously for 10 minutes to ensure adequate mixing. Excess lipid mixture, approximately 1 g, was loaded into the 150 ml solubilization vessel (Figure 3.1, (10)) to keep the level of lipid constant in the SC-CO_2 throughout each experimental run. After pressurization, the solution was allowed to equilibrate for 20 minutes at 10 MPa. The cargo solution consisted of 20mM Tris and 0.2M glucose adjusted to a pH of 7.4 using 1N HCl.

3.3.4. Niosome characterization

3.3.4.1. Lamellarity

Niosome lamellarity was determined following the TNBS assay as described by Gruber and Schindler (1994). The TNBS assay allows for a quantitative measure of lamellarity using a shift in the absorbance of DMPE when it reacts with TNBS. By determining the ratio of amount of DMPE marker lipid in the outermost lamella to the total amount of marker lipid in the niosome, lamellarity can be assessed. For determination of DMPE in the outermost lamella (external), 25 µl of a solution of 0.2 M borate and 1 M sucrose (pH 9) was added to 50 µl of niosome suspension in four separate Eppendorf tubes. 50 µl of TNBS (0.1% w/v in H_2O) was then added to each tube. The reaction was stopped at 15 min intervals using 50 µl 1.5 M HCl containing 2% (w/v) Triton-X100. For the total DMPE, the same procedure was performed, but the borate-sucrose solution contained 4% (w/v) Triton X-100 in order to disrupt the niosomes before addition of the TNBS reagent and the 1.5 M HCl "stop solution" contained no Triton X-100. At the conclusion of the 60 minute reaction period, each tube was dilute with 1 ml DI water.

Analyses were performed in duplicate and the absorbance of the samples was determined at 410nm using a Beckman Du640 uv-vis spectrophotometer (Fullerton CA, USA).

3.3.4.2. Particle size and zeta potential

Particle size analysis was performed using a Brookhaven 90 plus nanoparticle size analyzer (Holtsville, NY,USA). Niosome suspensions were diluted by a factor of 40 in deionized water and transferred to cuvettes, which were allowed to equilibrate in the size analyzer for 2.5 minutes before analysis. Zeta-potential was determined on the same Brookhaven 90 plus nanoparticle size analyzer equipped with the BI-zeta extension.

3.3.4.3. Encapsulation efficiency

Encapsulation efficiency was determined following the glucose dialysis method of Manosroi et al. (2008) with modification, as follows. Niosome suspensions were transferred to Pur-a-lyzer Midi dialysis tubes (Sigma-Aldrich, St. Louis, MO, USA) and dialyzed against 200x volume of 20 mM Tris buffer adjusted to pH 7.4 with 1 N HCl for 5 hours. The dialyzed suspensions were then disrupted with 4% Triton X-100 (w/v in H_2O). The glucose content of the dialyzed suspension was determined using the glucose hexokinase assay kit (Sigma-Alrdrich). Encapsulation efficiency was calculated as follows:

$$\text{Encapsulation efficiency (\%)} = 100 \text{ x } \frac{glucose\ concentration\ in\ dialyzed\ suspension}{glucose\ concentration\ of\ cargo} \quad (3.1)$$

3.3.4.4. Confocal laser scanning microscopy

For confocal laser scanning microscopy (CLSM), FITC (0.1mg/ml) was included in the cargo solution to view the aqueous phase. The niosome suspension was stained with 2% (w/v) nile red in order to view the lipophilic portion of the niosomal membrane and then centrifuged for 10s at 15,600g using an Eppendorf 5414 Centrifuge (Brinkmann Instruments, Westbury, NY,

USA) to remove the excess stain. CLSM images were obtained using a Leica Upright DMRE-7 confocal microscope fitted with HCX PL APO 100x objective (oil immersion). Excitation was performed at 488nm using and Argon laser to highlight FITC (green image) and at 543 using a helium-neon laser to highlight nile red (red image). Red-green composite images were created using ImageJ v. 1.48u.

3.3.5. Storage stability

In order to demonstrate the efficacy of the method and physical stability of the produced niosomes, suspensions were prepared for the simultaneous encapsulation of cholecalciferol (Vitamin D_3) and iron (II) sulfate heptahydrate (ferrous sulfate) as lipophilic and hydrophilic cargo, respectively. The cargo solution consisted of 0.9 M ferrous sulfate in in degassed 10 mM citric acid-sodium citrate buffer (pH 6.8) (Xia and Xu, 2005). The cargo solution was prepared immediately before use and care was taken to limit the exposure of the cargo solution to oxygen. The niosome formulation was prepared at a 1:1:0.16 molar ratio of Tween61 to cholesterol to Vitamin D_3. Niosome suspensions were prepared as described above using the venturi for cargo introduction, 0.762mm SC-CO_2 nozzle, 0.508 mm cargo introduction tube, 2.5 cm nozzle separation distance and all temperature controlled zones at 60°C. The suspension was subsequently passed over a 1cm x 30cm column of Amberlite IR-120 cationic exchange resin (Aldrich, Milwaukee, WI, USA) to remove the unencapsulated iron (Xia and Xu, 2005). The cleaned suspension was split into 15 ml batches, which were stored in air tight containers at 20°C and 4 °C, respectively. On day 0, 1, 7, 14, and 21, 1 ml samples from each container were withdrawn and analyzed for particle size, as described above, and for encapsulation efficiency of the two cargo compounds, as described below.

3.3.5.1. Ferrous sulfate content analysis

Niosome suspensions were transferred to Pur-a-lyzer Midi dialysis tubes (Sigma-Alrdrich, St. Louis, MO, USA) and dialyzed for 18 hours at room temperature against 200x volume of 10 mM citric acid-sodium citrate buffer. The dialyzed suspensions were then disrupted with 4% Triton X-100 (w/v in H_2O). The ferrous sulphate content of the dialyzed suspension was determined according to AOAC method 977.30.

3.3.5.2. Vitamin D_3 content analysis

Niosome suspensions were centrifuged for 2 minutes at 15,600g using an Eppendorf 5414 Centrifuge in order to separate out the unencapsulated vitamin D. The supernatant was reserved and the remaining niosomal material was disrupted with 1 mL 4% Triton X-100 (w/v in DI H_2O). The samples were stored frozen at -20°C until analysis. The Vitamin D2/D3 assay was completed by preforming a liquid-liquid-extraction (LLE) by Hearland Assays LLC (Ames, IA, USA). The samples were pipetted into boro-silicate test tubes and spiked with tri-deuterated Vitamin D_3, extracted with hexane, and dried. The samples were then re-constituted into LCMS grade methanol and water and injected onto an Agilent 1290 HPLC (Agilent, Santa Clara, CA, USA) coupled to an Agilent 6460 Triple-quad mass spec, using an Agilent Poroshell C18 analytical column for separation and isolation. Encapsulation efficiency was determined according to the following equation:

$$\text{Encapsulation efficiency (\%)} = 100 \text{ x } \frac{Vit.D_3 \text{ content in centrifuged niosomes}}{Vit.D_3 \text{ content in centrifuged niosomes} + Vit.D_3 \text{ content in supernatant}} \quad (3.2)$$

3.3.5.3. Cryogenic transmission electron microscopy

Niosome samples containing iron were visualized using cryogenic transmission electron microscopy (Cryo-TEM). Samples were pipetted onto Quantifoil holey carbon TEM grid, blotted, and plunge frozen in a mixture of liquid propane and liquid ethane. Samples were stored

in liquid nitrogen until analysis. Samples were transferred using a Gatan 626 cro-transfer holder (Gatan, Pleasanton, CA, USA) and visualized using an 200kV FEI Tecnai F20 (FEI, Hillsboro, OR, USA). Cryo-scanning transmission electron microscopy coupled with electron energy loss spectroscopy (EELS) using a Gatan Tridiem spectrometer were also performed in order to assess the distribution of iron within the sample.

3.3.5.4. Release kinetics

The release of ferrous iron was modeled using the Higuchi (1963) equation, the Hixon-Crowell model (1931), and the Korsmeyer-Peppas equation (Korsmeyer et al. 1983). According to the Higuchi equation, the quantity of drug released, M_t, when based purely on Fickian diffusion, was shown to be proportional to the square root of time:

$$\frac{M_t}{A} = \sqrt{Dc_s(2c_i - c_s)t} \quad (3.3)$$

Where D is the diffusivity of the drug in the homogenous media, c_s is the solubility of the drug in the matrix, c_i is the initial concentration of drug in the matrix, A is the surface area, and t is time (Siepmann and Peppas, 2011). When the initial concentration is much greater than the concentration at a given time ($c_i \gg c_s$), this equation can be simplified to:

$$M_t = k\sqrt{t} \quad (3.4)$$

$$\text{With } k = A\sqrt{2c_i Dc_s} \quad (3.5)$$

For release of bioactives from lipid vesicles (Fathi *et al.* 2011), equation (4) has been expressed as:

$$\frac{M_t}{M_\infty} = k_H\sqrt{t} \quad (3.6)$$

Where M_t is the total amount of the bioactive compound released from the lipid vesicles at time t, M_∞ is the total amount of bioactive compound released over infinite time, and k_H is the

Higuchi constant. The Hixson-Crowell model (Hixson and Crowell, 1931) has also been used to describe bioactive release from lipid vesicles, assuming release of entrapped content was proportional to change in total surface area:

$$C_0^{1/3} - C_t^{1/3} = kt \quad (3.7)$$

Where C_0 is the concentration of bioactive compound in the lipid vesicles initially, C_t is the concentration of the bioactive material in the lipid vesicle at time t, and k is the rate constant.

Release of drugs from lipid vesicles has also been studied using the Korsmeyer-Peppas equation (Korsmeyer et al. 1983):

$$\frac{M_t}{M_\infty} = kt^n \quad (3.8)$$

Where k is a constant and n is the diffusional exponent, which indicates the dominant transport mechanism. This model assumes limiting cases of Fickian diffusion and zero-order kinetics and is valid for the first 60% of fraction release. For spheres, $n \leq 0.45$ corresponds to Fickian diffusion, $0.45 < n < 0.85$ corresponds to so-called non-Fickian "anomalous" transport, and $n > 0.85$ corresponds to Type II transport (Vali et al. 2008). Equation (3.8) can be modified to include a parameter, b, to account for a burst release effect (Kim and Fassihi, 1996):

$$\frac{M_t}{M_\infty} = kt^n + b \quad (3.9)$$

When b = 0, equation (3.9) becomes identical to equation (3.8)

3.3.6. Statistical analyses

All statistical analyses were performed using JMP Pro 11 (SAS, Cary, NC, USA) at a significance level α=0.05 with two independent experimental repetitions. Data are represented as mean ± standard deviation of at least two experimental replicates. Data were compared using ANOVA with multiple comparisons using Fisher's LSD test where applicable. Particle size

distributions were analyzed using the normal mixtures function in JMP Pro 11 to assess relevant distribution statistics. Regression analysis was performed on particle size and encapsulation efficiency data to assess the influence of the tested parameters.

3.4 Results and discussion

3.4.1. Lamellarity

Gruber and Schindler (1994) observed an increase in TNBS labelling over time, caused by permeation of TNBS into the lipid vesicles produced with soy bean lecithin and phosphatidylcholine, respectively. The authors accounted for this by linearly extrapolating absorbance values to time zero, thus improving estimates of external labelling. However, in the current study, no change in labelling was observed over the course of the one hour assay period, indicating that the niosomal lamella was relatively impermeable to the TNBS reagent. This may be due to the rigidity of the membrane, as the assay was performed at room temperature, below the phase transition temperature of Tween61 (~40°C).

The effect of pre-expansion temperature and nozzle dimensions on E, the ratio of DMPE labelling in the external most layer of the niosome to total DMPE labelling in the niosomal suspension, is shown in Figure 3.2.

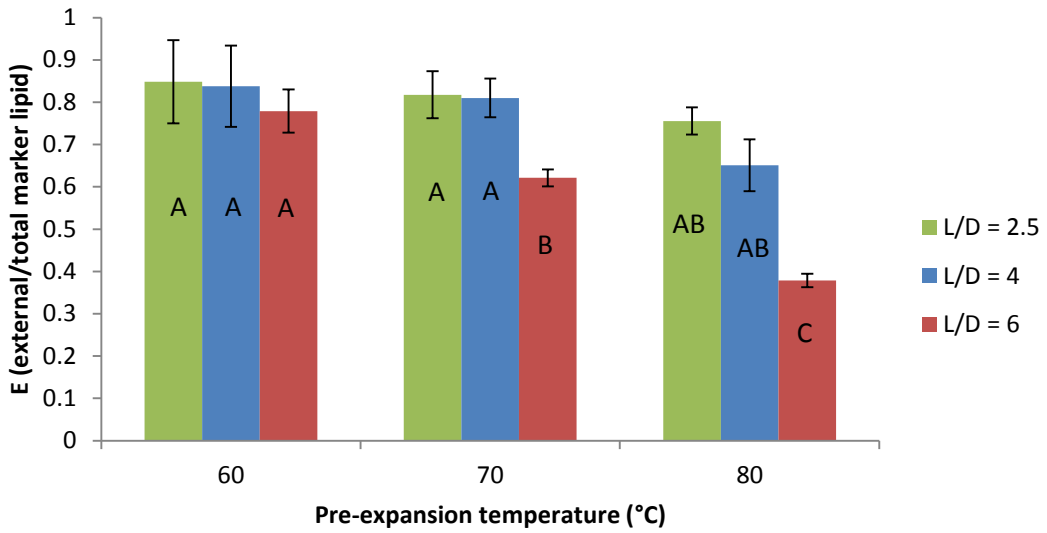

Figure 3.2. Ratio of external to total marker lipid in Tween 61 niosomes produced at 60°C, 10 MPa with varying pre-expansion temperature and nozzle L/D ratio. Different letters indicate significant difference (n=3, α=0.05)

In all cases, E is less than one, indicating the presence of multilamellar vesicles (MLVs). This corresponds with the studies of Frederiksen *et al.* (1997) and Castor and Chu (1994) who observed the formation MLVs using RESS-based liposome formation processes. Figure 3.2 also shows that as pre-expansion temperature increases, there is a decrease in E, indicating an increase in the lamellarity of the niosomal suspension. In supercritical solutions with solutes of sufficiently low volatility, increasing temperature causes a drop in fluid density, which in turn causes a reduction in the solubility of the dissolved solute, resulting in precipitation. In the present study, the precipitated lipid forms niosomal bilayer and greater precipitation of the lipid (higher pre-expansion temperature) prior to contact with the aqueous cargo appears to result in greater niosomal lamellarity. Further, E was observed to decrease slightly with increasing L/D ratio of the nozzle through which the SC-CO_2 solution was expanded. Debenedetti et al. (1993) showed that in RESS the density of the supercritical solution drops along the length of the nozzle, with an even greater density drop occurring in longer capillaries. The observed increase

in lamellarity with increasing L/D ratio of the nozzle may be due to the greater precipitation of the solute as a result of the greater drop in fluid density. Lasic (1988) proposed that lipid vesicle formation was dependent on the formation of bilayer phospholipid fragments (BPF), whose growth and formation can be manipulated through precipitation from organic solution. These BPF subsequently peel off during hydration and vesiculate at the water/organic interface. Similarly, growth of intermediary lipid structures in SC-CO_2 would be dependent on solubility conditions thus influencing the vesicular lamellarity upon hydration.

Lesoin *et al.* (2011) categorized current lipid vesicle formation methods into two categories those that hydrate the lipid formulation before depressurization, such as the SCRPE method (Otake et al., 2001), and those that hydrate the lipid formulation during depressurization, such as the injection method (Castor and Chu, 1994). Generally, it can be observed that unilamellar vesicles (UVs) are formed when the lipid formulation is hydrated before precipitation from solution upon depressurization (Lesoin et al., 2011), or prior to the removal of organic solvent as in the depressurization of expanded solutions into aqueous media (DESAM) method (Meure et al., 2008). Accordingly, it should be possible to produce MLVs and UVs using one preparation method by varying the point of lipid hydration, whether before or after precipitation is initiated.

Figure 3.3 shows the E ratio for niosomes produced using an alternate system configuration where the cargo solution in pumped directly into the SC-CO_2 solution before depressurization through the nozzle.

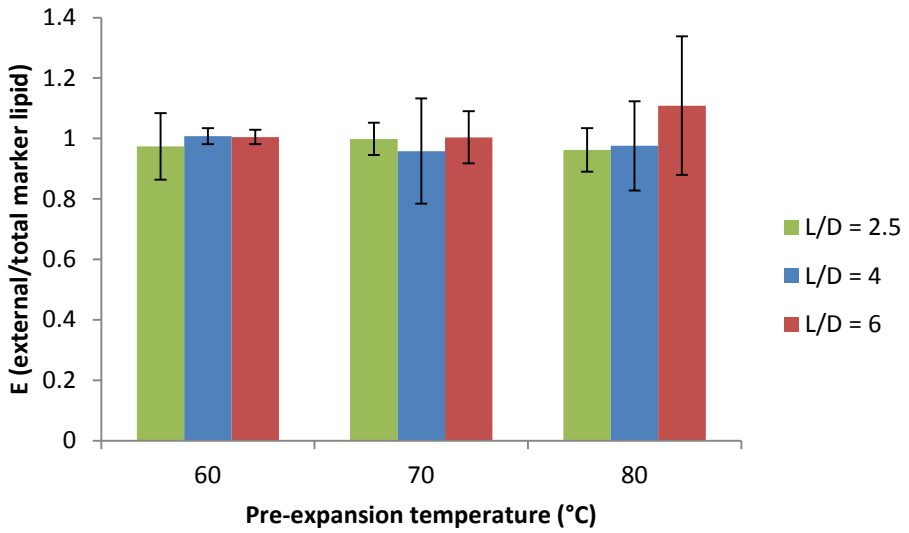

Figure 3.3. Ratio of external to total marker lipid in Tween 61 niosomes produced at 10 MPa with varying pre-expansion temperature and cargo introduction before expansion of the supercritical solution.

The ratio of external to total lipid labelling was nearly unity for all conditions tested, indicating near unilamellarity for the niosomal suspension. This is in agreement with other SC-CO_2 methods that produce lipid vesicles by hydrating the lipid formulation before precipitation from SC-CO_2 solution (Lesoin et al., 2011). Otake et al. (2006) suggested that when an aqueous solution is introduced into a phospholipid/SC-CO_2 solution, reverse micelles form to minimize the unfavorable energy at the water/CO_2 interface. Subsequent depressurization results in a phase inversion and the formation of a lipid vesicle suspension. This initial reverse micelle structure is critical to the formation of UVs in the SCRPE method (Otake et al., 2006) and in the reverse phase evaporation method with conventional organic solvents (Lasic, 1988).

Lamellarity was also qualitatively assessed using CLSM. FITC was included in the aqueous cargo solution in order to visualize the hydrophilic interior of the niosomes and nile red was used to visualize the lipophilic portion of the niosomal lamella. Figure 3.4 (A and B) shows niosomes produced using the ejector for introduction of cargo during depressurization. The

majority of the vesicles are multilamellar, with a small proportion of UVs. In Figure 3.4 (C and D), it can be seen that introduction of the cargo prior to depressurization through the nozzle results in vesicles that are mostly unilamellar, with a small proportion of MLVs.

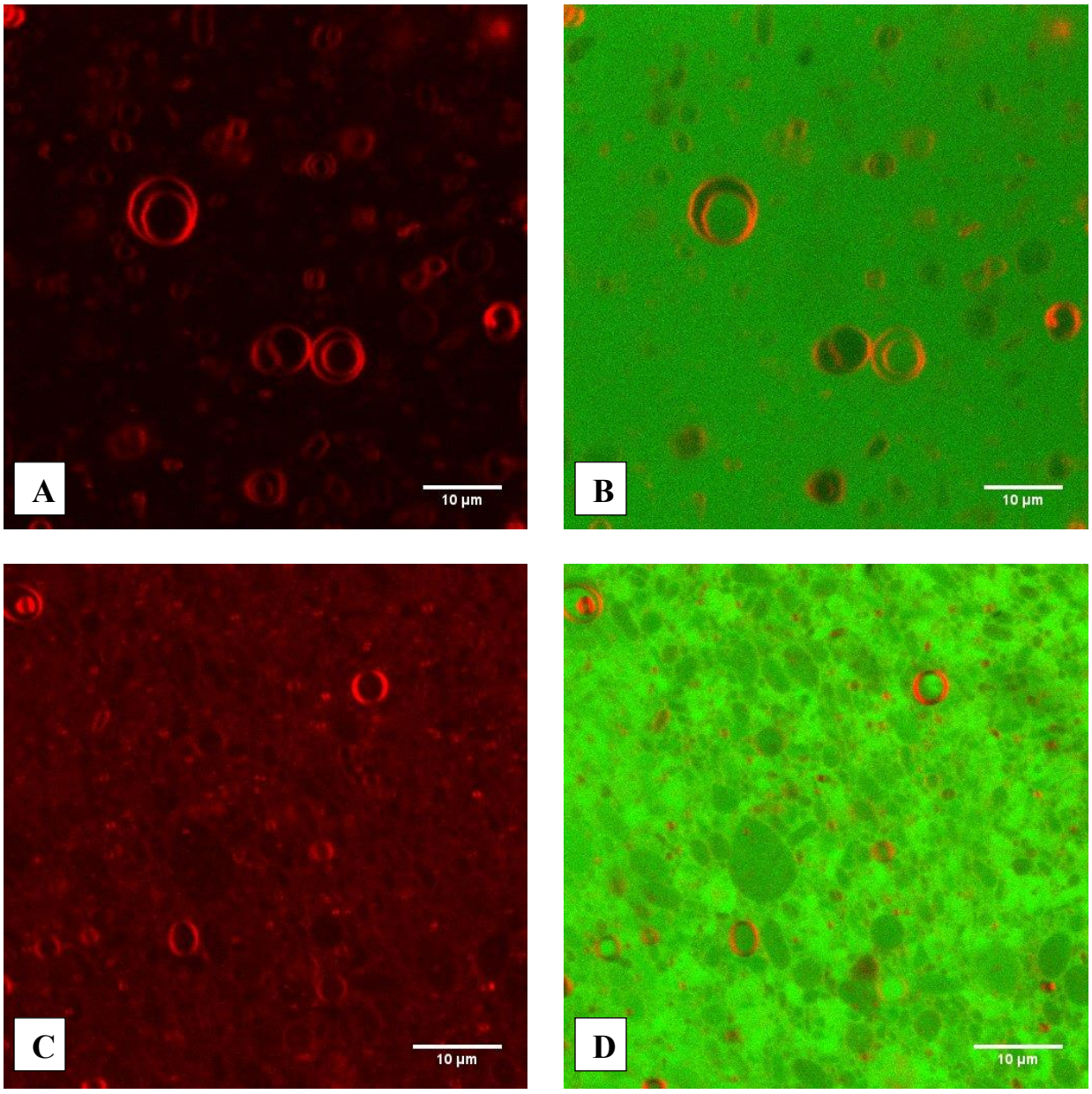

Figure 3.4. CLSM images of niosomes produced at 60°C, 10 MPa. Red fluorescent (A) and red-green fluorescent composite image (B) of niosomes produced using the ejector based introduction of cargo and red fluorescent(C) and red-green composite image (D) of niosomes produced using introduction of cargo prior to depressurization.

3.4.2. Particle size

Application of lipid vesicles is heavily dependent on particle size, which can range from 20 nm to tens of micrometers (Jesorka and Orwar, 2008). Under all conditions tested, both cargo introduction before depressurization and cargo introduction using the gas ejector produced bimodal particle size distributions, as shown in Figure 3.5.

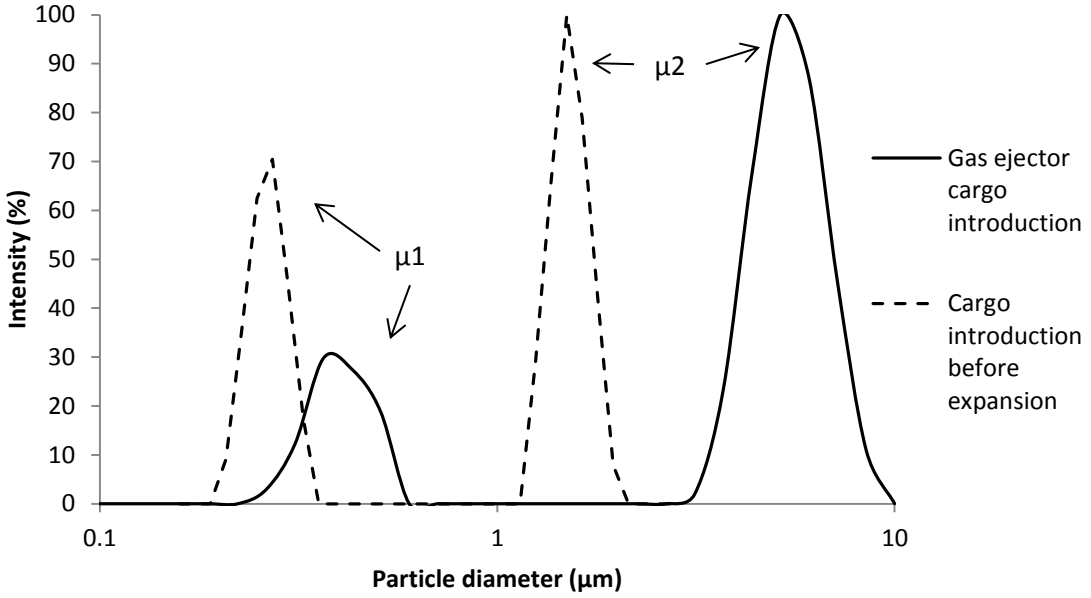

Figure 3.5. Representative particle size distribution for niosomes produced at 80°C and 10 MPa using the gas ejector for cargo introduction and cargo introduction before depressurization

Debenedetti *et al.* (1993) observed bimodal phenanthrene particle size distributions with RESS using short (L= 6mm) converging nozzle-capillary expansion devices and unimodal distributions using long (L= 12 mm) nozzle-capillary expansion devices of the same diameter profile (D= 30 μm entrance, 20 μm exit), suggesting that a longer device allows for growth of the smaller particle range. The relatively short nozzle length used in this study (< 5 mm in all cases) may have similarly limited the time for growth of the smaller lipid fragments as they precipitate from the supercritical solution. Santo et al. (2014) also observed bimodal particle size distributions of liposomes produced using an RESS based preparation method when nozzles with greater

diameter than 180μm were used for injection of cargo into the expanding supercritical solution, though no nozzle length was reported. In the current study, the smaller diameter peak (μ1) and the larger diameter peak (μ2) were treated as individual normal distributions using the statistical program JMP Pro 11.

3.4.2.1. Pre-expansion temperature and point of cargo introduction

Table 3.1. shows the effect of pre-expansion temperature on the mean particle size of each peak, produced using the gas ejector for cargo introduction and introducing the cargo prior to expansion through nozzle, respectively. In both cases, little difference was observed with increasing temperature for either the μ1 or μ2 peak. However, one way ANOVA showed a significant difference ($p<0.001$) in the mean particle diameter for the μ2 peak for niosomes when comparing the different methods of cargo solution introduction.

Table 3.1. Comparison of bimodal mean particle size of niosomes produced using a gas ejector for cargo introduction during depressurization and introduction of the cargo before depressurization*†

Method of cargo introduction	Temperature (°C)	μ1 peak mean (nm)	μ2 peak mean (nm)	Volume contribution of μ2 peak (%)
Gas ejector	60	421 ± 20[a]	5674 ± 161 [a]	83.5 ± 1.5[a]
	70	437 ± 69 [a]	6618 ± 671 [a]	82.01 ± 3.3[a]
	80	409 ± 21 [a]	6058 ± 752 [a]	80.5 ± 5.6[a]
Before depressurization	60	362 ± 169 [a]	1457 ± 134[b]	99.6 ± 0.9[b]
	70	272 ± 109 [a]	1437 ± 117 [b]	98.7 ± 1.0[b]
	80	354 ± 123 [a]	1576 ± 63 [b]	98.9 ± 1.0[b]

* Values in each column with different superscript letters are significantly different according to Tukey's HSD test (n=3, α= 0.05).
†Pressure = 10 MPa, 0.762mm nozzle used for SC-CO_2. 0.838 mm cargo introduction tube and 2.5 cm nozzle separation distance used for gas ejector.

The distribution of particles was closer to unimodal when the cargo was introduced before

depressurization, with the μ2 peak contributing 99% of the niosomal volume, in comparison to 82% contribution when the gas ejector was used to introduce the cargo solution (Table 3.1). Furthermore, the spread of each peak, measured as the standard deviation of the frequency distribution, was also smaller for niosomes produced by introducing the cargo before depressurization than those produced by introducing cargo through the ejector. The comparative uniformity of the niosomes produced when introducing the cargo before depressurization indicates some homogenizing effect of the nozzle, though the size and uniformity of the reverse micelle structures in the SC-CO_2 prior to depressurization, as discussed earlier, is not known. Due to the novelty and complexity, further investigation was focused on incorporation of the cargo solution using the gas ejector method only.

3.4.2.2. Nozzle and cargo introduction dimensions

Figure 3.6 shows the influence of the diameter of the cargo introduction tube and the diameter of the SC-CO_2 expansion nozzle on the particle size of niosomes produced by the gas ejector method. The length of each cargo introduction tube, and therefore point of introduction into the expanding CO_2 stream was kept constant with a nozzle separation distance of 2.5 cm. The volumetric flow rate of the cargo solution was kept at 1.2 ml/s using a needle valve for all cargo introduction tube and nozzle combinations.

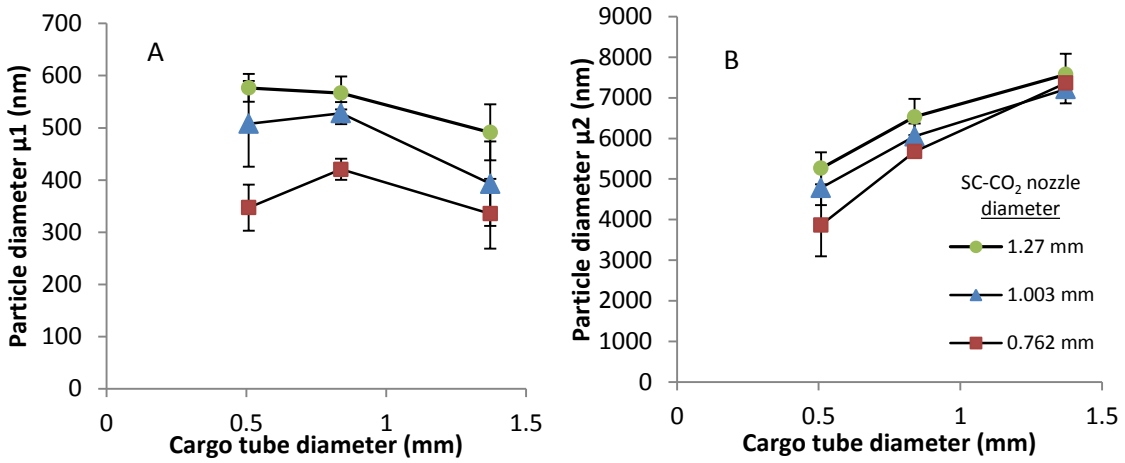

Figure 3.6. Effect of cargo introduction tube diameter and SC-CO2 expansion nozzle on particle size of niosomes produced at 60°C and 10 MPa. (A) Bimodal mean particle size µ1 (B) Bimodal mean particle size µ2

As the diameter of the cargo introduction tube was increased from 0.508 mm to 1.372 mm, the average diameter of the µ2 peak increased. Similar results were observed by Santo et al. (2014), who found that increasing nozzle size (80 to 1000 µm) to inject water into a high pressure mixture of CO_2 and phospholipids resulted in the generation of larger liposomes in the collected suspension (264 nm to 620.9 nm). In atomization processes involving a liquid stream in a gaseous cross-flow, the tendency of a fluid to break into droplets is governed by both the liquid properties and the aerodynamic forces acting on the jet and is typically characterized by the dimensionless Weber number, the ratio of the fluid's kinetic energy to surface tension (Sirignano, 1999). However the highly non-ideal behavior of an expanding supercritical fluid jet is difficult to model, even with modern computational fluid dynamics techniques (Seebald and Sojka, 2011), though some attempts have been made (Lin et al., 2003; Wu et al., 1996) From a practical standpoint, larger diameter orifices tend to result in larger liquid jets which are less susceptible to aerodynamic perturbations under otherwise equivalent conditions, resulting in larger droplets as the jet breaks up. The increase in niosome size with increase in diameter of the cargo introduction tube indicates that the atomization of the aqueous cargo within the expansion

device does influence the lipid vesicle size and that the lipid fragments do not simply vesiculate once they come in contact with the bulk suspension in the collection container, but instead may be coating the aqueous cargo droplets. The mean particle diameter of the μ2 peak increased slightly as the SC-CO_2 expansion nozzle diameter, except when used in conjunction with the largest diameter (1.372 mm) cargo introduction tube where the particle size seems to reach a limiting value. The converging design of the nozzles limits the exiting gas to sonic velocity at this pressure and temperature (10 MPa, 60°C). Because the pressure and the actuating time interval for the solenoid were kept constant for all configurations, larger SC-CO_2 nozzle diameters result in greater flow of the lipid-SC-CO_2 solution. The greater mass of gaseous flow would impart greater acceleration to the smaller cargo droplets in the ejector body and potentially limit their contact with the precipitated lipid fragments, preventing them from being coated with lipid and shifting the average niosomal diameter towards a larger size. This effect is reduced as the initial cargo droplet size is increased, as observed using the largest cargo introduction tube. As with temperature, the μ1 peak was relatively unaffected by nozzle and cargo introduction tube dimensions. This indicates that the smaller particle range of the bimodal distribution may be formed through a separate mechanism, such as vesiculation after coming into contact with the bulk aqueous solution in the collection container.

3.4.2.3. Nozzle separation

The size of particles produced in RESS processes has been shown to be dependent on growth due to coagulation after exiting the expansion nozzle (Weber and Thies, 2007). Growth of lipid fragments prior to contact with the aqueous cargo could affect resultant lipid vesicle characteristics. To investigate the influence of the expansion growth process on the size distribution of niosomes, the expansion device was modified to vary the distance between the

$SC\text{-}CO_2$ nozzle and the cargo introduction tube. Figure 3.7 shows the effect of the nozzle separation distance (distance between the $SC\text{-}CO_2$ expansion nozzle and the cargo introduction) on the bimodal mean particle size of niosomes produced at 10 MPa.

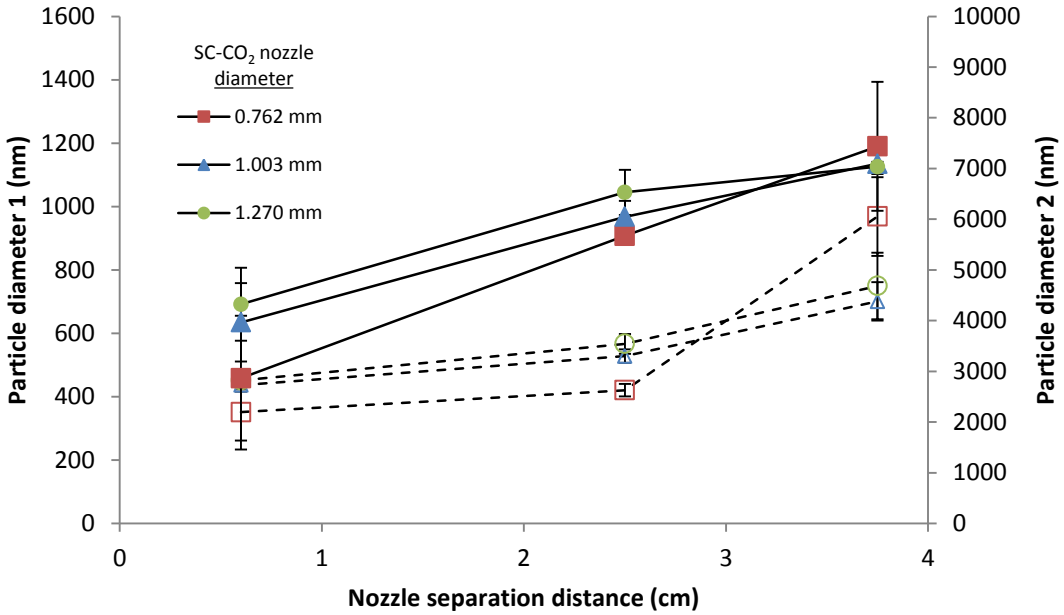

Figure 3.7. Effect of distance between carrier nozzle and cargo tube outlet on particle size. Open symbols represent the smaller mean peak size µ1 (primary axis) and filled symbols represent the larger mean peak size µ2 (secondary axis). Pressure= 10 MPa, pre-expansion temperature = 60°C, cargo tube diameter =0.838 mm.

As the distance between the two increases, the average diameter of each peak in the bimodal distribution increases. Increasing the relative distance between each fluid stream introduction point inside the expansion device increases the time for growth of the precursor lamellae from the precipitated lipid after exiting the $SC\text{-}CO_2$ expansion nozzle and decreases the velocity of the expanding gaseous stream at the point when it comes in contact with the atomized cargo fluid. The reduction of the gaseous stream velocity would reduce the momentum forces responsible for the breakup of the liquid cargo stream, resulting in an increase of the droplet diameter of the atomized liquid cargo. In addition, Weber and Thies (2007)showed that particle growth by coagulation after the nozzle exit in RESS processes could be minimized by restricting time for

growth, lowering particle collision efficiency, and lowering particle collision frequency. In the case of vesicle formation, this may allow for the growth of larger precipitated lipid fragments prior to contact with the aqueous cargo droplets.

3.4.2.4 Regression analysis

In an attempt to assess the influence of the tested parameters on the particle size of niosomes produced using the gas ejector for cargo introduction, multiple regression was performed with each peak mean as respective dependent variables. For the μ2 peak, regression analysis yielded an expression that explained 75% of the variation (R^2=0.75, R^2_{adj}=0.74 F=51.05, p<0.0001):

$$Niosome\ diameter\ (nm) = 1168.46N_{ID} + 2408.90C_{ID} + 1014.88S + 41.70 \quad (3.10)$$

Where N_{ID} is then CO_2 nozzle diameter (mm), C_{ID} is the cargo introduction tube diameter (mm), S is the nozzle separation distance (cm) and temperature and pressure are fixed at 60°C and 10 MPa. However, the variables with statistically significant predictive power on the μ2 peak mean diameter (Table 3.2) were the diameter of the tube used for cargo introduction and the nozzle separation distance.

Table 3.2. Parameter estimates for multiple regression* for the prediction of μ2 diameter†

Parameter	Coefficient of regression (β)	Standard error	t-ratio	p-value
Intercept	451.70	743.61	0.61	0.5463
Nozzle diameter (mm)	1168.46	624.54	1.87	0.0672
Cargo introduction tube diameter (mm)	2408.90	364.19	6.61	<0.0001
Nozzle separation distance (cm)	1014.85	98.61	10.29	<0.0001

* R^2=0.75, R^2_{adj} = 0.74, F=51.06, p<0.0001.
†Fixed conditions: P= 10 MPa, T= 60°C, cargo flow rate 1.2ml/s

While the regression analysis is specific to this system, it does suggest that controlling the atomization of the cargo stream, and there for the liquid droplet size, is critical to the resultant vesicle size for spray based mechanisms of liposome formation. Regression analysis for the μ1 peak mean diameter yielded a model with statistically insignificant explanatory power, further indicating that the niosomes formed at this size range may form from a separate mechanism.

3.4.3. Zeta potential

Zeta potential was also determined in order to assess the physical stability of the niosomes in suspension. For all samples tested, zeta potential ranged between -32 to -42 mV, which indicates good stability of the suspended particles, as the critical zeta potential to ensure mutual repulsion is generally ±30 mV (Everett et al., 2007). One way ANOVA showed a significant difference ($p=0.008$) between the zeta potential of niosomes prepared using the gas ejector and those prepared by introducing the cargo before depressurization. However, there was no statistically significant influence on zeta potential of the niosomal suspension by any other parameter tested which is to be expected, as chemical rather than physical preparation factors affect zeta potential of niosomal vesicles. The zeta potential of Span60 niosomes prepared by the reverse phase evaporation method was shown to be affected by the pH of the suspension as well as the addition of other surface active membrane additives, but ranged from -16 to -19 mV for the control formulation up to -49mV for Span60 niosomes containing dicetylphosphate (Junyaprasert et al., 2008).

3.4.4. Encapsulation efficiency

3.4.4.1. Temperature and point of introduction

The quality of microencapsulation processes is often assessed by the amount of cargo that

is encapsulated relative the amount of cargo that is fed into the process. Figure 3.8 shows the effect of temperature and method of cargo introduction on the encapsulation efficiency of niosomes. In both cases, temperature showed no statistically significant effect on encapsulation efficiency, but encapsulation efficiency did significantly differ across methods of cargo introduction according to one way ANOVA (p=0.0004).

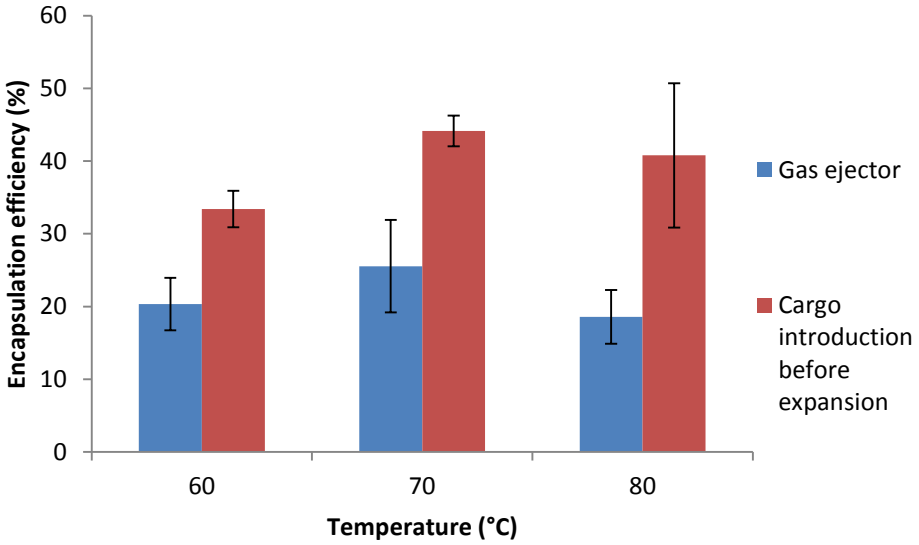

Figure 3.8. Effect of temperature and method of cargo introduction on glucose encapsulation efficiency of niosomes produced at 10 MPa. SC-CO_2 nozzle diameter = 0.762 mm. Cargo tube diameter for gas ejector = 0.838 mm. Nozzle separation distance for gas ejector = 2.5 cm

Introducing the cargo solution to the lipid formulation prior to depressurization likely resulted in greater mixing of the two streams. The encapsulation efficiency achieved using either method of cargo introduction was greater than that reported in previous studies for the production of Tween61 based niosomes (8-12%) using the SCRPE method (Kinka et al., 2005; Manosroi et al., 2008), but only cargo introduction before depressurization was comparable to the encapsulation efficiency of bioactive compounds from rice bran reported in Tween 61 niosomes (55-64%) reported by Manosroi (2010). The gas ejector method for cargo introduction used in this study did give comparable encapsulation efficiency to that reported by other RESS based methods

(~20%) for the formation of liposomes (Castor and Chu, 1994; Frederiksen et al., 1997). Again, due to the comparative novelty, further investigation of encapsulation efficiency was focused on the use of the gas ejector method for cargo introduction.

3.4.4.2. Nozzle and cargo introduction dimensions

Figure 3.9 shows the impact of nozzle dimensions and cargo introduction tube diameter on the encapsulation efficiency of niosomes produced at 10 MPa with pre-expansion temperature of 60°C using the gas ejector for introduction of cargo.

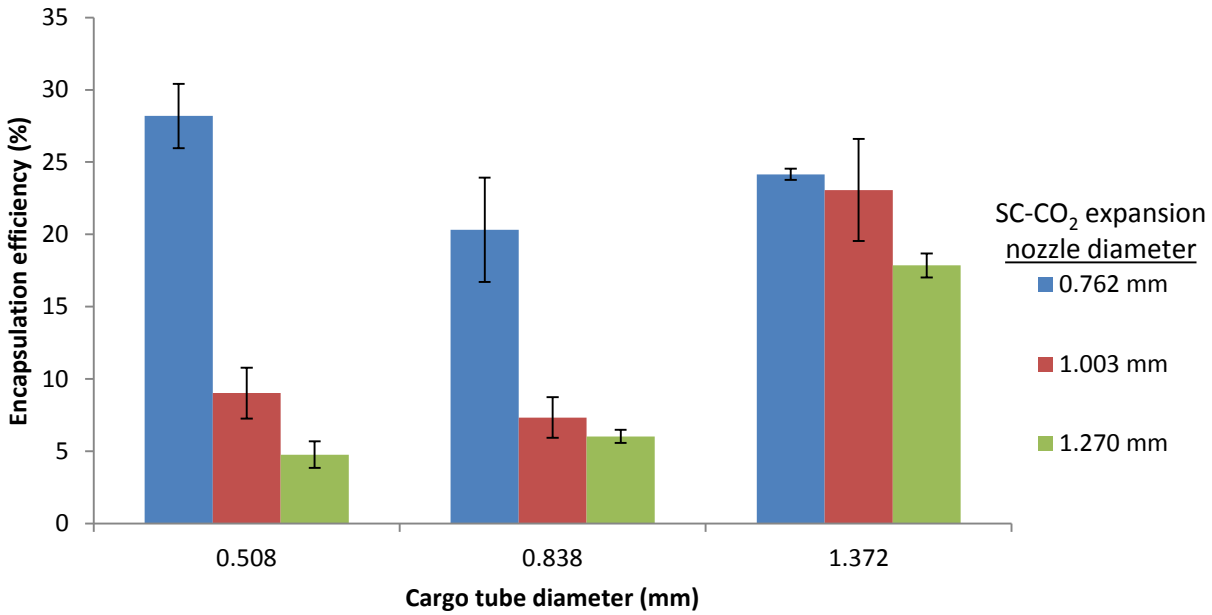

Figure 3.9. Effect of cargo tube and SC-CO_2 expansion nozzle dimensions on encapsulation efficiency of niosomes produced at 60°C and 10 MPa using the gas ejector for introduction of the cargo solution. Nozzle separation distance = 2.5 cm

For a given cargo introduction tube, encapsulation efficiency decreased with increasing diameter of the SC-CO_2 nozzle. The greatest encapsulation efficiency was observed with the smallest cargo introduction tube (0.508 mm) in conjunction with the smallest diameter nozzle (0.762 mm) tested. This observed difference may be due to the size of the cargo droplets generated using the different cargo tubes. Aerodynamic forces have a greater impact on smaller droplets than larger

droplets in atomization processes, causing smaller droplets to be accelerated and decelerated faster than larger droplets in a spray. The higher CO_2 mass flow rate using the larger diameter nozzles (1.270 and 1.008 mm) compared to the smallest nozzle (0.762 mm) give greater acceleration to the smaller droplets generated using the 0.508 mm and 0.838 mm diameter cargo introduction tubes, limiting the contact between the lipid fragments and the cargo droplets and subsequently the encapsulation efficiency.

A small increase was observed in the encapsulation efficiency when the distance between the SC-CO_2 expansion and cargo introduction point inside the expansion device was increased (Figure 3.10). Encapsulation efficiency is highly dependent on particle size and morphology in regards to lipid vesicles. The minor increase observed in encapsulation efficiency may be linked to the increase in particle size also observed when the distance between the SC-CO_2 expansion and cargo introduction point inside the expansion device was increased.

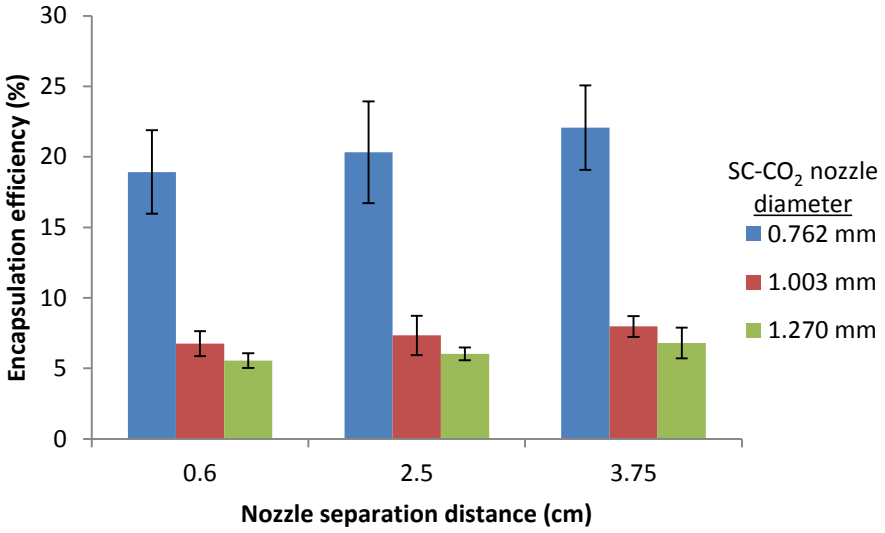

Figure 3.10. Effect of distance between carrier nozzle and cargo tube outlet on encapsulation efficiency of niosomes produced at 60 °C and 10 MPa.

It is important to note that this definition of encapsulation efficiency assumes there is sufficient

lipid present in order to encapsulate the aqueous cargo. The theoretical amount of lipid required to encapsulate a certain volume of aqueous cargo could be estimated geometrically for a known particle size a similar approach to Pidgeon and Hunt (1980). Assuming a homogenous population of spherical niosomes, the volume of lipid (V_L) required for a single vesicle could be estimated using the spherical shell equation:

$$V_L = {}^{4}/_{3}\,\pi\,(R^3 - (R - x)^3) \qquad (3.11)$$

Where R is the particle diameter and x is the bilayer thickness. And the total mass of lipid required to encapsulate a given volume of aqueous cargo can be estimated using:

$$m_L = NV_L\rho_L \qquad (3.12)$$

Where N is the total number of particles and ρ is the lipid mass density. For a fixed volume, the smallest particle size should have the largest surface area, and therefore the greatest lipid requirement. In the present study, the smallest particle diameter achieved for the μ2 peak was 3.86 μm using the gas ejector for cargo introduction and 1.44 μm using the pump for cargo introduction before depressurization (both using the 0.762 mm nozzle). The number of particles for complete encapsulation can be taken as the total aqueous volume included as cargo divided by the volume inside the aqueous compartment of one niosome. Assuming a bilayer thickness of 3.4 nm (Uchegbu and Florence, 1995) and a lipid mixture density of 1.08 g/ml, based on the initial mass ratio of lipids (1.5:1 Tween 61 to cholesterol) and densities at room temperature, the minimum mass of lipid required to fully encapsulate the aqueous cargo would be 15.5 mg / ml aqueous cargo while introducing the cargo before depressurization (diameter = 1.44 μm) and 5.7 mg / ml aqueous cargo using the gas ejector for cargo introduction (diameter =3.86). Based on the lamellarity assessment of niosomes produced using the gas ejector, approximately 80% of the total lipid is present in the outermost lamella. In order to account for the additional lipid required

for the internal lamella, the minimum lipid requirement using the gas ejector for cargo introduction would be closer to 6.9 mg/ ml aqueous cargo. Using the 0.762 mm nozzle in the current study, 19.8 ± 1.1 mg of lipid were introduced per milliliter of aqueous cargo, indicating that sufficient lipid was present to theoretically achieve 100% encapsulation efficiency.

3.4.4.3. Regression analysis

Multiple regression of glucose encapsulation efficiency data yielded an equation with a fit of R^2=0.71 (R^2_{adj}= 0.70, F=41.61, p<0.0001):

$$\sqrt{EE} = -35.82N_{ID} + 2.96C_{ID} + 0.83S + 46.53 \quad (3.13)$$

Where EE is encapsulation efficiency (%) N_{ID} is then CO_2 nozzle diameter (mm), C_{ID} is the cargo introduction tube diameter (mm), S is the nozzle separation distance (cm) and temperature and pressure are fixed at 60°C and 10 MPa. Taking the square root of the dependent variable was necessary to maintain the assumption of homoscedacity. Of the parameters tested, only the nozzle diameter was shown to be statistically significant (Table 3.3). Considering all factors simultaneously, this indicates that nozzle diameter and therefore mass flow of the gaseous stream has the most influence on encapsulation efficiency in this system. While a true predictive equation for encapsulation efficiency is likely more complicated than what is presented, it does suggest that further efforts for improving and predicting encapsulation efficiency using this process should focus on the dynamics of the gaseous stream.

Table 3.3. Parameter estimates for multiple regression* for the prediction of glucose encapsulation efficiency†

Parameter	Coefficient of regression (β)	Standard error	t-ratio	p-value
Intercept	46.53	3.90	11.94	<0.0001
Nozzle diameter (mm)	-35.82	3.27	-10.95	<0.0001
Cargo introduction tube diameter (mm)	2.96	1.90	1.55	0.1272
Nozzle separation distance (cm)	0.83	0.52	1.61	0.1130

* R^2=0.71, R^2_{adj} = 0.70, F=41.61, p<0.0001

†Fixed conditions: P= 10 MPa, T= 60°C, cargo flow rate 1.2ml/s

3.4.5. Bioactive compound encapsulation and physical stability

3.4.5.1. Encapsulation efficiency

Niosomes were prepared containing iron (II) sulphate and Vitamin D_3 to demonstrate the unique quality of niosomes to deliver hydrophilic as well as lipophilic solutes. Figure 3.11 shows the change in encapsulation efficiency of iron sulphate in niosomes stored at room and refrigeration temperatures over time.

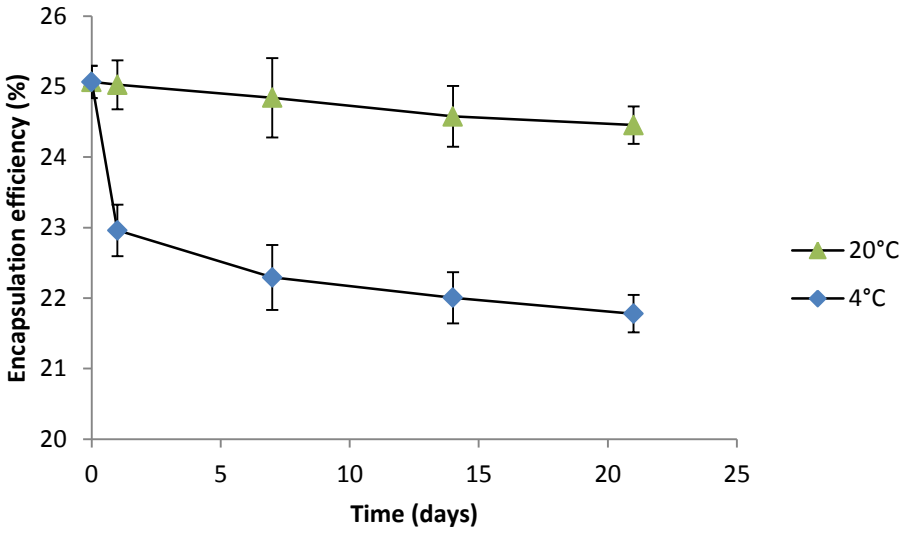

Figure 3.11. Change in encapsulation efficiency of iron sulphate in niosomes during storage at 20°C and 4°C.

At 20°C, encapsulation efficiency dropped slightly over the course of time with a total retention at the conclusion of 21 days of 97.56 $\pm$ 1.61 %. At 4°C, encapsulation efficiency dropped rapidly within 1 day and then slowly continued to decrease resulting in a total retention at the conclusion of 21 days of 86.90 $\pm$ 1.86%. It is likely that the iron sulphate precipitated on cooling at 4°C, as the initial concentration of the cargo solution 20% (mass) was above the equilibrium solubility of iron (II) sulphate at 4°C of 15.0% mass (CRC Handbook, 2014). Subsequent crystal growth may have damaged the membrane, causing rupture, as reported by Johnsson et al. (1999), who observed rupture of liposomal membranes by crystals of precipitated boronated drug compounds.

At the prepared concentration, iron (II) sulphate should begin to precipitate as the solution is cooled below 17°C. To test if precipitation of the cargo solution was related to leakage during storage, the release of Fe^{2+} from the niosome suspension was determined after storage for 24 hours 4°C, 15°C, and 18°C, and 20°C. Figure 3.12 shows that little Fe^{2+} release was observed after 24 hours of storage at 18 and 20°C, but considerably more was released at 4 and 15°C. The sharp increase in Fe^{2+} release as the storage temperature drops below the precipitation temperature of 17°C supports the idea that precipitation of the cargo material may have caused rupture of the membrane resulting in greater release.

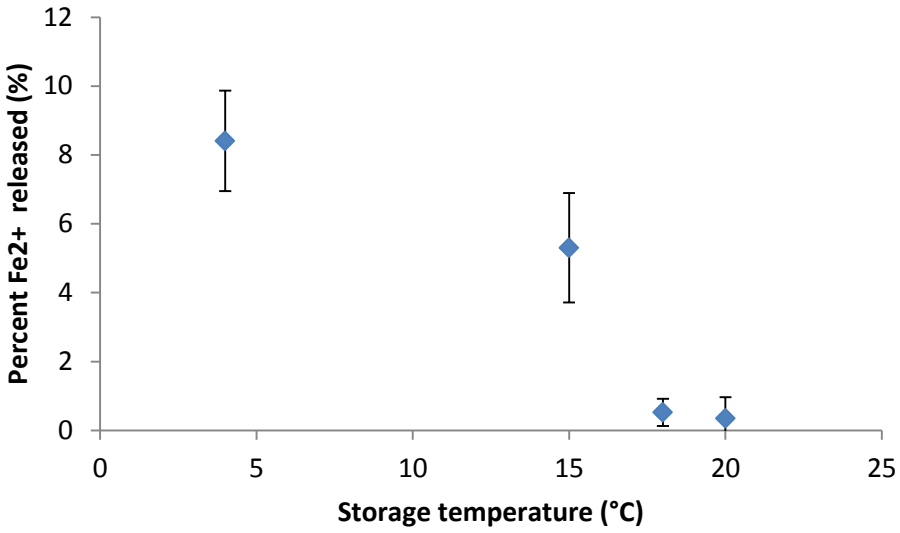

Figure 3.12. Release of Fe^{2+} from niosomes after storage at 24 hours.

To investigate possible rupture of the niosome, samples were viewed using Cryo-TEM. Cryo-TEM images of niosomes containing iron (II) sulphate are shown in Figure 3.13. The niosomes were stored at 4°C prior to analysis. Needle like crystals were clearly observed in the sample (Figure 3.13 (A)). No clear image of the crystals piercing the bilayer was obtained, however considerable warping of the outer most bilayer was observed in one particular image at the sample well wall (Figure 3.13 (B)) which may indicate prior damage to the membrane and release of entrapped iron. EELS confirmed the presence of iron atoms within the crystals observed in the sample well and the spectra suggest that iron remained in the unoxidized divalent form (Colliex, et al. 1994; Van Aken et al. 1998) though no literature is available on EELS spectra of iron (II) sulphate crystals. Iron could not be detected over the background within the niosomes, possibly due to the sample thickness.

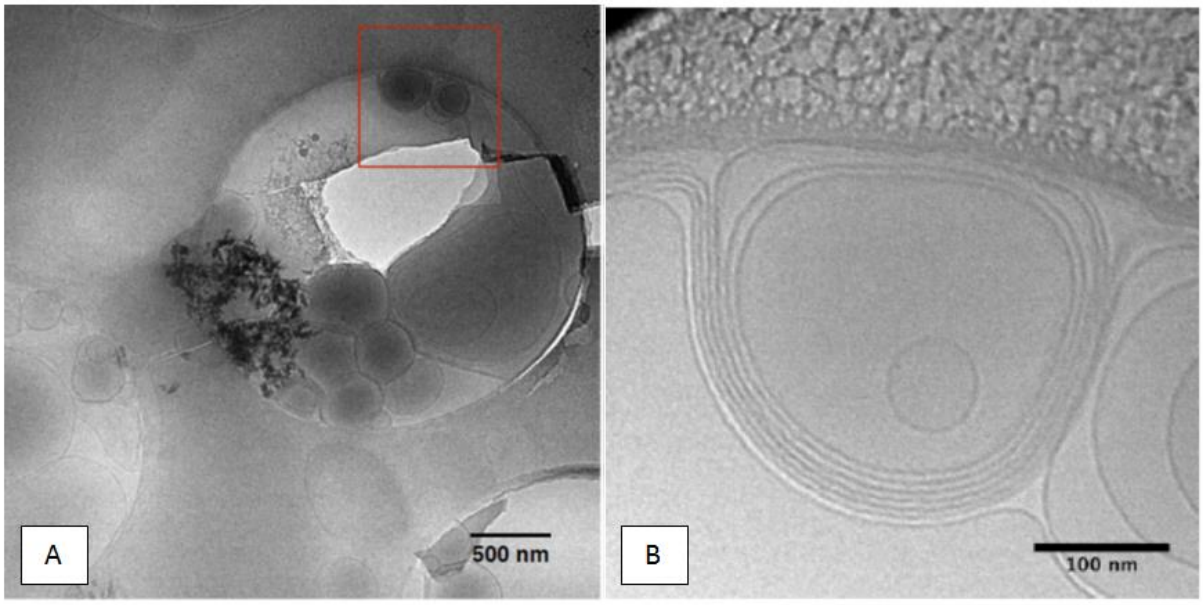

Figure 3.13. Cryo-TEM images iron (II) sulphate containing niosomes within the sample well (A). Zoomed in image (marked in red square on image A) of niosome with distorted outer membrane at sample well wall (B).

The Vitamin D_3 content of niosome suspensions stored at room and refrigeration temperatures over time is shown in Figure 3.14.

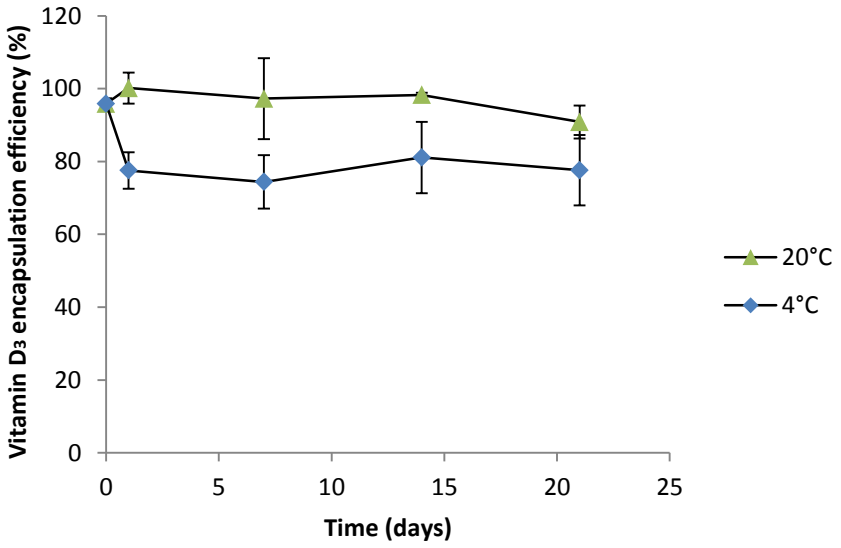

Figure 3.14. Change in Vitamin D_3 encapsulation efficiency of niosomal suspension during storage at 20°C and 4°C.

Encapsulation efficiency (according to equation (3.2)) at day 0 was determined to be 95.9 $\pm$ 1.47%. This is in accordance with Mohammadi *et al.* (2014) who reported >90% encapsulation efficiency of Vitamin D_3 in phosphatidylcholine based liposomes prepared using thin film hydration and sonication. As with iron, an initial drop in Vitamin D_3 content was observed in the niosomes stored at 4°C after 1 day of storage. This lends further support to the idea that cold storage may have caused rupture of some of the lipid vesicles, as vesicle shrinkage alone should result in constant levels of Vitamin D_3 in the bilayer. However, little change was observed in Vitamin D_3 content during storage at 20°C and 4°C after the first day of storage.

As a demonstration of the utility of these lipid based nanocapsules as food ingredients or supplements, the bioactive content of the niosome suspensions after removal of unentrapped material is shown in Table 3.4. Not accounting for bioavailability, 30 mg of lipid carrier (Tween61/ cholesterol) would be sufficient to encapsulate enough iron (II) sulphate to meet the RDA for iron for both men and women ages 19-50. High incorporation of Vitamin D_3 levels was possible, with 1 mg of lipid carrier encapsulating sufficient Vitamin D_3 to exceed the current RDA. Reduction of Vitamin D_3 to lower levels would be relatively simple, requiring only reduction of the proportion of Vitamin D_3 added to the initial lipid formulation.

Table 3.4. Nutritional composition of niosome suspensions

Component	Content in niosome* (mg/mg lipid carrier)	Content in prepared suspension (mg/ml)	Recommended Daily Allowance (mg)**
Fe^{2+}	0.64	12.5	Men: 8 Women: 18
Vitamin D_3	0.023	0.42	0.015

*Based on initial levels of niosomes produced using gas ejector for cargo introduction after removal of unencapsulated bioactives

**Based on normal adults ages 19-50 for Fe^{2+} and ages 19-70 for Vitamin D (National Institute of Health, 2014)

3.4.5.2. Particle size and zeta potential

The iron sulphate and Vitamin D_3 containing niosomes, as expected, also exhibited a bimodal particle size distribution but in this case, the smaller peak with mean diameter 1.4 μm comprised the majority of the niosomal volume (98.8%). The size limits for the production of stable vesicles is determined by the properties of the contributing membrane lipids, such as molecular weight, critical packing parameter and the interaction between the hydrophilic and hydrophobic portions of the molecules (Antonietti and Förster, 2003). The inclusion of Vitamin D_3 in the niosomal membrane likely interfered with the tight packing of the Tween61 surfactant in the bilayer, reducing the maximum possible curvature of the membrane and subsequent minimal stable vesicle size. Similar observations were made by Junyaprasert *et al.* (2008) for the inclusion of dicetylphosphate in Span 60 niosomes prepared using the reverse phase evaporation method. Figure 3.15 shows the mean particle size of the smaller peak throughout the storage period. Niosomes stored at room temperature (20°C) showed good physical stability over time, with very little change in average size.

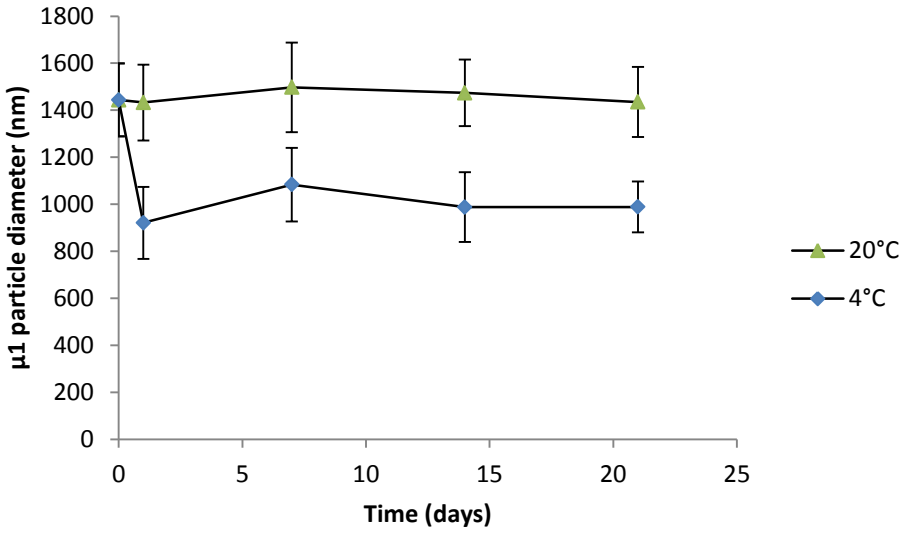

Figure 3.15. Change in mean particle size of iron sulphate and Vitamin D_3 containing niosomes during storage at 20°C and 4°C.

Similar results were reported by Nasr *et al.* (2008) who observed little change in the size of Span60 niosomes with entrapped aceclofenac over the course of three months. Niosomes stored at refrigeration temperature (4°C) showed an initial drop in size after 1 day. The size reduction after the first day corresponded to a 59.3% change in volume ($\Delta V/V_{initial}$) based on a weighted average diameter with a 16°C temperature change, which is considerably larger than the 20% change in volume with 50°C temperature change of phospholipid based vesicles reported previously (Raudino et al., 1990). The observed reduction in particle size may be attributed to rupture of the vesicles upon cold storage as described previously, shifting the average particle diameter to a smaller value. However, after the initial drop, relatively little difference in particle size was observed during storage. Zeta potential measured on the first day was -57.96 ± 0.27 mV and -54.71 ± 0.49 mV for niosome suspensions stored at 4°C and 20°C, respectively, indicating good stability. No appreciable change was observed during storage.

3.4.5.3. Release kinetics

From an application standpoint, release of Fe^{2+} during storage would be unfavorable, as it could potentially cause harmful oxidative reactions with susceptible compounds, like unsaturated fatty acids, impacting product quality. Three models were applied to assess the release of Fe^{2+} into the bulk fluid over time. Figure 3.16 shows the cumulative release of Fe^{2+} in the niosomes throughout the storage period for both room and refrigeration temperatures and comparison with the three literature models investigated. Based on the mean squared error (MSE) shown in Table 3.5, the best fit for the release of Fe^{2+} from the niosomes at 4°C and 20°C over this period of time was obtained using the Korsmyer-Peppas model.

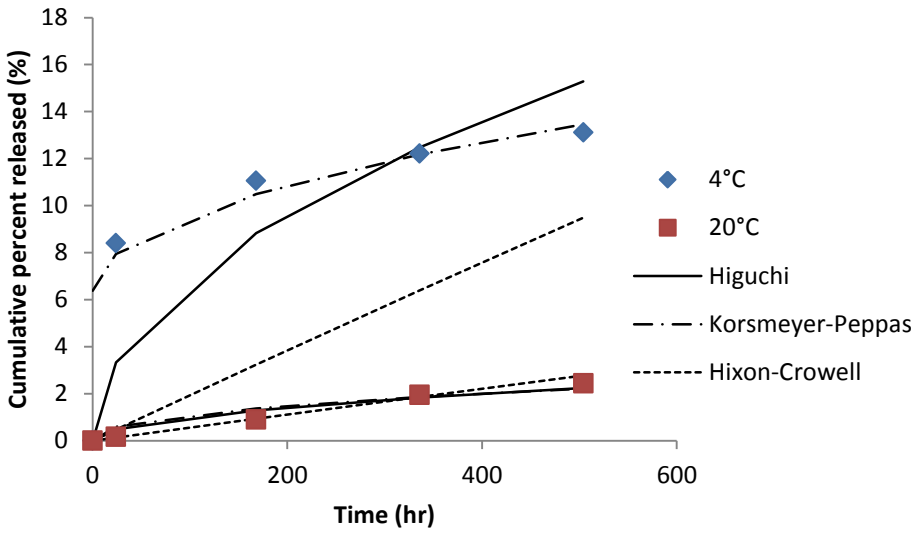

Figure 3.16. Release of Fe^{2+} from niosomes in storage at 4° and 20°C and comparison with bioactive release models.

Table 3.5. Kinetic parameters and descriptive statistics of models for release of Fe^{2+} from niosomes during storage

		Storage temperature (°C)	
Model	Parameter	4	20
Higuchi	k_H ($hr^{-0.5}$)	0.681	0.100
	MSE*	2.5	0.064
Hixson-Crowell	k (hr^{-1})	1.0×10^{-4}	2.0×10^{-5}
	MSE*	0.018	3.9×10^{-5}
Korsmeyer-Peppas	k (hr^{-1})	0.0032	0.0015
	n	0.495	0.890
	B	0.064	0
	MSE*	8.3×10^{-4}	9.5×10^{-6}

*Mean squared error between experimental and model predicted values

With the greatest number of adjustable parameters of the three models and the ability to account for the burst effect observed at 4°C, this is to be expected, however it does offer insight into the transport mechanism. In both cases, the exponent *n* of the Korsmeyer-Peppas equation fell in the anomalous transport region. After accounting for the burst effect at 4°C, transport was near the pure Fickian cut-off described by (Ritger and Peppas, 1987). At 20°C, the exponent approached the limit for Type II transport, indicating increased importance of relaxation within the bilayer as membrane fluidity increases.

3.5. Conclusions

A novel method for the production of niosomes based on RESS coupled with a gas ejector for the introduction of cargo solution has been presented. Based on this study, the following conclusions can be drawn:

1) Vesicle lamellarity was related to the solubility of lipid formulation at the point of introduction for the aqueous cargo. Greater precipitation of the lipid formulation before exposure to the aqueous cargo resulted in a greater degree of lamellarity according to a TNBS labelling assay and results were supported using CLSM imaging.
2) Vesicle size was largely dependent on the atomization conditions of the liquid cargo, indicating a possible spray coating method of the droplets by the lipid material
3) Interaction between the lipid and aqueous cargo was critical to increasing encapsulation efficiency. Interaction and thus, encapsulation efficiency was limited by higher mass flow of the SC-CO_2 solution
4) Niosomes showed good physical stability over time at room temperature with little appreciable loss of Fe^{2+} or Vitamin D_3 over 21 days. Storage at 4°C however may have caused rupture of the niosome, resulting in greater leakage of both Fe^{2+} and vitamin D_3 , suggesting that niosomes should be kept above precipitation temperatures for the given cargo concentration or, conversely, concentration of the cargo solution should be kept below the precipitation limit at the desired storage temperature.
5) Release data was modeled using the Korsmeyer-Peppas equation and transport of Fe^{2+} fell within the “anomalous” regime.
6) Further understanding the dynamic interactions of the lipid formulation in the expanding CO_2 jet and the atomized aqueous cargo droplets is critical to fully understanding the mechanism of formation of lipid vesicles in aerosol sprays.

References

Antonietti M., Förster S. (2003). Vesicles and liposomes: a self-assembly principle beyond lipids. *Advanced Materials*, 15(16), 1323-1333.

Bayindir Z.S., Yuksel N. (2010). Characterization of niosomes prepared with various nonionic surfactants for paclitaxel oral delivery. *Journal of pharmaceutical sciences*, 99(4), 2049-2060.

Beh C.C., Mammucari R., & Foster N.R. (2012). Lipids-based drug carrier systems by dense gas technology: A review. *Chemical Engineering Journal*, 188(0), 1-14.

Castor T.P., Chu L. (1994). Methods for making liposomes containing hydrophobic drugs. (WO9615774).

Chakrabarti A.C., Veiro J.A., Wong N.S., Wheeler J.J., & Cullis P.R. (1992). Generation and characterization of iron- and barium-loaded liposomes. *Biochimica et Biophysica Acta (BBA) - Biomembranes*, 1108(2), 233-239.

Chang H.I., Yeh M.K. (2012). Clinical development of liposome-based drugs: formulation, characterization, and therapeutic efficacy. *International journal of nanomedicine*, 7, 49-60.

Chemical Rubber Company. (2014). Aqueous solubility of inorganic compounds at various temperatures. In Anonymous CRC handbook of chemistry and physics. (95th edn.). CRC Press, Boca Raton, Fla.

Cocero M.J., Martín Á., Mattea F., & Varona S. (2009). Encapsulation and co-precipitation processes with supercritical fluids: Fundamentals and applications. *The Journal of Supercritical Fluids*, 47(3), 546-555.

Colliex, C., Manoubi, T., & Ortiz, C. (1991). Electron-energy-loss-spectroscopy near-edge fine structures in the iron-oxygen system. *Physical Review B,44*(20), 11402.

Cullis P.R., Mayer L.D., Bally M.B., Madden T.D., & Hope M.J. (1989). Generating and loading of liposomal systems for drug-delivery applications. *Advanced Drug Delivery Reviews*, 3(3), 267-282.

Debenedetti P.G., Tom J.W., Sang-Do Y., & Gio-Bin L. (1993). Application of supercritical fluids for the production of sustained delivery devices. *Journal of Controlled Release*, 24(1–3), 27-44.

Everett, D. H., Sankey,Otto Francis.,. (2007). Basic principles of colloid science. .

Fathi M., Mozafari M.R., & Mohebbi M. (2012). Nanoencapsulation of food ingredients using lipid based delivery systems. *Trends in Food Science & Technology*, 23(1), 13-27.

Frederiksen L., Anton K., Hoogevest P.v., Keller H.R., & Leuenberger H. (1997). Preparation of liposomes encapsulating water-soluble compounds using supercritical carbon dioxide. *Journal of pharmaceutical sciences*, 86(8), 921-928.

Gianasi E., Cociancich F., Uchegbu I.F., Florence A.T., & Duncan R. (1997). Pharmaceutical and biological characterisation of a doxorubicin-polymer conjugate (PK1) entrapped in sorbitan monostearate Span 60 niosomes. ***International journal of pharmaceutics,*** **148(2), 139-148.**

Gruber H.J., Schindler H. (1994). External surface and lamellarity of lipid vesicles: a practice-oriented set of assay methods. ***Biochimica et Biophysica Acta (BBA)-Biomembranes,*** **1189(2), 212-224.**

Guinedi A.S., Mortada N.D., Mansour S., & Hathout R.M. (2005). Preparation and evaluation of reverse-phase evaporation and multilamellar niosomes as ophthalmic carriers of acetazolamide. ***International journal of pharmaceutics,*** **306(1–2), 71-82.**

Higuchi T. (1963). Mechanism of sustained-action medication. Theoretical analysis of rate of release of solid drugs dispersed in solid matrices. ***Journal of pharmaceutical sciences,*** **52(12), 1145-1149.**

Hixson A.W., Crowell J.H. (1931). Dependence of Reaction Velocity upon surface and Agitation. ***Industrial & Engineering Chemistry,*** **23(8), 923-931.**

Hougeir F.G., Kircik L. (2012). A review of delivery systems in cosmetics. ***Dermatologic Therapy,*** **25(3), 234-237.**

Imura T., Gotoh T., Otake K., Yoda S., Takebayashi Y., Yokoyama S., Takebayashi H., Sakai H., Yuasa M., & Abe M. (2003). Control of physicochemical properties of liposomes using a supercritical reverse phase evaporation method. ***Langmuir,*** **19(6), 2021-2025.**

Jesorka A., Orwar O. (2008). Liposomes: technologies and analytical applications. ***Annu.Rev.Anal.Chem.,*** **1, 801-832.**

Johnsson M., Bergstrand N., & Edwards K. (1999). Optimization of drug loading procedures and characterization of liposomal formulations of two novel agents intended for boron neutron capture therapy (BNCT). Journal of Liposome Research, 9(1), 53-79.

Jung J., Perrut M. (2001). Particle design using supercritical fluids: literature and patent survey. ***The Journal of Supercritical Fluids,*** **20(3), 179-219.**

Junyaprasert V.B., Teeranachaideekul V., & Supaperm T. (2008). Effect of charged and non-ionic membrane additives on physicochemical properties and stability of niosomes. ***AAPS PharmSciTech,*** **9(3), 851-859.**

Kim H., Fassihi R. (1997). Application of binary polymer system in drug release rate modulation. 2. Influence of formulation variables and hydrodynamic conditions on release kinetics. Journal of pharmaceutical sciences, 86(3), 323-328.

Kinka R., Gotoh T., Wongtrakul P., Hashimoto S., & Abe M. (2005). Preparation of niosomes by a supercritical reverse phase evaporation method without using co-solvents-Effects of the pressure on the trapping efficiency-. ***MATERIAL TECHNOLOGY,*** **23(4), 241-246.**

Korsmeyer R.W., Gurny R., Doelker E., Buri P., & Peppas N.A. (1983). Mechanisms of solute release from porous hydrophilic polymers. International journal of pharmaceutics, 15(1), 25-35.

Kunastitchai S., Pichert L., Sarisuta N., & Müller B.W. (2006). Application of aerosol solvent extraction system (ASES) process for preparation of liposomes in a dry and reconstitutable form. *International journal of pharmaceutics*, 316(1–2), 93-101.

Lasic D.D. (1988). The mechanism of vesicle formation. *The Biochemical journal*, 256(1), 1-11.

Lesoin L., Boutin O., Crampon C., & Badens E. (2011). CO2/water/surfactant ternary systems and liposome formation using supercritical CO2: A review. *Colloids and Surfaces A: Physicochemical and Engineering Aspects*, 377(1–3), 1-14.

Lin K., Cox-Stouffer S., Kennedy P., & Jackson T. (2003). Expansion of supercritical methane/ethylene jets in a quiescent subcritical environment. *AIAA Paper*, 483, 2003.

Liu J., Han B., Wang Z., Zhang J., Li G., & Yang G. (2002). Solubility of Ls-36 and Ls-45 surfactants in supercritical CO2 and loading water in the CO2/water/surfactant systems. *Langmuir*, 18(8), 3086-3089.

Makino K., Yamada T., Kimura M., Oka T., Ohshima H., & Kondo T. (1991). Temperature- and ionic strength-induced conformational changes in the lipid head group region of liposomes as suggested by zeta potential data. *Biophysical chemistry*, 41(2), 175-183.

Manosroi A., Chutoprapat R., Abe M., & Manosroi J. (2008). Characteristics of niosomes prepared by supercritical carbon dioxide (scCO< sub> 2</sub>) fluid. *International journal of pharmaceutics*, 352(1), 248-255.

Manosroi A., Chutoprapat R., Abe M., & Manosroi J. (2010). Characteristics of niosomes entrapped with rice bran bioactive compounds prepared by supercritical carbon dioxide. In *Nanoscience and Nanotechnology (ICONN), 2010 International Conference on, .*

Meure L.A., Knott R., Foster N.R., & Dehghani F. (2008). The depressurization of an expanded solution into aqueous media for the bulk production of liposomes. *Langmuir*, 25(1), 326-337.

Mohammadi M., Ghanbarzadeh B., Hamishehkar H., Mokarram R.R., & Mohammadifar M.A. (2014). Physical properties of vitamin D3-loaded nanoliposomes prepared by thin layer hydration-sonication. *Iranian Journal of Nutrition Sciences & Food Technology*, 8(4), 175-188.

Nasr M., Mansour S., Mortada N.D., & Elshamy A.A. (2008). Vesicular aceclofenac systems: A comparative study between liposomes and niosomes. *Journal of microencapsulation*, 25(7), 499-512.

National Institute of Health. (2014). Dietary Supplement Fact Sheet. , 2014(July).

Pidgeon, C., & Hunt, C. A. (1981). Calculating number and surface area of liposomes in any suspension. Journal of pharmaceutical sciences, 70(2), 173-176.

Otake K., Imura T., Sakai H., & Abe M. (2001). Development of a new preparation method of liposomes using supercritical carbon dioxide. *Langmuir*, 17(13), 3898-3901.

Otake K., Shimomura T., Goto T., Imura T., Furuya T., Yoda S., Takebayashi Y., Sakai H., & Abe M. (2006). Preparation of liposomes using an improved supercritical reverse phase evaporation method. ***Langmuir*****, 22(6), 2543-2550.**

Raudino A., Zuccarello F., La Rosa C., & Buemi G. (1990). Thermal expansion and compressibility coefficients of phospholipid vesicles: experimental determination and theoretical modeling. ***Journal of Physical Chemistry*****, 94(10), 4217-4223.**

Ritger P.L., Peppas N.A. (1987). A simple equation for description of solute release I. Fickian and non-fickian release from non-swellable devices in the form of slabs, spheres, cylinders or discs. Journal of Controlled Release, 5(1), 23-36.

Santo I.E., Campardelli R., Albuquerque E.C., de Melo S.V., Della Porta G., & Reverchon E. (2014). Liposomes preparation using a supercritical fluid assisted continuous process. ***Chemical Engineering Journal*****, 249(0), 153-159.**

Schwartz J.B., Simonelli A.P., & Higuchi W.I. (1968). Drug release from wax matrices I. Analysis of data with first-order kinetics and with the diffusion-controlled model. ***Journal of pharmaceutical sciences*****, 57(2), 274-277.**

Seebald P., Sojka P. (2011). Supercritical and Transcritical Injection. In Anonymous ***Handbook of Atomization and Sprays.*** **(, pp. 255-261). Springer.**

Siepmann J., Peppas N.A. (2011). Higuchi equation: Derivation, applications, use and misuse. ***International journal of pharmaceutics*****, 418(1), 6-12.**

Sirignano W.A.,. (1999). ***Fluid dynamics and transport of droplets and sprays.*** **(). Cambridge University Press, Cambridge, U.K.**

Taylor T.M., Weiss J., Davidson P.M., & Bruce B.D. (2005). Liposomal Nanocapsules in Food Science and Agriculture. ***Critical reviews in food science and nutrition*****, 45(7-8), 587-605.**

Thoman C.J. (1999). The versatility of polysorbate 80 (tween 80) as an ionophore. ***Journal of pharmaceutical sciences*****, 88(2), 258-260.**

Thoman C.J. (1986). Lonophoric properties of polysorbate 80. ***Journal of pharmaceutical sciences*****, 75(10), 983-986.**

Uchegbu I.F., Vyas S.P. (1998). Non-ionic surfactant based vesicles (niosomes) in drug delivery. ***International journal of pharmaceutics*****, 172(1–2), 33-70.**

Uchegbu, I. F., & Florence, A. T. (1995). Non-ionic surfactant vesicles (niosomes): physical and pharmaceutical chemistry. Advances in colloid and interface science, 58(1), 1-55.

Van Aken, P. A., Liebscher, B., & Styrsa, V. J. (1998). Quantitative determination of iron oxidation states in minerals using Fe L 2, 3-edge electron energy-loss near-edge structure spectroscopy. ***Physics and Chemistry of Minerals, 25*****(5), 323-327.**

Weber M., Thies M.C. (2007). A simplified and generalized model for the rapid expansion of supercritical solutions. ***The Journal of supercritical fluids*****, 40(3), 402-419.**

Wen Z., Liu B., Zheng Z., You X., Pu Y., & Li Q. (2010). Preparation of liposomes entrapping essential oil from Atractylodes macrocephala Koidz by modified RESS technique. ***Chemical Engineering Research and Design*****, 88(8), 1102-1107.**

Wu P., Chen T.H., Nejad A.S., & Carter C.D. (1996). Injection of supercritical ethylene in nitrogen. ***Journal of Propulsion and Power*****, 12(4), 770-777.**

Xia S., Xu S. (2005). Ferrous sulfate liposomes: preparation, stability and application in fluid milk. ***Food Research International*****, 38(3), 289-296.**

Section II

Chapter 4: Supercritical fluid extraction of oil from potato chips: two scale comparison and mathematical modeling

4.1. Abstract

Oil was extracted from fried chipped potatoes using supercritical carbon dioxide. The goals of the study were to determine the effect of process parameters on the extraction, explore the scalability of the process, and determine useful kinetic parameters. Extraction conditions range 27.6-41.4MPa (4000-6000 PSI), 35-80°C and solvent flow rate of 0.5-5.0g CO_2/min. Up to 100% of the oil was recovered from the potato chips at the highest pressure and temperature conditions. Two process conditions were chosen for comparison of performance with a larger scale (1:5) system, maintaining the same CO_2 flow rate to feed mass ratio. Good agreement between scales was seen at the higher pressure and temperature settings. Kinetic parameters, calculated using a literature model, indicated that, as expected, the extraction is limited by internal diffusion.

4.2. Introduction

Fried snack foods are ubiquitous in supermarkets today, but as public demand for healthier food increases, the ability to provide a low-fat alternative to these consumer favorites will be economically advantageous. Post-frying oil extraction is one approach that can be used to produce lower-fat fried snack foods.

Supercritical fluid extraction (SFE) offers a safe alternative to conventional solvent extraction. Supercritical fluids have properties in between those of a gas and a liquid. With gas like-diffusivity and liquid-like density supercritical fluids have desirable solvating and mass

transport properties, but leave no solvent residue and can be employed using physiologically benign chemicals, such as carbon dioxide. The physicochemical properties of supercritical fluids are well established and the advantages have been documented in many publications (McHugh and Krukonis, 1994; Rizvi *et al.* 1986a; Rizvi *et al.* 1986b).

Supercritical carbon dioxide (SC-CO_2) has been used for many years in the food industry for the decaffeination of coffee and flavor extraction from hops (Sahena *et al.* 2009). Though industrial success is largely limited to high value extracts, research has demonstrated that SC-CO_2 can also be used for the extraction of lipids from a variety of food matrices such as chicken nuggets and french fried potatoes (Devineni *et al.* 1997), omega-3 fatty acids from fish by products (Rubio-Rodriguez *et al.* 2008), and oil from oil seeds (Seal *et al.* 2008). The high capital investment required for SFE limits its use in fat reduction for snack foods, but post-frying oil extraction could allow for the recovery of high value flavor compounds or oil to be recycled into the fryer, thus offsetting the cost.

In order to assess the feasibility of industrial scale SFE for the reduction of fat from snack foods, the scalability of the process must be investigated. Several studies have been done on the extraction of oil from potato chips (Vijayan *et al.*, 1994; Levy *et al.,* 1994; Neff *et al.* 2002), but information on scalability and modeling of oil extraction in the literature is limited. Clavier and Perrut (2004) suggested strategies for approaching scale up of SC-CO_2 processes based on the mass transfer mechanism:

1) For processes where solubility is the limiting mechanism, the ratio of solvent mass to feed mass should be kept constant between small and large scales

2) For processes where internal diffusion is the limiting mechanism, the solvent flow rate to mass of feed ratio should be kept constant between small and large scales

3) For process where both diffusion and solubility are limiting, both the ratio of solvent mass to mass of feed ratio and the solvent flow rate to mass of feed ratio should be kept constant between small and large scales

Several mathematical models based on differential mass balance and equilibrium relations have been developed to describe and quantify SFE of various natural products (King and Catchpole 1993; Reverchon *et al.* 1993; Goto *et.al* 1993). Sovova (1994; 2005) described extraction of oil from milled vegetable containing a proportion of broken and intact cells. The model assumes broken cells at the particle surface contain easily accessible solute which is directly transferred to the fluid phase and controlled by phase equilibrium, giving rise to a constant extraction rate. Intact cells inside the particle contain solute that must diffuse into intercellular space before being swept into the fluid phase. Internal solid phase mass transfer occurs at a rate several orders of magnitude lower than the fluid phase mass transfer, giving rise to falling extraction rates and diffusion controlled segments of the extraction process. The Sovova model has been applied to the extraction of non-polar compounds from many substances including clove buds, eucalyptus leaves, ginger rhizomes (Rodrigues *et al.* 2002), apricot kernels (Ozkal *et al.* 2005), chamomile flowers (Povh *et al.* 2001), and rosemary leaves (Bensebia *et al.* 2009).

The objectives of the present study were to:

1) Investigate, the effects of temperature, pressure, and flow rate on the extraction of oil from potato chips
2) Determine kinetic parameters using the model of Sovova
3) Compare extraction profiles at two scales
4) Fractionate extract in line with sequential pressure step downs and investigate the fraction compositions.

4.3. Materials and methods

4.3.1. Raw material

Potato chips were commercial products prepared without salt and fried in sunflower oil. The chips pale yellow in color and elliptical in shape with an average area of 14.8 cm^3 and had an average thickness of 0.13 cm. Bent, broken, and discolored chips were discarded. Chips were kept sealed and frozen at -20°C and brought to room temperature before use. Total available oil content of the sample was determined by Soxhlet using a FOSS Tecator Soxtec HT2 (Hillerod, Denmark). The solvent used was petroleum ether.

4.3.2. Extraction procedure

Laboratory scale extractions were carried out using an SFT-250 SFE/SFR System (Supercritical Fluid Technologies, Newark, DE, USA) equipped with a 100 ml extraction vessel and a single separator (denoted as E100). The vessel had a length to diameter ratio of 4.6 (13.97cm height, 3.02 cm internal diameter) and a porous disc at the solvent inlet for even solvent distribution. For each experiment 10g of sample was loaded into a stainless steel mesh basket with glass beads at the base to ensure evenly distributed flow of solvent through the bed. The basket was then lowered into the extraction vessel, which was then preheated to 8°C below the desired extraction temperature in order to account for the increase in temperature that occurs when pressure builds up in the vessel. The solvent used was carbon dioxide (siphon tube tank, 99.9% purity, Airgas, Elmira, NY, USA). The dynamic extraction method was employed with the collection valve constantly open. Extract weight was measured every ten minutes. The experiment was stopped when the amount of extract remained constant for two sampling periods. The collection valve was left open as the system depressurized to allow any oil remaining in the separator to be collected and the total mass was determined after the system completely depressurized. Three repetitions were performed for each extraction experiment.

4.3.3. Scale up

In order to determine the scalability of the extraction of oil from potato chips, a custom built extraction/fractionation system equipped with a 500 ml extraction vessel (denoted as E500) was used (Figure 4.1.).

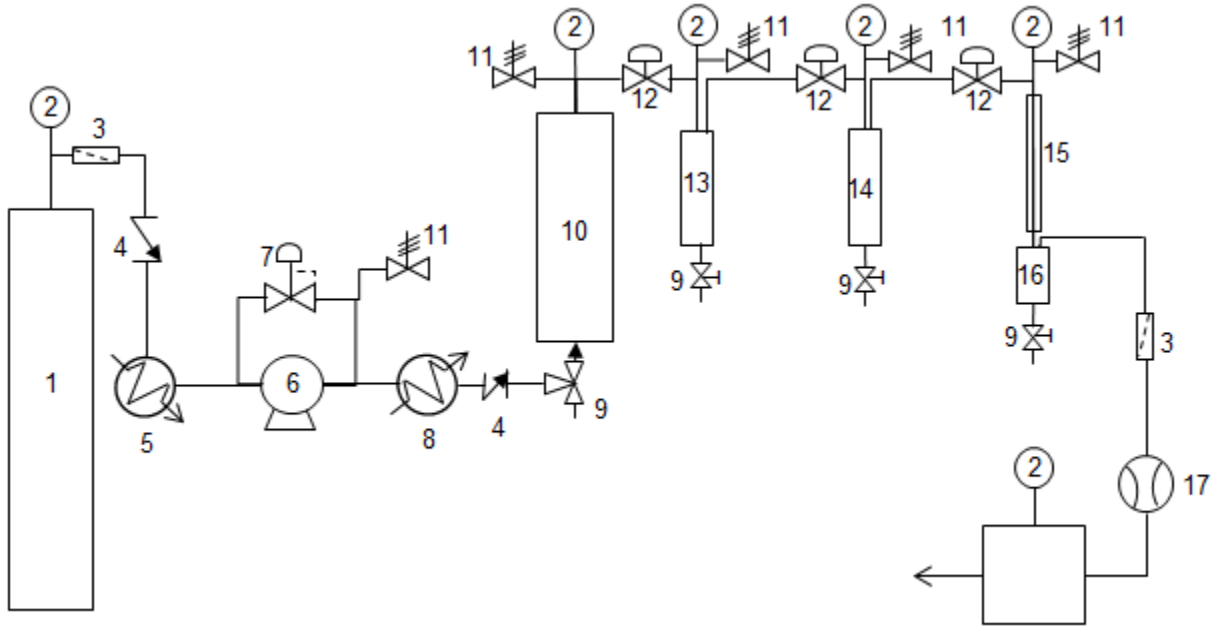

Figure 4.1. E500 extraction unit diagram. 1) CO_2 tank 2) pressure gauge 3) filter 4) check valve 5) cooling bath 6) pump 7) back pressure regulator 8) preheating water bath 9) drain valve 10) extraction vessel 11) pressure relief valve 12) forward pressure regulator 13) separator 1 14) separator 2 15) condenser 16) separator 3 17) flow meter 17) gas totalizer

The vessel had a length to diameter ratio of 4 (22.2 cm length, 5.6 cm internal diameter) and a porous disc at the solvent inlet for even solvent distribution. Whole, unbroken chips were placed in a custom built stainless steel basket and then lowered into the extraction vessel. The scale up criterion selected for this experiment was to maintain the solvent mass flow rate to feed mass ratio, as suggested by Clavier and Perrut (2004) where internal diffusion is the limiting factor in extraction. Extraction procedure was the same except that collection valve was opened only for a short time before measurement of extract weight. This should not affect extraction yield

(Prado *et al.* 2011).

4.3.4. Oil fractionation

Oil was also fractionated concurrently with extraction using E500. Three separators were used in series. The first separator was maintained at 10.3MPa and 80°C. The second separator was maintained at atmospheric pressure and 80°C. The third separator was maintained at atmospheric pressure and was kept cold using condenser circulating water at 5°C in an attempt to trap volatile portions of the extract that may pass through the first two separators. Three repetitions were performed for each fractionation experiment.

4.3.5. Fractionated extract analysis

Fatty acid composition of the fractionated extract was determined using an HP 5890A Gas Chromatograph (GC) equipped with a Supelco SP-2380 capillary column (30m x 0.25mm x 0.25 μm) and a flame ionization detector (FID). Helium was used as the carrier gas with a linear velocity of 20cm/sec. The oven was held at 150°C for 4 minutes, then ramped up to 250°C at 4°C/min and held at 250°C for 5 minutes. The detector was held at 300°C and the injector was operated at 250°C with a split ratio of 1:100. SC-CO_2 fractionated oil samples were derivitized to fatty acid methyl esters (FAMEs) following AOAC Method 965.49 and composition calculations were performed following AOAC method 963.22. A standard solution of FAMEs (Sigma-Aldrich) was prepared for peak identification and area correction.

Triglyceride composition of the fractionated extract was determined using the same HP5890A GC using cool-on-column injection with a Supelco MET-Biodiesel column (14m x 0.53mm x 0.16 μm) with an integrated 2 m guard. AOAC method 986.19 was followed in order to determine the triglyceride composition with the following oven conditions: hold at 200°C for

one minute, then ramp up at 25°C/min to 370°C and hold for 5 minutes. The FID was set to 390°C. Helium was used as a carrier gas and the column head pressure was set to 62 kPa. Triglyceride analytical standard mix used for peak identification and response factor determination was purchased from Sigma-Alrdrich. Six total repetitions were performed for each fatty acid and triglyceride analysis.

4.3.6. Particle size

In this study three different particle sizes were used. For experiments performed in E100, potato chips were ground using a mortar and pestle and then sieved between 0.24cm and 0.14m. Because the varying shape and size of the potato chips could cause non-uniformities in the extraction bed and problems with modeling, grinding was used to standardize the particle size. However, the end goal of the study was to extract oil from intact potato chip. In order to determine the effect of particle size, whole chips were broken into pieces small enough to fit into E100 (area 3.25cm^2, average thickness 0.13cm) and the extraction results were compared with those of ground chips. For experiments performed in E500, whole unbroken chips were used with average thickness of 0.13cm.

4.3.7. Mathematical modeling and kinetic parameters

The model of Sovova (1994) was used to determine the mass transfer coefficient from the fluid phase, $k_y a$, and from the solid phase, $k_x a$. The model assumes pseudo-steady state, plug flow with constant pressure, temperature, and solvent velocity with homogenous bed composition. The mass balance for the solid and fluid phase is given as:

Solid phase:

$$-\rho_s(1-\varepsilon)(\partial X/\partial t) = J(X,Y) \qquad (4.1)$$

Fluid phase:

$$\rho_f (U)(\partial Y/\partial h) = J(X,Y) \qquad (4.2)$$

Where ρs and ρf are the solid and fluid phase densities, respectively, X and Y are the solute mass ratio in the solid and fluid phase respectively, ε is the void fraction in the bed, U is the superficial velocity, *t* is time, *h* is the axial coordinate, and J(X,Y) is the interfacial mass transfer rate per volume of fixed bed (kg/m^3s).

The overall extraction curve was modeled in three regimes corresponding to the constant extraction rate (CER) period, falling extraction rate (FER) period, and diffusion controlled (DC) period. The equation solved by Sovova (1994) can be written (Povh *et.al* 2001):

For the CER period $t<t_{CER}$ $\quad m_{extract}=Y^*[1-\exp(-Z)]Q_{CO2}t \qquad (4.3)$

For the FER period $t_{CER}<t<t_{FER}$ $\quad m_{extract}=Y^*[(t-t_{CER}\exp(z_w-Z)]Q_{CO2} \qquad (4.4)$

For the DC period $t>t_{FER}$ $\quad m_{extract}=N\{X_o-(Y^*/W)\ln\{1+[\exp(WX_o/Y^*)-1]\}\exp[(WQ_{CO2}/N)(t_{CER}-t)](X_k/X_o)\} \qquad (4.5)$

With the following definitions:

$$Z= (Nk_{Ya}\rho_{CO2})/(Q_{CO2}(1-\varepsilon)\rho_s) \qquad (4.6)$$

$$t_{cer} = [(X_o-X_k)/(Y^*Z)][N/Q_{CO2}] \qquad (4.7)$$

$$X_p = X_o-X_k \qquad (4.8)$$

$$z_w/Z = (Y^*/WX_o)\ln\{[(X_o\exp\{(WQ_{CO2}/N)(t-t_{cer})-X_k\}]/[X_o-X_k]\} \qquad (4.9)$$

$$W= [Nk_{Xa}]/[Q_{CO2}(1-\varepsilon)] \qquad (4.10)$$

$$t_{FER} = t_{CER} + (N/Q_{CO2}W)\ln[X_k + \{X_o-X_k)\exp(WX_o/Y^*)\}/X_o] \qquad (4.11)$$

Where m_{ext} is the mass of extract at time t, N is the mass of inert solid, Y* is the solubility of the extract in the solvent, Q_{CO2} is the solvent mass flow rate, k_{Ya} is the fluid phase mass transfer coefficient (min^{-1}), k_{Xa} is the solid phase mass transfer coefficient (min^{-1}), X_o is the initial solute mass ratio in the solid phase, X_k is the solute mass ratio for un-ruptured cells in the

solid phase, X_p is the solute mass ratio for the easily accessible solute also in the solid phase, t_{CER} is the time at the end of the constant extraction rate period, t_{FER} is the time at the end of the falling extraction rate period, and Z and W are adjustable parameters of the model. Excel 2007 Solver function was used to fit the model to the experimental data.

4.3.8. Statistical analysis

ANOVA was used to assess the influence of particle size on extraction and Fisher's LSD test was applied to determine the influence of operating parameters. ANOVA was also used to assess the differences among separator oil profiles after fractionation. All statistical analyses were performed using JMP 9 (SAS, Cary, NC, 27513).

4.4. Results and discussion

4.4.1. Effect of particle size

In order to determine if particle size reduction had a statistically significant influence on extraction, two different particle sizes were compared in E100 at 34.5 MPa and 57.5°C. The comparison of overall extraction curves for ground chips (0.14-0.24cm diameter) and broken chips (area 3.25cm^2, thickness 0.13cm) can be seen in Figure 4.2.

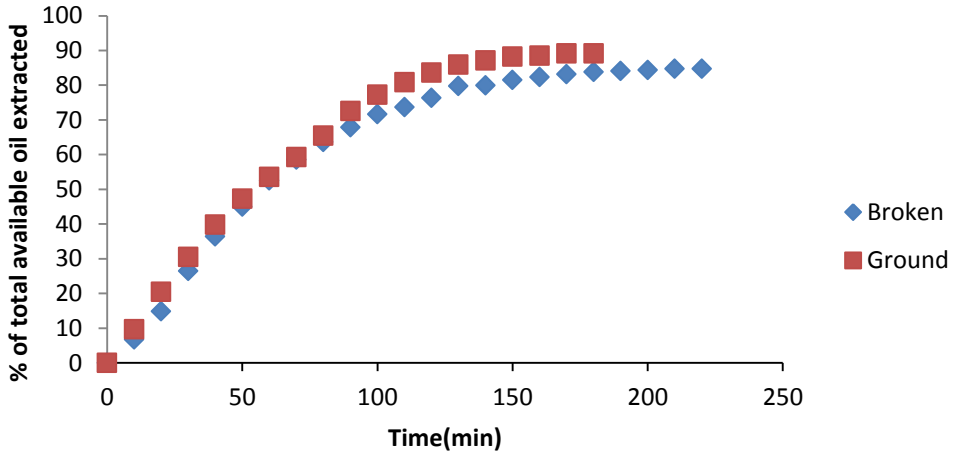

Figure 4.2. Comparison of total percentage of oil extracted from ground potato chips and broken potato chips at 34.5 MPa and 57.5°C with a flow rate of 5g CO_2/min

Data did not show a statistically significant difference in total amount of oil extracted ($p=0.53$) and one way ANOVA did not indicate a statistically significant effect of particle size on the extraction ($p=0.0786$). Grinding of the sample is common for SFE when the matrix limits solvent to solute contact or could cause channeling of the solvent through the sample bed. Potato chips are porous in structure and therefore tend to have a large surface area, allowing for high exposure of the solute to the solvent. The increase in surface area as a result of grinding to this particle size does not seem to enhance extraction, indicating that in this case the chip thickness is the controlling factor.

4.4.2. Effect of operating conditions on extraction

Table 4.1. presents a summary of the operating conditions used in this study, percentage of total available oil extracted, and time to reach constant weight of extract. Total percentage of oil extracted is in keeping with the results of other studies on potato chips (Vijayan *et al.*, 1994; Levy *et al.,* 1994). As pressure increases from 27.6 MPa to 34.6 MPa, the time to reach constant extract weight decreases. This is expected due to the increased density and therefore increased solvating power of SC-CO_2. As pressure increases from 34.5MPa to 41.4MPa, little difference is seen in the duration of the extraction.

The influence of temperature on extraction is illustrated in Figures 4.3. and 4.4. At 27.6 MPa and 34.5 MPa, as expected, as temperature increases, the total amount of extracted oil tends to decrease due to a decrease in SC-CO_2 density. However, at 41.4 MPa, as temperature increases, an increase in the total amount of extracted oil is observed. At higher pressures, as temperature increases the density of SC-CO_2 decreases more slowly than at lower pressures. With this higher pressure setting, the increase in vapor pressure of the solute that occurs with

increasing temperature is able to overcome the decreased solvating power of the SC-CO_2. This phenomenon of divergent effect of temperature is often referred to as the "crossover" point in the literature.

Table 4.1. Effect of operating conditions[a] on percentage of oil extracted

Pressure (MPa)	Temperature (C)	ρ_{CO2} (g/ml)	Oil extracted (%)[b]	Time (min)
41.4	80	0.8280	$100.9^{a} \pm 5.05$	180
	57.5	0.9023	$96.1^{ab} \pm 1.10$	180
	35	0.9752	$89.5^{bc} \pm 3.74$	210
34.5	80	0.7812	$91.7^{ab} \pm 0.79$	173
	57.5	0.8662	$93.5^{ab} \pm 2.11$	177
	35	0.9480	$97.2^{ab} \pm 2.65$	240
27.6	80	0.7150	$80.1^{c} \pm 4.35$	340
	57.5	0.8184	$91.4^{ab} \pm 2.52$	280
	35	0.9142	$91.6^{ab} \pm 1.89$	330

[a]ground chip particle size=0.14-0.24cm; flow rate = 5g CO_2 /min

[b]Percentage based on soxhlet results for total oil; data reported as mean ± standard deviation, n=3; data with same letter superscripts were not significantly different (Fisher's LSD, $a = 0.05$)

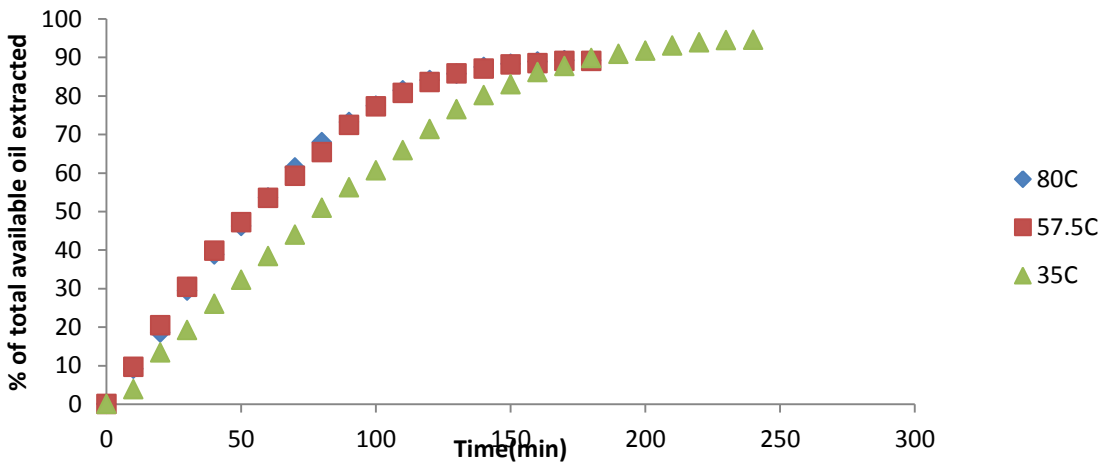

Figure 4.3. Effect of temperature on OEC of ground potato chips at 34.5 MPa with a flow rate of 5g CO_2/min

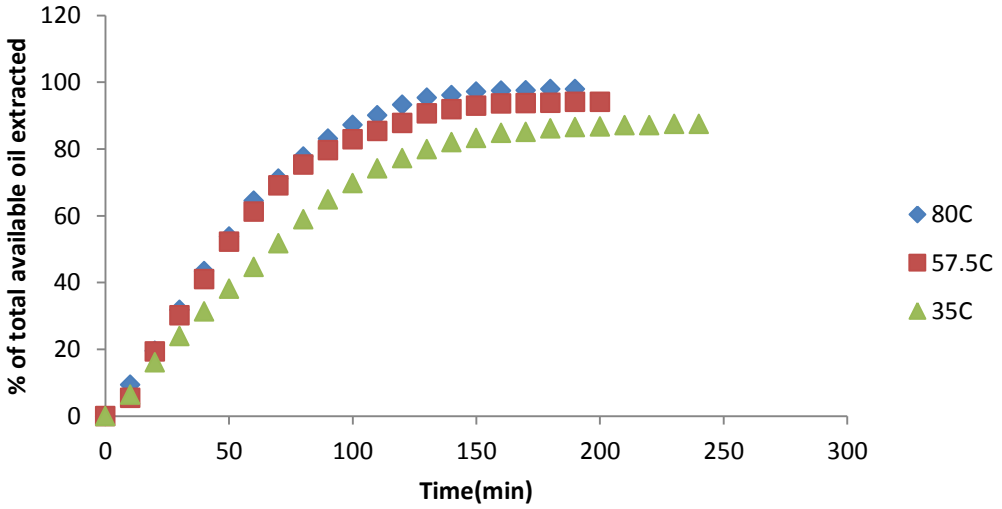

Figure 4.4. Effect of temperature on OEC of ground potato chips at 41.4 MPa with a flow rate of 5g CO_2/min

At a fixed temperature, increased pressure generally leads to greater extraction because of increased solvent density and therefore solvating power. Figure 4.5. shows the effect of increasing pressure at 80°C.

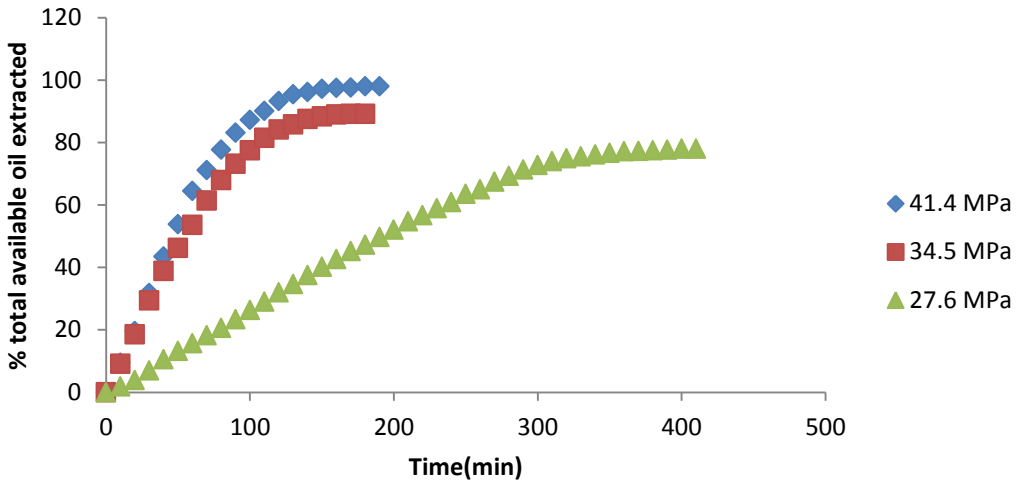

Figure 4.5. Effect of pressure on OEC of ground potato chips at 80°C with a flow rate of 5g CO_2/min

Not only is the total amount that can be extracted higher at 41.4 MPa in comparison to 27.6 MPa, but the rate of extraction was nearly twice as fast . Similar results were seen for extractions performed at 57.5°C. Because the time to reach constant extract weight was different for each experimental setting, the percentage of total oil extracted was compared at a fixed time interval of 180 minutes in Figure 4.6.

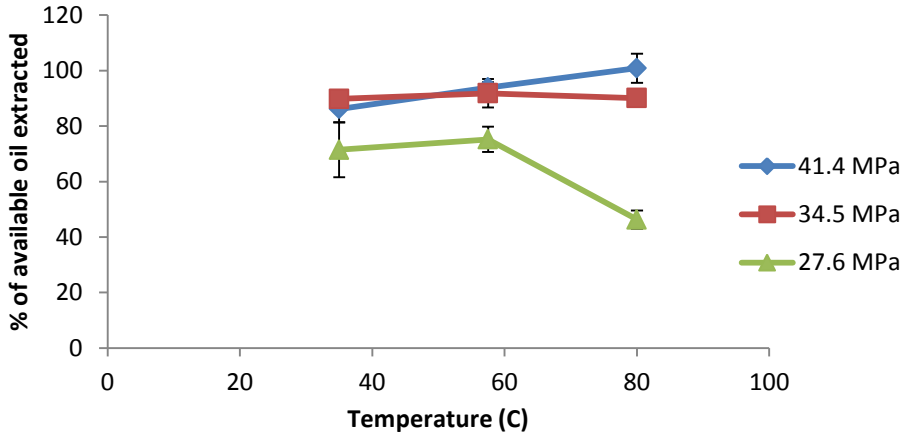

Figure 4.6. Comparison of total percentage of oil extracted from ground potato chips at 180 min with a flow rate of 5g CO_2/min

The relationship of increased total extraction with increased pressure holds for the two higher

temperatures, but not for the low temperature of 35°C. At this low temperature, total extraction increases from 27.6 MPa to 34.5 MPa, but decreases from 34.5 MPa to 41.4 MPa. Similar results were seen using SC-CO_2 extraction of lycopene from tomato skins (Topal *et al.* 2006), fatty acids from trout powder (Nei *et al.* 2008), and loquat seeds (Machmuda *et al.* 2008). Vijayan *et al.* (1994) observed similar results with potato chips where increasing from 41.4 MPa to 55.2 MPa at 50°C caused a decrease in extraction. Mixtures of vegetable oils in SC-CO_2 exhibit Type III phase behavior, as classified by van Konynenburg and Scott (1980), so isothermal increases in pressure can result in a solubility maximum for vegetable oils(Lira 1996).

The effect of flow rate on the overall extraction curve at 41.4 MPa and 80°C can be seen in Figure 4.7. No difference was observed in the total amount of available oil extracted, however there was a clear difference in the rate of extraction as well as the total time required to reach constant extract weight.

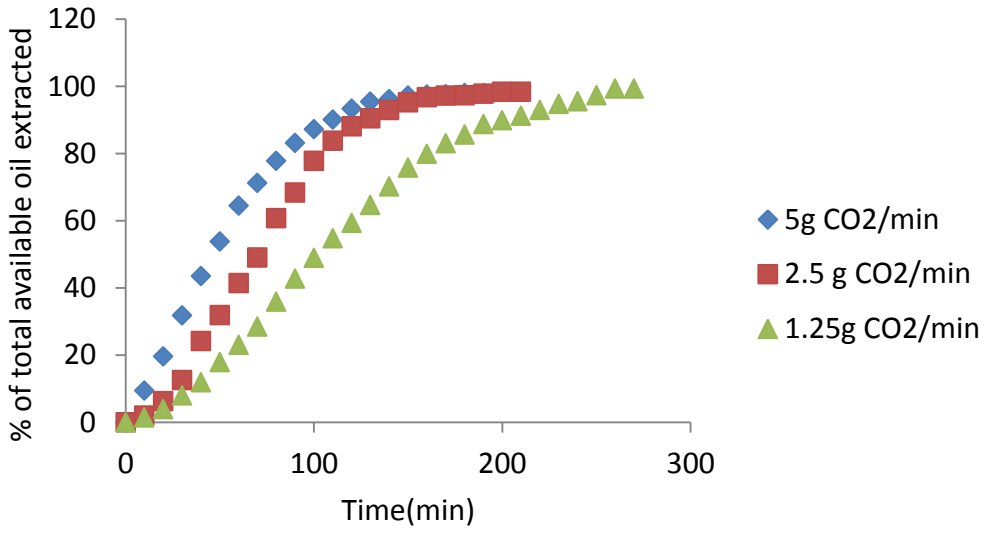

Figure 4.7. Effect of varying flow rate on OEC's at 41.4 MPa and 80°C

The initial straight line portion of the extraction curve is marked by extraction of solute that is freely available at the surface. Thus, the concentration of solute in the supercritical fluid

is independent of matrix effects during this time and can be considered equivalent to solubility. If an overall extraction curve (OEC) has a constant extraction period, it does not necessarily indicate that the true solubility of solute was obtained (Rodrigues *et al.* 2002), but only its flow rate dependent "extractability". The effect of flow rate on extractability, calculated as the slope of the CER period divided by the mass flow rate of CO_2, can be seen in Figure 4.8.

In all cases, as flow rate decreases from 5g CO_2/min to 1.25g CO_2/min, the extractability increases. As the flow rate decreases further below 1.25g CO_2/min, the extractability decreases. This phenomenon is explained by Rodrigues *et al.* (2002). At flow rates above this peak value, the solvent may move too quickly through the bed and exit the extractor unsaturated. At slower flow rates, axial dispersion, or back-mixing, may decrease the concentration gradient and cause the solvent to leave the vessel unsaturated.

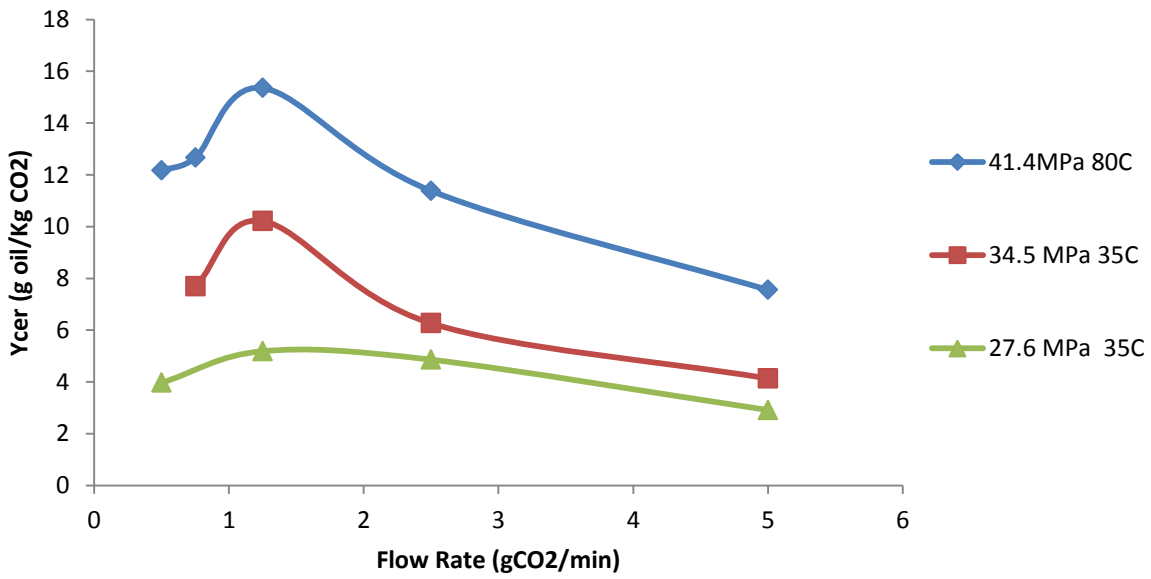

Figure 4.8. Influence of flow rate on extractability of oil from ground potato chips

Understanding the influence of solvent flow rate is important for optimization at an

industrial level. Table 4.2. illustrates the trade-off between speed and efficient use of resources in this process.

Table 4.2. Effect of flow rate on time to reach 50% total oil reduction and CO_2 usage

Flow rate (g CO_2/min)	M_{CER} [ab] (g/min)	M_{CER} [c] (%/min)	Time to 50% of total oil extracted (min)	CO_2 used (g)
5	0.038	1.08	46	230
2.5	0.028	0.81	62	155
1.25	0.019	0.55	91	114
0.75	0.0095	0.27	185	139
0.5	0.0061	0.17	294	147

[a]M_{CER} = slope of the initial constant extraction rate period
[b]Data from extraction of ground chips in E100 at 41.4 MPa and 80°C
[c]Percentage based on average initial oil content of chips

At a flow rate of 1.25g CO_2/min, 50% of the total oil can be extracted in about 91 minutes, consuming 114 g of CO_2. At a flow rate of 5g CO_2/min, the same amount can be extracted in about half the time, but CO_2 consumed roughly doubles. Higher flow rates allow for faster processing, but require greater inputs of energy.

4.4.3. Kinetic parameters Estimation

Sovova's model was fitted to the experimental data using Excel 2007 Solver function to determine the model parameters Z, W, and X_k by minimizing the sum of squared differences between the experimental and model predicted data. Y* was taken as the greatest measured extractability determined from the flow rate experiments. Comparisons of the experimental and model predicted data are presented in Figure 4.9.

X_k remained fairly constant, which is reasonable because this should be independent of the extraction conditions. Kinetic parameters calculated using Sovova's model are presented in Table 4.3.

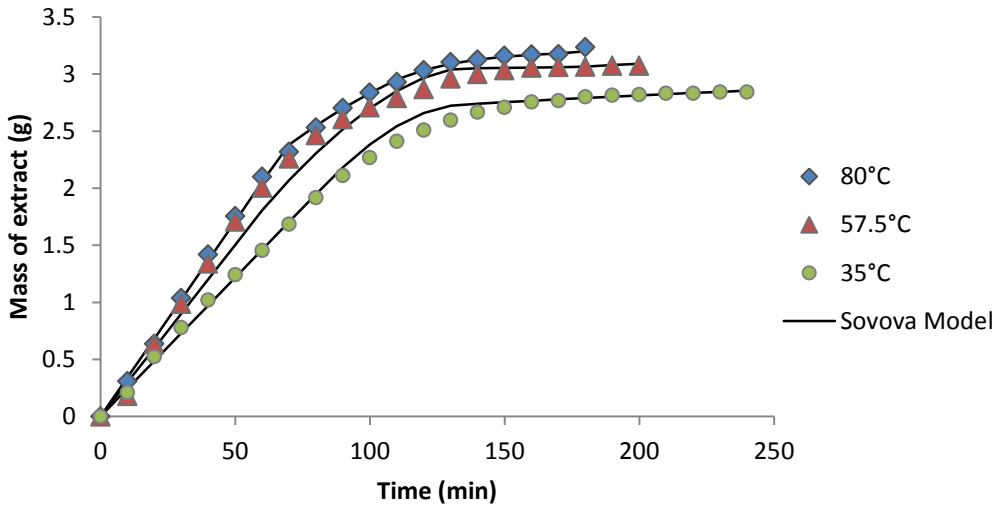

Figure 4.9. Comparison of experimental data with Sovova's model at 41.4MPa

Table 4.3. Kinetic parameters estimated using Sovova's model

P(MPa)	T(°C)	M_{CER} X 10^2 (g/min)[a]	T_{CER} (g/min)	Y_{CER} (g/kg CO_2)[a]	CO_2 density (kg/m^3)	k_{ya} (min^{-1})	k_{xa} x 10^3 (min^{-1})	MSE[b]
41.4	80	3.78 ± 0.60	60.25	7.55 ± 1.19	828	0.704	4.02	0.0009
	57.5	3.35 ± 0.62	64.90	6.71 ± 1.24	902	0.646	3.57	0.0108
	35	2.54 ± 0.55	80.25	5.08 ± 1.10	975	0.603	2.70	0.0037
34.5	80	3.26 ± 0.84	65.03	6.51 ± 1.68	781	1.223	3.47	0.0190
	57.5	3.26 ± 0.41	72.33	6.53 ± 0.83	866	1.018	3.47	0.0114
	35	2.07 ± 0.23	102.45	4.13 ± 0.47	949	0.472	2.20	0.0026
27.6	80	0.86 ± 0.12	138.25	1.73 ± 0.23	715	2.666	0.92	0.0005
	57.5	1.44 ± 0.11	156.54	2.89 ± 0.21	818	1.590	1.54	0.0012
	35	1.46 ± 0.44	194.97	2.91 ± 0.88	914	0.849	1.55	0.0017

[a]Data presented as average of three ± standard deviation
[b]MSE= mean squared error for model curve fit to experimental data

M_{CER} was calculated as the slope of the initial constant portion of the extraction. T_{CER} was calculated as the intersection of the line fitted to the CER period and the line fitted to the FER period. The mass transfer coefficient from the fluid phase, k_{Ya}, was calculated using equations (1) and (4). The mass transfer coefficient from the solid phase, k_{Xa}, was calculated using the following definitions presented by Povh *et al.* (2001).

$$k_{Xa} = [K_{Ya}\rho_{CO2}\Delta Y]/[\rho_s \Delta X] \quad (4.12)$$

$$\Delta Y = M_{CER}/(\rho_{CO2} S H k_{Ya}) \quad (4.13)$$

$$\Delta X = (X_p + X_k)/2 \quad (4.14)$$

The results in Table 4.3. agree with the findings of Ozkal *et al.* (2005). The mass transfer coefficient of the fluid phase, k_{Ya}, decreases with increasing pressure because the diffusivity of SC-CO_2 decreases with increasing pressure (Ozkal *et al.* 2005; Rezaei *et al.* 2000; Liong *et al.* 1992). The mass transfer coefficient of the solid phase, k_{Xa}, increased with increasing pressure, which may be due to greater destruction of the internal cellular structure at high pressure (Ozkal *et al.* 2005). When the extracted sample was removed from the extraction vessel, a small amount of very fine particles could be seen inside the vessel, indicating destruction of some of the cellular structures within the chip.

4.4.4. Scale up

The two experimental settings that resulted in the highest extraction using E100, 34.5 MPa at 35°C and 41.4 MPa at 80°C, were selected for scalability trials. The feed mass to solvent mass flow rate ratio in E100 was 2:1, which was maintained in the scale up experiments performed in E500. In the interest of investigating the usefulness of this process to manufacturers and because little effect of particle size reduction was observed, whole chips were used. Figure 4.10. and Figure 4.11. show OEC's at 41.4 MPa and 80°C and 34.5 MPa and 35°C,

respectively, using E100 and E500.

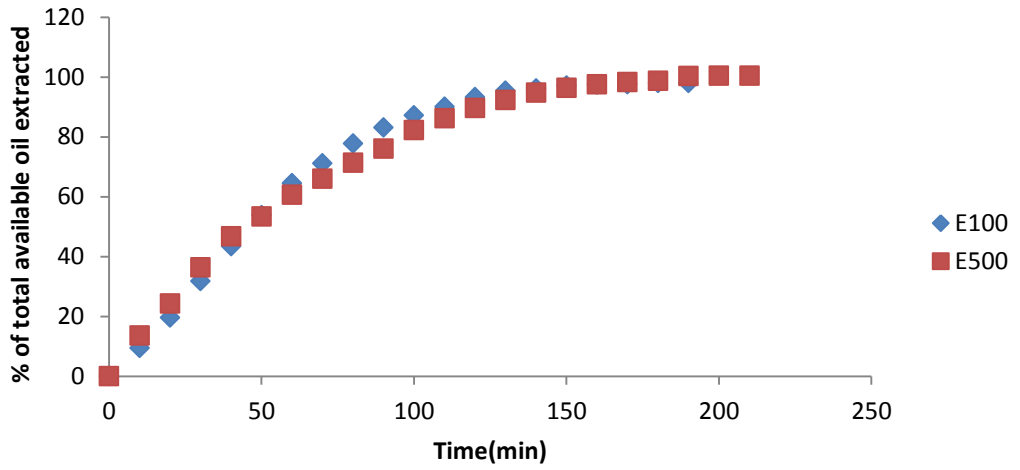

Figure 4.10. Comparison of OEC's at 41.4 MPa and 80°C of small scale (E100) and larger scale (E500). Extractions in E100 carried out with 10g sample and a flow rate of 5g CO_2/min. Extractions in E500 carried out with 40g sample and a flow rate of 20g CO_2/min.

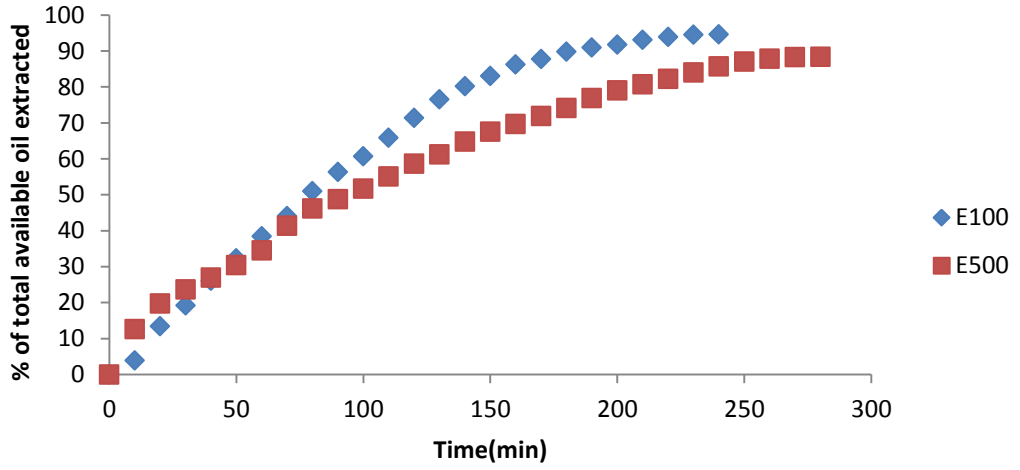

Figure 4.11. Comparison of OEC's at 34.5 MPa and 35°C of small scale (E100) and larger scale (E500). Extractions in E100 carried out with 10g sample and a flow rate of 5g CO_2/min. Extractions in E500 carried out with 40g sample and a flow rate of 20g CO_2/min.

At 41.4 MPa and 80°C, a one way ANOVA showed no difference between the small and large scale ($p=0.76$). However, a statistically significant difference was observed at the 34.5 MPa and 35°C setting ($p=0.028$). This indicates that maintaining mass to solvent flow rate ratio alone

may be inadequate for scaling up, and that additional parameters, such as solvent linear velocity, should also be taken into account.

Kinetic parameters were also calculated for the large scale unit and are compared with the small scale unit in Table 4.4. As with the OEC, very good agreement is seen with the small and large scale at 41.4 MPa and 80°C. Though the total amount extracted agreed well at 34.5 MPa and 35°C, but as expected, the calculated kinetic parameters did not show as good agreement due to the statistically significant differences in the OECs.

Table 4.4. Comparison of kinetic parameters at different experimental conditions using E100 and E500

	41.4 MPa, 80°C		34.5 MPa, 35°C	
	E100[a]	**E500[b]**	**E100[a]**	**E500[b]**
% Oil Extracted	101	102	97	96
Mcer(g/min)	0.038	0.15	0.021	0.066
Mcer(%total/min)	1.16	1.12	0.63	0.51
Ycer (g/Kg CO_2)	7.55	7.66	4.13	3.30
Tcer (min)	60.26	56.48	102.4	89.68
kya(min^{-1})	0.790	0.82	0.33	0.25
kxa (min^{-1})	0.004	0.002	0.0022	0.00076

[a]Vessel size = 100ml
[b]Vessel size = 500ml

4.4.5. Fractionated oil analysis

Higher molecular weight triglycerides are less soluble in SC-CO_2 and are expected to drop out of SC-CO_2 before the lower weight triglycerides as pressure is decreased. Fatty acid composition of each oil fraction is presented in Table 4.5.

Table 4.5. Fatty acid percent composition of fractionated extracts

	Sunflower oil [a]	41.4 MPa, 80°C		34.5 MPa, 35°C	
Fatty Acid		**S1[b]**	**S2[c]**	**S1**	**S2**
C16:0	3.83	3.75	4.86	4.53	4.51
C18:0	3.54	3.49	3.37	3.40	3.48
C18:1	63.76	63.19	58.86	63.41	63.63
C18:2	27.22	28.76	27.10	27.81	27.56
C18:3	0.19	0.27	0.27	0.27	0.29
C20:0	0.39	0.21	0.20	0.25	0.29
C20:1	0.39	0.21	0.21	0.24	0.23
C22:0	0.68	0.12	0.01	0.09	0.01

[a] All values reported as percent, n = 5
[b] S1= Separator 1, 10.13MPa
[c] S2= Separator 2, atmospheric pressure

Fatty acid composition of the oil is comparable to literature values reported for potato chips fried in mid-oleic sunflower oil (Lee and Pangloli, 2011). The first fraction obtained at 41.4MPa and 80°C shows a greater concentration of higher molecular weight fatty acids like oleic (18:1), linoleic (18:2), and behenic acid (22:0) than the second, lower pressure fraction. The fractions obtained at 34.5 MPa and 35°C show little difference in composition when compared to each other or the un-extracted oil. In all cases, the concentration of behenic acid was much lower than that of the un-extracted oil, which may indicate limited solubility of these fatty acids in SC-CO_2 at these conditions. However, triglyceride composition of the fractions may be more informative as separation occurs because of triglyceride molecular weight, as opposed to that of individual fatty acids.

Though high sensitivity and rapid analysis is possible trough GC-FID, alteration of triglycerides, especially those with unsaturated fatty acids, is a concern due to the high temperatures used and response factors must be checked to appropriately interpret data (Carelli and Cert, 1993). Response factors ranged from 0.98-1.02, indicating little difference between

measured and actual proportions of triglycerides (Molkentin and Precht, 2000). Figure 4.12. shows the triglyceride composition of pressure fractions collected during extraction at 41.4 MPa and 80°C.

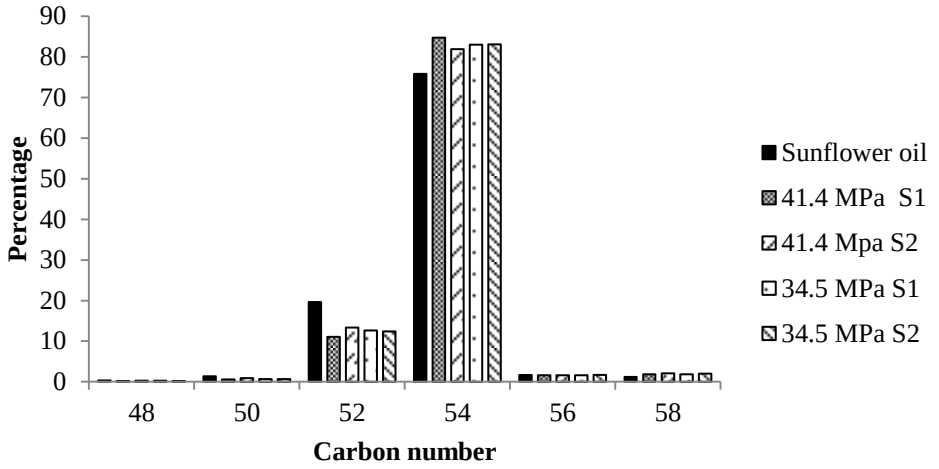

Figure 4.12. Comparison of triglyceride composition of extract pressure fractions at 41.4 MPa and 80°C and 34.5 MPa and 57.5°C. Separator 1(S1) held at 10.13 MPa. Separator 2 (S2) held at atmospheric pressure.

Comparing extracts within each carbon number, one way ANOVA indicated a statistically significant effect of the separators for C50, C52, and C58 and statistically significant effect of pressure for C52 only. The composition of extract in the first separator reflected a slightly greater concentration of larger molecular weight triglycerides (C54-58) while the extract in the second separator showed a greater concentration of the lower molecular weight triglycerides (C48-52). In keeping with the fatty acid results, the fractions obtained at 34.5 MPa and 35°C showed little difference from each other and the un-extracted oil. Greater resolution of triglyceride separation may be possible with more pressure step-downs at smaller intervals.

4.5. Conclusion

The following conclusions could be drawn from the presented work:

1) Up to 100% of the oil in potato chips can be extracted using SC-CO_2.
2) Total oil extracted increased as pressure increased from 27.6-41.4 MPa. The crossover effect of temperature was observed within this range of conditions, indicating the relative influence of solvent density and solute vapor pressure on oil extraction.
3) Extractability showed a dependence on flow rate, indicating that an optimum flow rate value may exist for different vessel dimensions.
4) The Sovova model showed a good fit to the experimental data. As expected, calculated kinetic parameters indicated that internal diffusion limits the mass transfer.
5) The process showed good agreement between small and large scale systems at 41.4 MPa and 80°C.
6) Fractionated oil analysis showed some preferential separation, but isolation of specific compounds would require further investigation.

References

Bensebia O., Barth D.,Bensebia B., Dahmani A., (2009). Supercritical CO2 extraction of rosemary: Effect of extraction parameters and modeling. *Journal of Supercritical Fluids*, 49(2), 161-166.

Carelli A.A., Cert A. (1993). Comparative study of the determination of triacylglycerol in vegetable oils using chromatographic techniques. *Journal of Chromatography A*, 630(1-2), 213-222.

J.-Y. Clavier, M. Perrut. (2004). Scale-Up Issues for Supercritical Fluid Processing in Compliance with GMP, vol. 1, Champigneulles, France

Devineni N., Mallikarjunan P., Chinnan M.S., & Phillips M.S. (1997). Supercritical Fluid Extraction of Lipidsfrom Deep-Fried Food Products. *JAOCS*, 74(12), 1517-1523.

Goto M., Sato M., & Hirose T. (1993). Extraction of Peppermint Oil by Supercritical Carbon Dioxide. *Journal of Chemical Engineering of Japan*, 26(4), 401-407.

King, M. B.; Catchpole, J. R. (1993). Physico-chemical data required forthe design of near critical fluid extraction process. In *Extraction of natural products using near-critical solvents*; King, M. B.,Bott, T. R., Eds.; Chapman and Hall: New York; 184-228.

Lee J.H. and Pangloli P., (2011). Volatile compounds and storage stability of potato chips fried in mid-oleic sunflower oil. *International Journal of Food Properties.* DOI: 10.1080/10942912.2010.526279

Levy J.M., Danielson V., Ravey R., & Dolata L. (1994). Routine determination of fats in foods using supercritical fluid extraction. *LC-GC*, 12(12), 920-923.

Liong K.K., Wells P.A., & Foster N.R. (1992). Diffusion of fatty acid esters in supercritical carbon dioxide. *Industrial & Engineering Chemistry Research*, 31(1), 390-399.

Lira C.T. (1996). Thermodynamics of Supercritical Fluids. In J. W. King, G. R. List (Eds.), *Supercritical Fluid Technology in Oil and Lipid Chemistry*. pp. 1-17. AOCS Press, Champaign, IL.

Machmudah S., Kondo M., Sasaki M., Goto M., Munemasa J., & Yamagata M. (2008). Pressure effect in supercritical CO2 extraction of plant seeds. *The Journal of Supercritical Fluids*, 44(3), 301-307.

McHugh, M. A., and V. J. Krukonis. (1994). *Supercritical fluid extraction principles and practice*. 2nd ed. Boston: Butterworth-Heinemann.

Molkentin J., Precht D. (2000). Equivalence of packed and capillary GC columns for detection of foreign fat in butter by use of the triglyceride formula method. *Chromatographia*, 52(11), 791-797.

Neff W.E., Eller F., & Warner K. (2002). Composition of oils extracted from potato chips by supercritical fluid extraction. *European Journal of Lipid Science and Technology*, 104(12), 785-791.

Nei H.Z.N., Fatemi S., Mehrnia M.R., & Salimi A. (2008). Mathematical modeling and study of mass transfer parameters in supercritical fluid extraction of fatty acids from Trout powder. *Biochemical engineering journal*, 40(1), 72-78.

Official Methods of Analysis of AOAC International. (2005). 18th Ed., AOAC International Gaithersburg, MD, USA, Official Method 963.22

Official Methods of Analysis of AOAC International. (2005). 18th Ed., AOAC International Gaithersburg, MD, USA, Official Method 969.33

Official Methods of Analysis of AOAC International. (2005). 18th Ed., AOAC International Gaithersburg, MD, USA, Official Method 986.19

Özkal S.G., Yener M.E., & Bayındırlı L. (2005). Mass transfer modeling of apricot kernel oil extraction with supercritical carbon dioxide. *The Journal of Supercritical Fluids*, 35(2), 119-127.

Povh N.P., Marques M.O.M., & Meireles M.A.A. (2001). Supercritical CO2 extraction of essential oil and oleoresin from chamomile (Chamomilla recutita [L.] Rauschert). *The Journal of Supercritical Fluids*, 21(3), 245-256.

Prado J.M., Prado G.H.C., & Meireles M.A.A. (2011). Scale-up study of supercritical fluid extraction process for clove and sugarcane residue. *The Journal of Supercritical Fluids*, 56(3), 231-237.

Reverchon E., Donsi G. Osseo LS. (1993). Modeling of supercritical fluid extraction from herbaceous matrices. *Ind. Eng. Chem. Res.* 32(11), 2721-2726

Rezaei K.A., Temelli F. (2000). Using supercritical fluid chromatography to determine diffusion coefficients of lipids in supercritical CO2. *The Journal of Supercritical Fluids*, 17(1), 35-44.

Rizvi, S. S. H., A. L. Benado, J. A. Zollweg, and J. A. and Daniels. (1986a). Supercritical fluid extraction: Fundamental principles and modeling methods. *Food Technology* 40 (6): 55-65.

Rizvi, S. S. H., A. L. Benado, J. A. Zollweg, and J. A. and Daniels. (1986b). Supercritical fluid extraction: Operating principles and food applications. *Food Technology* 40 (7): 57-64.

Rodrigues V.M., Sousa E.M.B.D., Monteiro A.R., Chiavone-Filho O., Marques M.O.M., & Meireles M.A.A. (2002). Determination of the solubility of extracts from vegetable raw material in pressurized CO2: a pseudo-ternary mixture formed by cellulosic structure+solute+solvent. *The Journal of Supercritical Fluids*, 22(1), 21-36.

Rubio-Rodríguez N., de Diego S.M., Beltrán S., Jaime I., Sanz M.T., & Rovira J. (2008). Supercritical fluid extraction of the omega-3 rich oil contained in hake (Merluccius capensis–Merluccius paradoxus) by-products: Study of the influence of process parameters on the extraction yield and oil quality. *The Journal of Supercritical Fluids*, 47(2), 215-226.

Sahena F., Zaidul I.S.M., Jinap S., Karim A.A., Abbas K.A., Norulaini N.A.N., & Omar A.K.M. (2009). Application of supercritical CO2 in lipid extraction – A review. *Journal of Food Engineering*, 95(2), 240-253.

Seal C.E., Kranner I., & Pritchard H.W. (2008). Quantification of seed oil from species with varying oil content using supercritical fluid extraction. *Phytochemical Analysis*, 19(6), 493-498.

Sovova H. (1994). Rate of the vegetable oil extraction with supercritical CO2, I. Modeling of extraction curves. *Chemical Engineering Science*, 49, 409-414.

Sovova H. (2005). Mathematical model for supercritical fluid extraction of natural products and extraction curve evaluation. *Journal of Supercritical Fluids.* 33(1), 35-52

Topal U., Sasaki M., Goto M., & Hayakawa K. (2006). Extraction of Lycopene from Tomato Skin with Supercritical Carbon Dioxide: Effect of Operating Conditions and Solubility Analysis. *Journal of Agricultural and Food Chemistry*, 54(15), 5604-5610.

van Konynenburg PH and Scott RL., (1980). Critical lines and phase equilibria in binary Van der Waals mixtures. *Phil. Trans. R. Soc. Lond. A.*, 298(1442), 495-540.

Vijayan S., Byskal D.P., & Buckley L.P. (1994). Separation of oil from fried chips by a supercritical extraction process: an overview of bench-scale test experience and process economics. In S. S. H. Rizvi (Ed.), *Supercritical fluid processing of food and biomaterials.* (1st edn., pp. 75-92). Blackie Academic & Professional, New York.

Chapter 5: Supercritical Fluids in Foods: Economic Analysis

5.1 Introduction

Food processing offers a set of unique challenges to the industry as not only must food be nutritious, have desirable organoleptic qualities for the consumer, and be safe to consume, but these objectives must be achieved while operating within the relatively low profit margins typical of the food industry. Therefore novel food processes must be evaluated for their efficacy, but before they can be implemented commercially, they must be evaluated for their financial feasibility. One novel processing strategy that has been explored for the past few decades is the use of supercritical fluids. Supercritical fluids (SCFs) have properties between those of liquid and gas. With liquid like densities and gas like mass transport properties, they have been used extensively for industrial separations processes (McHugh and Krukonis 1994). Separation processes that require the use of toxic organic solvents are typically avoided in food processing, as traces of solvent could cause harm to the consumers. There are some conventional solvents that are suitable for food use such as ethanol, but generally their removal from the final product can be energetically expensive and solvent disposal can have financial and environmental impacts. Supercritical fluids are particularly useful in food processes, because when brought back to atmospheric pressure they evaporate into the gaseous phase, leaving no solvent residue. Supercritical carbon dioxide (SC-CO_2) has been researched extensively for use in foods (Brunner 2005) due to its relatively low critical temperature and pressure (T_c = 31°C; P_c = 7.38 MPa), physiological innocuity, and low cost. SC-CO_2 is most commonly used for separation processes, particularly in lipid extraction (Sahena *et al.* 2009), bioactive compound extraction (Pereira and Meireles, 2010), and chromatography (Taylor, 2009). SC-CO_2 has also seen application in microbial inactivation (Perrut, 2012), enzymatic inactivation (Balaban and Ferrentino 2012), polymer foaming through extrusion (Rizvi *et al.* 1995), and several other unique processes

(Perrut, 2000).

Despite their benefits, SCFs are often considered too expensive for many applications due to the relatively high capital costs associated with the high pressure rated equipment required for their implementation. Therefore, a thorough investigation of the manufacturing cost of any supercritical fluid based process is necessary to establish its viability. The goal of this study was to assess feasibility of a recently described SC-CO_2 extraction process using a literature estimate for cost of manufacturing.

5.2. Associated costs

5.2.1. Fixed costs

Limited published information is available for the estimation of SCF equipment costs. Lack and Seidlitz (2001) published a cost breakdown associated with the production of extracts from hops. They indicated that the annualized capital investment cost (accounting for depreciation) represented about one third of the total operating costs, without taking into account the raw material costs. Perrut (2000) presented data regarding the cost of SCF units designed for extraction, fractionation, impregnation, or atomization at laboratory, pilot, and industrial scales based on a standardized design. The author presented a simple price index for SCF units:

$$PI = A(10V_TQ)^{0.24} \qquad (5.1)$$

Where PI is the dimensionless price index, A is a proportionality constant, V_T is the total volume, and Q is the solvent flow rate. Though Perrut cautions that this correlation should be interpreted carefully and is based on the experience of the author working for the Separex corporation (Champigneuelle, France) the construction of SCF units, it does demonstrate that the cost of an SCF unit increases by the square root of its capacity. This indicates economies of scale for SCF processes, though aside from the current major industrial applications (coffee

decaffeination, hops flavor extraction, essential oil extraction), much of SCF processing is for niche markets. Because of the economies of scale, Perrut (2000) suggests that building multiproduct facilities operating on a "time-share" basis would be more economical than using smaller scale single product dedicated units. However, processing standards and cleaning costs could be significant depending on the industry requirements.

5.2.2 Variable Costs

5.2.2.1. Materials

The two major input materials for SCF extraction are the supply fluid, typically CO_2 in food processing, and the raw feed material containing the desired solute. Supply fluid cost is generally low, due to the inexpensive nature of the fluids used and recovery of the fluid after decompression for recycling (Perrut, 2000). Raw materials to be extracted can vary in impact on costs, ranging as much as 27-94% of the total cost of manufacturing (Pereira and Meireles, 2010). Agricultural waste streams have also been investigated as potential feed materials for valuable extracts. Comim *et al.* (2010) investigated the extraction of oils from dried banana peel, a major agricultural byproduct in Brazil, and estimated the cost of manufacturing assuming no cost for acquiring the raw materials. However, pre-extraction processing, such as grinding or drying, cannot be ignored as necessary preparative steps for the feed prior to extraction (Comim *et al.*, 2010).

5.2.2.2 Labor

Perrut (2000) suggested that the most significant operating cost for SCF processes was manpower. The batch nature of many SCF systems along with the difficulty of automation for raw and spent material handling tend to contribute to this requirement. However, as expected, more sophisticated automation along with larger systems and long duration batch times would

reduce this cost.

5.2.2.3 Other

Perrut (2000) also stressed the importance of proper cleaning and maintenance when assessing the cost of a SCF system. Due to the high pressure associated with these processes, preventative maintenance, regular inspection, proper calibration, and documentation are key to the safe and successful application of this technology.

5.3. Estimating cost of manufacturing

Rosa and Meireles (2005) presented a rapid method for determining the cost of manufacturing (COM) of extracts using supercritical fluids by analyzing the contribution of fixed, variable, and general costs. The expression originally proposed by Turton *et al.* (1998) was designed for feasibility assessment of a broad range of chemical processes. It divides COM into five main costs: raw material, operational labor, utilities, waste treatment, and capital investment:

$$COM = 0.304\ FCI + 2.73\ C_{OL} + 1.23\ (C_{UT} + C_{WT} + C_{RM}) \qquad (5.2)$$

Where COM is the cost of manufacturing ($/yr), FCI is the annualized fixed capital investment, COL is the operation labor cost, CUT is the cost of utilities, CWT is the cost of waste treatment, and CRM is the cost of raw materials. The component costs ($/yr) are based on an assumed manufacturing capacity, specific to the processing equipment and operation schedule. The cost of raw materials takes into account any cost associated with raw materials including cost of preparative processes that may be required, such as drying. The fixed capital investment is the total cost of the SFE system. Cost of CO_2 is also factored into the FCI, though this is generally insignificant in comparison to the initial equipment investment (Rosa and Merieles, 2002).

Operational labor cost is estimated according to Ulrich (1984) and utility costs were estimated using the energy solvent cycle of pure CO_2, suggested by Brunner (1994). The expression itself was developed from a combination of the Lang (1947) factor method, which surveyed fourteen different chemical processing plants, and the Guthrie (1969) method, which surveyed 42 chemical processing plants. The processes surveyed were standard chemical operations including solids processing (milling, pelletizing, etc.), separations (solvent extraction, distillation, etc.), and reaction based processing (polymerization, catalysis, etc.). Regression of the data reported by Lang (1947) and Guthrie (1969) led to the coefficients used in the equation above which have been updated over time to account for inflation and technology based cost changes using the *Marshall and Swift all industry and process-industry equipment indexes, Engineering New-Record construction index, the Nelson refinery construction index, and the chemical Engineering plant cost index* (Peters and Timmerhaus, 1991). The coefficients are also used to indirectly adjust for costs associated with the process using the known input costs. For example, local taxes and insurance costs for chemical processing equipment can be estimated as 1.4-5% of the capital investment cost per year, which contributes to the coefficient for FCI in the equation above (Turton *et al.*, 2012). Because the equation is based on surveys of many types of chemical processing plants it is subject to error for any single process and can only serve as an initial estimate of the manufacturing cost. However, in the absence of more detailed information on processing costs as is the case with SC-CO_2 based operations, it can be a useful tool in assessing the feasibility of a particular chemical process.

Rosa and Meireles (2005) analyzed the COM for the production of clove bud oil and ginger oleoresin, two flavor extracts with potential application in the food industry, using supercritical fluid extraction (Figure 5.1.).

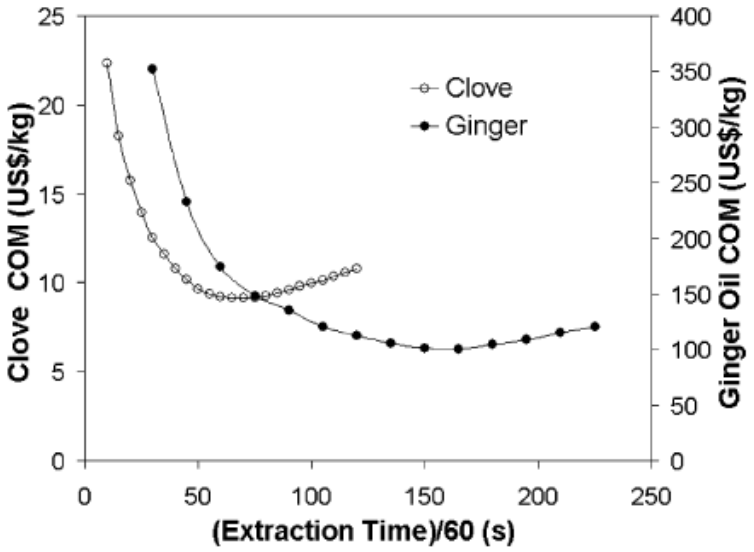

Figure 5.1. Estimated COM for clove and ginger extracts based on total extraction time (Rosa and Meireles 2005)

The authors estimated that the specific COM, defined as the manufacturing cost divided by the total mass of extract produced, reached a minimum value at the conclusion of the constant extraction rate period of the SCFE process, as described by Sovova (1994). The constant extraction rate (CER) period is marked by the convection dominated mass transport of the solute from the feed bed. Typically, this represents a linear portion of the overall extraction curve (extract mass over time) with the greatest rate of extraction. After the freely available solute is extracted, further extraction is limited by diffusion of the solute through the bed and thus the extraction rate decreases with time. Extraction beyond the conclusion of the CER period allows for the production of more extract per weight of feed, thus decreasing the total raw material costs, but increases total variable costs, such as labor and utilities. Accordingly, Rosa and Meireles (2005) found that for extraction times before the conclusion of the CER period, raw material costs dominated the COM, whereas after the CER period the fixed capital investment dominates. Several other studies were published using this same approach on estimating the COM for the production of extracts from plant materials (Table 5.1.)

Table 5.1. Estimated cost of manufacturing (COM) for various extracts*

Feed material	Target extract	COM ($US/kg)	Reference
Anise (*Pimpinella anisum*)	Anethole	14.43	Pereira and Meireles (2007a)
Banana peel (*Musa* spp.)	Peel oil	0.08-2.17	Comim *et al.* (2010)
Brazilian ginseng (*Pfaffia glomerata*)	Ecdysterone	1,648	Leal *et al.* (2006)
Clove (*Eugenia caryophyllus*)	Essential oil	9.18–10.97	Rosa and Meireles (2005)
Spent coffee grounds	Bioactive oil	7.35	de Melo *et al.* (2014)
Grape bagasse	Phenolics	133.16	Farías-Campomanes *et al.* (2013)
Mango (*Manguifera indica*)	Extract	151	Pereira and Meireles (2007b)
Palm (*Elaeis guineensis*)	Carotenoids	19.46-20.66	Assis *et al.* (2007)
Rosemary (*Rosmarinus officinalis*)	Essential oil	30.29	Pereira and Meireles (2007a)

*COM estimated assuming the same operating capacity, i.e. a 2 x 400 L column SC-CO_2 extraction system operated on a 24 hour basis for 330 days/year. Extraction conditions were specific to the feed and target extract. For further information the reader is directed to Pereira and Meireles (2010) and Pereira *et al.* (2013)

5.4. Cost of manufacturing for SC-CO_2 extraction and fractionation of oil from potato chips

Wagner *et al.* (2013) detailed the SC-CO_2 extraction of oil from fried potato chips at two scales. The goal of this additional processing step was to produce potato chips with reduced oil content, but still possessing the flavor and texture of a fried chip. As an added benefit, the extract obtained could be recycled back into the fryer, potentially reducing cost for replacing fryer oil (sunflower oil). Alternatively, the extract could be fractionated in order to produce a more concentrated flavor extract which could in turn be applied baked chips or other products to impart a desirable fried flavor. In this case, chips unsuitable for sale that would otherwise be

discarded, such as broken chip fragments and those that had spent too long in the fryer, would be valuable feed stock for extraction. In order to assess the cost of this process, several critical parameters and assumptions needed to be set:

- Capital Investment: SFE unit with two 400L extraction vessels operating in tandem (one in operation while the other depressurizes), $2,000,000 (Rosa and Meireles, 2005)
- Equipment depreciation: 10%/yr (Turton *et al.* 2012)
- Operating time: 3 shifts over 24 hours each day, 330 days per year
- Labor: 2 equipment operators (Rosa and Meireles, 2005) at the average rate for miscellaneous plant and system operators, $28.64/hr (Turton *et al.* 2012)
- Feed cost: $0, performed with normal chip manufacturing or using waste chips as feed stock
- Feed preparation (milling etc.): $30/metric ton (Rosa and Meireles, 2005)
- CO_2 supply: $0.53/kg (Airgas Inc.), with 2% (lost during extraction process) replacement (Rosa and Meireles, 2005). Factored in as a raw material cost according to Turton *et al.* (2012).
- Utilities: Saturated steam for heating, $0.0133/Mcal; Cold water for system cooling, $0.0837/Mcal; Electricity (pump operation) $0.0703/Mcal (Rosa and Meireles, 2005); Refrigeration for CO_2 cooling, $0.0789/Mcal (Turton *et al.* 2012)
- Utility requirements estimated using pure CO_2 solvent cycle, as suggested by Brunner (1994). Entropy values obtained from NIST Chemistry Webbook (Lemmon *et al.*, 2014)
- Extraction conditions: 80°C, 41.4 MPa, CO_2 flow rate of 4.81 metric tons/ hr. Extraction time (constant extraction rate period) 60.25 minutes. Chips before extraction are roughly 33% oil by weight and 13% oil by weight after extraction (Wagner *et al.* 2013)

- Solid waste treatment: $36/ metric ton (Turton *et al.* 2012)

Given these parameters, the cost of manufacturing SC-CO_2 extract from fried potato chips is presented in Table 5.2. using the method presented by Rosa and Meireles (2005).

Table 5.2. Cost of manufacturing SC-CO_2 extract from potato chips

Component	Cost ($/yr)
Raw materials	38,315
Labor	453,658
Utilities	291,267
Waste treatment	45,544
Cost of Manufacturing*	2,307,889
Cost per unit input ($/ kg feed)	1.82
Specific cost ($/kg extract)	8.02

*Computed from equation (5.2)

The specific cost of potato chip extract production was in line with typical SC-CO_2 processes and lower than most of the high cost extracts of spices and herbs. Recycling of the whole extract as oil for the fryers might not be worthwhile, as fresh sunflower oil is typically around $1/kg (less than the specific cost of the extract), and the extracted oil still may contain a significant portion of oxidized fatty acid (Wagner *et al.* 2013), which could impact the chemical stability of the fryer oil as well as the sensory qualities of the final product. The relatively low preparative feed costs and the use of feed that would otherwise go to waste makes this process advantageous for the production of a fried flavor extract. Based on the specific cost of extract reported in Table 5.2. and assuming extract specific gravity of 0.91 (typical of vegetable oils),the cost of producing this flavor extract would be about $0.21/fl. oz. Though no comparable product could be found commercially, typical liquid extracts sell for anywhere from $0.50/ fl. oz. at the low end to several dollars per fluid ounce at the high end. Assuming the quality of the extract is sufficient,

sale of the extract could be profitable. Potato chips at a typical grocery store sells for $9.52/kg and in order to maintain the same profit on a comparable reduced fat potato chip, the price would need to increase by about 19% to compensate for the added cost of the SC-CO_2 extraction process. As a non-essential good with a number of substitutes, price elasticity is expected to be high and therefor an increase in price would likely result in a decrease in revenue. However, if the price was kept comparable to the full fat version, increased unit sales could compensate for the reduced margin assuming the product was marketed to the consumer in a way that would justify the added cost. Additionally, offering a reduced fat version may benefit the image of a snack food company looking to shift towards a healthier product portfolio. This analysis should be interpreted with caution however, as the level of desired fat reduction could be reduced depending on the preference of the producer, resulting in varied extraction times and rates as well as different material handling costs.

5.5. Conclusion

SC-CO_2 extraction offers a promising alternative separation process to conventional organic solvent extraction. Though characterized by a high capital investment, it has been applied commercially with some success in the food industry and may continue to experience growth in niche markets for specific food extracts. Further establishment of this technology requires economic assessments for each application and several publications are available detailing a relatively simple analysis method that can be used to determine manufacturing costs associated with each product. Based on the current investigation, the following conclusions can be drawn:

1) An initial estimate of the cost of manufacturing defatted potato chips using SC-CO_2 could be determined using a commonly applied literature approach

2) Production of defatted potato chips using this SC-CO_2 based method would increase the cost of the product by 19% in comparison to conventional potato chips
3) Use of the extract as a flavorant may justify the additional cost of the process, though further investigation of extract quality and use would be required.

References

Assis, A. R., Prado, J. M., Maróstica, M. R. Jr. & Meireles, M. A. A. 2007. Manufacturing cost of carotene and lipids extracted via supercritical Technology from pressed palm fiber. In: Proceedings of the I Iberoamerican Conference on Supercritical Fluids-PROSCIBA, 10-13 April 2007, Foz do Iguaçu, PR, Brazil (CD-ROOM).

Balaban, M.O., and Ferrentino, G. Dense phase carbon dioxide food and pharmaceutical applications. in John Wiley & Sons [database online]. Hoboken, 2012.

Brunner, G. 1994. Gas extraction: An introduction to fundamentals of supercritical fluids and the application to separation processes. New York: Springer.

Comim, S. R., Madella, K., Oliveira, J. V., & Ferreira, S. R. S. 2010. Supercritical fluid extraction from dried banana peel (Musa spp., genomic group AAB): Extraction yield, mathematical modeling, economical analysis and phase equilibria. The Journal of Supercritical Fluids, 54(1), 30-37.

de Melo, M. M., Barbosa, H., Passos, C. P., & Silva, C. M. 2014. Supercritical fluid extraction of spent coffee grounds: Measurement of extraction curves, oil characterization and economic analysis. The Journal of Supercritical Fluids, 86, 150-159.

Farías-Campomanes, A. M., Rostagno, M. A., & Meireles, M. A. A. 2013. Production of polyphenol extracts from grape bagasse using supercritical fluids: Yield, extract composition and economic evaluation. The Journal of Supercritical Fluids, 77(0), 70-78.

Guthrie, K. M. (1969). Data and techniques for preliminary capital cost estimating. Chemical Engineering, 76(6), 114.

Lack, E., H. Seidlitz, G. Luft, A. Bertucco, A. Striolo, and F. Zanette. 2001. Economics of high pressure processes. *Industrial Chemistry Library* 9 : 437-71.

Lang, H. J. (1947). Engineering approach to preliminary cost estimates. Chemical Engineering, 54(9), 130-133.

Leal, P. F., Alexandre, F. C., Kfuri, M. B., & Meireles, M. A. A. 2006. Preliminary estimative of the cost of manufacturing SFE extracts from Brazilian Ginseng. In: Eighth Conference on Supercritical Fluids and Their Applications, pp. 157-160, 28-31 May, 2006, Ischia, Italy.

Lemmon E.W., M.O. McLinden and D.G. Friend. 2014. Thermophysical Properties of Fluid Systems. NIST Chemistry WebBook, NIST Standard Reference Database Number 69, Eds. P.J. Linstrom and W.G. Mallard. National Institute of Standards and Technology, Gaithersburg MD, 20899, http://webbook.nist.gov, (retrieved March 13, 2014).

McHugh, M. A., & Krukonis, V. J. (1994). Supercritical fluid extraction principles and practice (2nd ed.). Boston: Butterworth-Heinemann.

Pereira, C. G., Prado, J. M., Meireles, M. A. A., Rostagno, M., & Prado, J. 2013. Economic evaluation of natural product extraction processes. Natural Product Extraction: Principles and Applications, (21), 442.

Pereira, Camila G., and M.A.A. Meireles. 2010. Supercritical fluid extraction of bioactive compounds: Fundamentals, applications and economic perspectives. *Food and Bioprocess Technology* 3 (3): 340-72.

Pereira, C. G., & Meireles, M. A. A. 2007a. Economic analysis of rosemary, fennel and anise essential oils obtained by supercritical fluid extraction. Flavour and Fragrance Journal, 22, 407–413.

Pereira, C. G., & Meireles, M. A. A. 2007b. Evaluation of global yield, composition, antioxidant activity, cost of manufacturing of extracts from lemon verbena (Aloysia triphylla L'Herit Britton) and mango (Mangifera indica L.) leaves. Journal of Food Process Engineering, 30, 150–173.

Perrut, M.. 2012. Sterilization and virus inactivation by supercritical fluids (a review). *The Journal of Supercritical Fluids* 66 : 359-71.

Perrut, M. 2000. Supercritical fluid applications: Industrial developments and economic issues. *Industrial & Engineering Chemistry Research* 39 (12): 4531-5.

Peters, M.S. and K.D. Timmerhaus.1980. *Plant design and economics for chemical engineers*. New York: McGraw-Hill.

Rizvi, SSH, SJ Mulvaney, and AS Sokhey. 1995. The combined application of supercritical fluid and extrusion technology. *Trends in Food Science & Technology* 6 (7): 232-40.

Rosa, Paulo T. V., and M.A.A. Meireles. 2005. Rapid estimation of the manufacturing cost of extracts obtained by supercritical fluid extraction. *Journal of Food Engineering* 67 (1–2) (3): 235-40.

Sovova, H. 1994. Rate of the vegetable oil extraction with supercritical CO2, I. modeling of extraction curves. Chemical Engineering Science, 49, 409-414.

Taylor, L.T. 2009. Supercritical fluid chromatography for the 21st century. *The Journal of Supercritical Fluids* 47 (3): 566-73.

Turton, R., R.C. Bailie; W.B. Whiting; J.A. Shaeiwitz and D. Bhattacharyya,.1998. Analysis, synthesis, and design of chemical processes. in Prentice Hall . Upper Saddle River, NJ, .

Ulrich, G. D. 1984. A guide to chemical engineering process design and economics. New York: John Wiley & Sons.

Wagner, M. E., French, J., & Rizvi, S. S. 2013. Supercritical fluid extraction of oil from potato

chips: Two scale comparison and mathematical modeling. Journal of Food Engineering, 118(1), 100-107.